

Fast Blind Adaptive Equalisation for Multiuser CDMA Systems

by Adel Daas

Centre for Signal and Image Processing (CeSIP)
Department of Electronic and Electrical Engineering
University of Strathclyde

A Doctoral thesis submitted in partial fulfillment of the requirement for the
award of Doctor of Philosophy at the University of Strathclyde

April 2018

Supervised by:

Prof. Stephan Weiss

Declaration

This thesis is the result of the author's original research. It has been composed by the author and has not been previously submitted for examination which has led to the award of a degree.

The Copyright of this thesis belongs to the author under the terms of the United Kingdom Copyright Acts as qualified by University of Strathclyde Regulation 3.50. Due acknowledgment must always be made of the use of any material contained in, or derived from, this thesis.

Signed: Adel Daas

Date: 05/04/2018

Acknowledgements

I am truly and deeply indebted to my supervisor Prof. Stephan Weiss for his insightful direction, never ending kindness, and supreme friendship. His intuitive spontaneity, exceptional sense of humour, and shrewd wisdom make him a unique advisor.

My immense gratitude goes undoubtedly to my dear mother Sakina, my father Elhadj for their overwhelming tenderness, incredible support and persistent encouragements. Special thanks are also devoted to my wife Hanane Cherfaoui, my brothers Abderezak and Amer, and sisters Mofida and Aida who have kindly cheered me up by their optimism and motivation.

I would like to thank my dearest friends and colleagues Samir Bendoukha and Shahzad Ahmed Bhatti, for listening to ideas, and generating new ones, and our lunch time chats to try and clear the head.

My special gratitude goes out to the Algerian Government for granting me the opportunity to obtain the PhD.

To all these wonderful people, many thanks again.

Abstract

In order to improve communication over a dispersive channel in a CDMA system, we have to re-establish the orthogonality of codes which are used when combining input signals from many users onto a single communication path, as otherwise the performance of such system is limited significantly by inter-symbol interference (ISI) and multiuser access interference (MAI). In order to achieve this, adaptive filters are employed. A variety of adaptive schemes to remove ISI and MAI have been reported in the literature, some of which rely on training sequences, such as the Least Mean Squares (LMS) and Recursive Least Squares (RLS) algorithms, or on blind adaptation, such as the Constant Modulus Algorithm (CMA) or the Decision Directed algorithm (DD), which has similar convergence properties as the LMS in the absence of decision errors, the CMA is relatively slow compared to the DD algorithm but more robust in converging to a suitable solution.

This thesis is concerned with developing a new robust and low-complexity blind multiuser equalisation over frequency selective channels.

A robust pilot-assisted equalisation strategy is developed for the partially loaded time-division duplex (TDD) component of the universal mobile telecommunications system (UMTS). In addition to training-based equalisation performed using the midamble of a data packet, some of the unused spreading codes are exploited to upload pilots in order to perform an additional semi-blind adaptation over the payload of a packet. The latter ensures continu-

ous adaptation and better tracking performance. The affine projection concept along with the concurrent constant modulus algorithm (CMA) and decision-directed (DD) mode are implemented to update the equaliser weights. Computer simulations are used to assess the performance of the proposed adaptation strategy over various UMTS TDD time bursts.

A new low complexity adaptive technique is derived for blind multiuser equalisation based on fitting the probability density function (PDF) of the equalizer output to the desired PDF of the corresponding symbol alphabet, i.e. matched-PDF. The cost function of the proposed technique can be measured by a stochastic gradient descent approach. The performance of the proposed adaptation strategy is assessed by a number of simulations, and benchmarked against FIRMER-CMA under QPSK modulation.

The matched-PDF algorithm is used for the equalisation of Space-Time Block Coding (STBC) and Time-Reversal Space Time Block Coding (TR-STBC) signals transmitted over dispersive MIMO channels. The performance is demonstrated in a number of simulations and benchmarked against other blind schemes such as: CMA, Newton's method, and the Conjugate Gradient method. A thorough evaluation is carried out taking into consideration the complexity of each implementation in terms of multiply-accumulate (MAC) operations required per iteration.

Finally, some variations of matched-PDF algorithm are proposed to improve the equaliser performance, including concurrent matched-PDF and decision directed, matched-PDF with affine projection algorithm, as well as pilot assisted equalisation based on matched-PDF algorithm for partially loaded systems.

Contents

Acronyms	xiii
Mathematical Notation	xvi
1 Introduction	3
1.1 Research Motivation	3
1.2 Original Contributions	6
1.3 Outline of Thesis	8
2 Algorithms for Adaptive Equalisation	10
2.1 General Concept of Adaptive Equalisation	10
2.2 Mean Square Error Criterion	11
2.3 Wiener-Hopf Solution	15
2.4 Least Mean Square Algorithm	16
2.4.1 Method of Steepest Descent	16
2.4.2 Gradient Estimate	17
2.4.3 Computational Complexity	18
2.5 Least Squares Algorithm	18
2.5.1 Least Squares Formulation	19
2.5.2 Recursive Least Squares Algorithm	20
2.5.3 Computational Complexity	23

2.6	Affine Projection Algorithm	23
2.6.1	APA Formulation	24
2.6.2	Geometrical Interpretation	26
2.6.3	Complexity Issues	26
2.7	Training versus Blind Equalisation	27
2.8	Decision Directed Adaptation	28
2.9	Constant Modulus Algorithm	29
2.9.1	Convergence Speed of CMA	30
2.9.2	Ill-Convergence and Initialisation	31
2.10	Concluding Remarks	32
3	Firmer-CMA and Variations	33
3.1	Blind Multiuser FIRMER-CMA Equaliser	33
3.1.1	Demultiplexed User Signals	34
3.1.2	Cost Function	36
3.1.3	Blind Adaptation	37
3.2	Concurrent FIRMER-CMA and Decision Directed Updating	39
3.2.1	Concurrent Cost Function	41
3.2.2	Concurrent Adaptation	43
3.2.3	Simulation Results	45
3.3	Concurrent FIRMER-CMA+DD with Affine Projection	47
3.3.1	Modified Cost Function	48
3.3.2	Formulation	49
3.3.3	Performance	52
3.4	Semi-Blind Adaptation	55
3.4.1	UMTS TDD Physical channel	55
3.4.2	Signal Model	56

3.4.3	Semi-Blind Equalisation Criterion	57
3.4.4	Demultiplexed User and Pilot Signals	58
3.4.5	Cost Functions	58
3.4.6	Phase ambiguity	59
3.4.7	Modified Cost Function	60
3.4.8	Concurrent Affine Projection Adaptation	61
3.4.9	Simulation Results	64
3.4.10	Effect of Pilot Loading on BER Performance	65
3.4.11	Summary	67
3.5	Concluding Remarks	67
4	Fast Adaptation for Time-Varying Channels	69
4.1	PDF Matching Algorithm	70
4.1.1	Demultiplexed User Signals	71
4.1.2	Cost Function	72
4.1.3	Stochastic Gradient Algorithm	75
4.2	PDF Algorithm Performance	76
4.2.1	Implementation Details	77
4.2.2	Results	77
4.2.3	Summary	79
4.3	Time-Varying Channels and Tracking Performance	80
4.3.1	Time-Varying Channel Model	80
4.3.2	Implementation Details	85
4.3.3	Simulation Results	86
4.3.4	Summary	88
4.4	Concluding Remarks	89

5 PDF Matching Algorithm for MIMO systems	90
5.1 MIMO STBC Based on PDF Matching	91
5.1.1 Channel and Signal Model	93
5.1.2 PDF-Matching Based Cost Function	96
5.1.3 Stochastic Gradient Algorithm	101
5.1.4 Algorithm Performance	103
5.1.5 Summary	106
5.2 MIMO TR-STBC Based on PDF Matching	106
5.2.1 Channel and Signal Model	107
5.2.2 Cost Function	111
5.2.3 Algorithm Performance	113
5.2.4 Complexity Study	114
5.2.5 Summary	116
5.3 Concluding Remarks	117
6 Conclusions and Future Work	119
6.1 Conclusions	119
6.2 Future Work	122
Appendices	125
A Wirtinger’s Calculus	126
B Matched Filters	130
Bibliography	132

List of Figures

2.1	Basic communication system model with channel \mathbf{g} and equaliser \mathbf{w}	11
2.2	Geometrical interpretation of affine projection algorithm	27
3.1	Signal model of DS-CDMA downlink with a Firmer-CMA equaliser	35
3.2	Cost function ξ_c in dependency of a single complex valued coefficient w_0	37
3.3	Signal model with a concurrent equaliser	40
3.4	Cost function ξ_c in dependency of a single complex valued coefficient w_0	42
3.5	Cost function ξ_d in dependency of a single complex valued coefficient w_0	42
3.6	Comparison of convergence speed and steady state MSE between the concurrent FIRMER-CMA+DD algorithm and the standard FIRMER-CMA.	46
3.7	The decoded signal constellations of user $l = 0$ after adaptation of 5×10^3 symbols with (a) no equalisation (b) standard FIRMER-CMA equaliser and (c) concurrent FIRMER-CMA+DD.	47
3.8	Configuration of the desired response for the CM criterion.	49
3.9	MSE curves of the FIRMER-CMA+DD ($p = 1$) and AP-FIRMER-CMA+DD ($p =$ 5).	53
3.10	BER curves of the matched filter receiver, FIRMER-CMA ($p = 1$), and AP- FIRMER-CMA+DD equalisers for two different projection orders with $p = 3$ and $p = 5$	54
3.11	Time structure in UMTS TDD: (a) basic frame structure, and (b) burst structure.	56

3.12	Signal model of a partially loaded DS CDMA downlink with a concurrent equaliser	57
3.13	Cost function ξ_c for a partially loaded system with 10 active users and 6 pilots.	60
3.14	MSE curves of FIRMER-CMA, FIRMER-CMA+DD, and AP-FIRMER-CMA+DD	64
3.15	Effect of the number of pilots on the BER performance.	65
3.16	Effect of the training sequence length and pilot loading on the BER performance.	66
4.1	Signal model of DS-CDMA downlink with a PDF-Matching equaliser $\mathbf{w}[m]$. . .	71
4.2	The PDF-matching cost function for one output.	75
4.3	MSE curves of the proposed Matched-PDF Algorithm and the FIRMER-CMA.	78
4.4	BER vs SNR curves of the Matched-PDF Algorithm and FIRMER-CMA.	79
4.5	ISI curves of the Matched-PDF Algorithm and FIRMER-CMA.	80
4.6	Channel Impulse Response at time n	81
4.7	Mobility of a terminal causes Doppler Shift.	82
4.8	Magnitude response of the Doppler filter or PSD of a channel coefficient.	84
4.9	Implementation of a single Rayleigh fading coefficient	85
4.10	Trajectories of moduli of Rayleigh fading channel coefficients.	86
4.11	MSE curves of Matched-PDF and CMA under time-varying channel.	87
4.12	MSE curves of Matched-PDF and CMA with averaging	88
5.1	A Multiple-Input Multiple-Output system with M transmit and N receive antennas	91
5.2	Channel and signal model with transmit STBC signals $s_i[n]$, a 2×2 MIMO channel with CIRs $h_{j,i}[n, \nu]$, received signals $r_j[n]$, equaliser components $\mathbf{w}_{i,j}[n]$ and equaliser outputs $y_i[n]$ which should adhere to the STBC structure. . .	93
5.3	The PDF-matching cost function for one output. Part of the surface has been removed to visualise the shape near the origin.	99

5.4	Complexity of the different equalisers, in number of complex multiply-accumulate (MAC) operations per iteration.	104
5.5	MSE curves of STBC-PDF and STBC-CMA	105
5.6	Block structure in Time-Reversal STBC: (a) regular burst, (b) regular and reverse bursts.	108
5.7	Data model for a 2×2 TR-STBC system	109
5.8	Equaliser structure for Time-Reversal STBC.	110
5.9	MSE curves for the different implementations of the TR-STBC-CMA	115
5.10	BER for the different implementations of the TR-STBC-CMA, SNR = 10dB	116
5.11	Number of MACs required per iteration for proposed algorithms.	117
B.1	Synchronous DS-CDMA system with matched filters	130

List of Tables

2.1	Equations for channel equalisation by LMS adaptive algorithm	18
2.2	Equations for channel equalisation by RLS adaptive algorithm	22
2.3	Equations for the filter update by the APA adaptive algorithm.	26
2.4	Equations for channel equalisation by DD adaptive algorithm	29
2.5	Equations for channel equalisation by CMA at symbol rate n	30
3.1	Equations for multiuser channel equalisation by FIRMER-CMA	39
3.2	Concurrent FIRMER-CMA+DD algorithm.	45
3.3	Concurrent affine projection algorithm (AP-FIRMER-CMA+DD) for pilot-assisted multiuser equalisation.	52
3.4	Parameter values of the generalised cost function ξ_m	61
5.1	Complexity of the different equalisers, in number of MAC operations.	103
5.2	Delay-power profile of the MIMO system's channel impulse responses	104
5.3	Simulation parameters for the different blind equalisers.	113
5.4	Complexity of the different equalisers, in terms of MAC and LDR operations	116

Acronyms

2G	second generation
3G	third generation
4G	fourth generation
5G	fifth generation
8PSK	eight phase shift keying
AM	amplitude modulation
AoA	angle of arrival
APA	affine projection algorithm
AWGN	additive white Gaussian noise
BER	bit error ratio
CDMA	code division multiple access
CM	constant modulus
CMA	constant modulus algorithm
CIR	channel impulse response
CG	conjugate gradient
DD	decision directed
DFE	decision feedback equaliser
DL	downlink
DS-CDMA	direct sequence CDMA
FAPA	fast affine projection algorithm
FDMA	frequency division multiple access
FIR	finite impulse response
FIRMER	filtered-R multiple error
FQN	fast quasi-Newton
FMT	frequency multi-tone

IEEE	institute of electrical and electronics engineers
iid	independent identically distributed
ISI	inter-symbol interference
ITU	international telecommunications union
ITU-R	radio-communication sector of ITU
LCMA	Lattice CMA
LMS	least mean square
LS	least squares
LTE	long term evolution
MAC	multiply-accumulate
MAI	multiple access interference
MBER	minimum BER
MIMO	multiple input multiple output
MF	matched filters
MOE	minimum output energy
MSE	mean square error
MMSE	minimum MSE
NLMS	normalised LMS
OFDM	orthogonal frequency division multiplexing
PDF	probability density function
PSK	phase shift keying
QAM	quadrature amplitude modulation
QPSK	quadratic phase shift keying
RLS	recursive least squares
RQN	recursive quasi-Newton
Rx	receive antenna
SDMA	space division multiple access
SISO	single input single output
SOS	second order statistics
SNR	signal to noise ratio
STBC	space time block coding
STBC-CMA	CM equaliser for STBC
STBC-PDF	Matched-PDF equaliser for STBC
TDD	time division duplex
TDMA	time division multiple access

TR-STBC	time reversal STBC
TR-STBC-CMA	CM equaliser for TR-STBC
TR-STBC-PDF	Matched-PDF equaliser for TR-STBC
Tx	transmit antenna
UMTS	universal mobile telecommunications system
UMTS-TDD	time division duplex for UMTS
UL	uplink

Mathematical Notation

General Notations

h	scalar quantity
\mathbf{h}	vector quantity
\mathbf{H}	matrix quantity
$h(t)$	a function of the continuous variable t
$h[n]$	a function of the discrete variable n
h_n	short hand form for $h[n]$ for dense notation
$\mathbf{H}(z)$	z-transform of a discrete function $h[n]$

Relations and Operators

$(\cdot)^*$	complex conjugate
$(\cdot)^T$	transpose
$(\cdot)^H$	Hermitian (conjugate transpose)
$(\cdot)^{-1}$	inverse
$(\cdot)^\dagger$	pseudo-inverse
$\mathcal{E}\{\cdot\}$	expectation operator
∇_x	gradient operator with respect to x
$\text{diag}(\cdot)$	diagonal matrix with elements (\cdot)
$ \cdot $	magnitude operator
\min	minimum
$\mathcal{C}_{\{\cdot\}}$	complexity of algorithm $\{\cdot\}$
$\mathcal{O}(\cdot)$	complexity in the order of (\cdot)
$\stackrel{!}{=}$	must be equal to

$\frac{\partial f}{\partial w}$	derivative of f with regards to w
$q(\cdot)$	maps (\cdot) into the nearest constellation point
δ	produces 1 if (\cdot) is equal to 0 and 0 otherwise
\sum	sum
$\bullet \rightarrow \circ$	Laplace transform

Sets and Spaces

\mathbb{R}	set of real numbers
$\mathbb{R}^{M \times N}$	set of $M \times N$ matrices with real entries
\mathbb{Z}	set of integer numbers
$\mathbb{Z}^{M \times N}$	set of $M \times N$ matrices with integer entries
\mathbb{C}	set of complex numbers
$\mathbb{C}^{M \times N}$	set of $M \times N$ matrices with complex entries

Symbols and Variables

α	weighting between two cost terms
α_n	a priori estimation error
β	forgetting factor
δ	delay
Δ	a delay of one symbol period
η	regulating weight
γ	constant modulus
γ_p	the dispersion constant of the constellation
\mathbf{h}_l	l th user's spreading code vector
$\tilde{\mathbf{h}}_l[nN]$	l th user's modified and time-varying code vector
\mathbf{H}	matrix of active user's spreading sequences
$\mathbf{H}_l[nN]$	convolutional time-varying matrix
μ	adaptive algorithm step size
μ_c	step size of the CM adaptive algorithm
μ_d	step size of the DD adaptive algorithm
μ_{PDF}	step size of the Matched-PDF adaptive algorithm

τ	delay index
Φ_n	inverse of autocorrelation matrix \mathbf{R}_n^{-1}
\mathbf{c}	scrambling code vector
$c[m]$	scrambling sequence
ξ	cost function
ξ_{CM}	CMA cost function
ξ_{DD}	DD cost function
ξ_{LS}	Least Squares cost function
ξ_{MSE}	MSE cost function
ξ_{PDF}	Matched-PDF cost function
φ	phase rotation
ϑ	angle of movement with respect to the reception path
\mathbf{g}	channel impulse response vector
$g[m]$	channel chip rate impulse response
\mathbf{g}_n	a gain vector
\mathbf{I}	identity matrix
\mathbf{H}	$N \times N$ Hadamard matrix
l	user index
L	length of equaliser
L_a	length of the source data
L_c	length of channel
L_h	length of MIMO channel
L_p	length of guard period
L_s	length of burst
L_w	length of space-time equaliser
K	number of active users
N_p	number of pilots signals
n	symbol index
m	chip index
$K_\sigma(z)$	Gaussian kernel
σ	variance
p	order of Godard's algorithm
p	order of APA
$p_l[n]$	l th pilot signal
$p_A(z)$	probability density function of A

$\hat{p}_A(z)$	probability density function estimate of A
\mathbf{p}	the cross-correlation vector
\mathbf{R}	the auto-correlation matrix
\mathbf{r}_{nN}	received vector signal
$u[n]$	single user transmitted signal
$\hat{u}[n]$	single user decoded signal
$u_l[n]$	l th user's transmitted signal
$\hat{u}_l[n]$	l th user's decoded signal
$s[n]$	chip rate transmitted signal
\mathbf{s}_n	transmitted signal vector
$v[m]$	noise chip rate sequence
\mathbf{v}_n	noise vector
v	speed of movement
λ	wavelength
\mathbf{w}	coefficient vector of an equaliser
\mathbf{w}_{opt}	optimum coefficient vector
$z_l[n]$	l th inactive signal
$x[n]$	input sequence to single user equaliser
\mathbf{x}_n	input vector to single user equaliser
$y[m]$	equaliser's chip rate output signal
f_{Doppler}	Doppler shift
f_{max}	maximum Doppler frequency
$s_i[n]$	transmitted signal of antenna i
$r_j[n]$	received signal from antenna j
$h[n, v]$	doubly-dispersive channel with n time index and v coefficient index
$h_{j,i}[n, v]$	time varying channel between the i th transmit and j th receive antenna
$\mathbf{H}_{n,v}$	MIMO channel matrix
$e[n]$	error at time n
\mathbf{e}	error vector
$e_i[n]$	error corresponding to output i at time n
r_{rs}	cross-correlation function between $r[n]$ and $s[n]$
L	size of Kernal window

Chapter 1

Introduction

1.1 Research Motivation

Over the last decades, mobile communications research has supported the shift in focus from voice transmission with moderate data rate to more inclusive communications with internet support and multimedia capabilities. This has been achieved with the introduction of 2G and 3G mobile communications technology standards, which allowed a data rate of up to 2 Mb/s. This trend continued with the adoption of the long term evolution (LTE) standard, pushing the data rate limit to up to 300 Mb/s for downlink and 75 Mb/s for uplink [1]. This advancement in mobile communication systems was enabled by a huge leap in mobile phone technology bringing sophisticated devices with high processing power which are hungrier than ever for data, and was accompanied by new requirements for 4G mobile cellular system standards. In March 2008, the radio-communications sector of the International Telecommunications Union (ITU-R) defined a set of specifications for systems to qualify as 4G, requiring peak data rate of 100 Mb/s for high mobility communication and 1 Gb/s for low mobility communication [2]. Since the first release of LTE did not meet the requirements for 4G, research efforts have been ongoing to achieve new standards meeting

these specifications [3]. This brought LTE-Advanced [4], a major enhancement to the LTE standard which was accepted by ITU-R as a candidate for 4G technology. Although, 5G is still under development, it promises to offer throughput as high as 10 Gb/s.

Many of the contemporary wireless network standards rely on orthogonal frequency division multiplexing (OFDM) rather than code division multiple access (CDMA) as promoted as part of the universal mobile telecommunications system (UMTS). Initially introduced to avoid equalisation, OFDM has since been driven to higher data rates in situations where its benefits are often negated, such as in mobility scenarios where complex equalisation schemes will be required [5, 6, 7], in order to re-establish the orthogonality on which OFDM so fundamentally relies. Just as OFDM has seen a revival of frequency division multiplexing techniques that had previously been popular several decades back in the form of techniques such as frequency multi-tone (FMT), CDMA-based approaches may experience a renaissance of spread-spectrum ideas in future communications applications; therefore, the contributions of this thesis are aimed at such systems, with simulation parameters drawn from current UMTS packet structures.

The increasing demand for high data throughput and multimedia services in the downlink (DL) transmission drives research towards achieving higher capacity gain through multi-input multi-output (MIMO) transmission and multiuser detection. In fact, DL signals are perfectly synchronised at the transmitter, and they experience the same dispersive channel using orthogonal spreading sequences. In most communication systems the channel is considered broadband, i.e the channel frequency response varies across the whole frequency bandwidth, which results in inter symbol interference (ISI) and multiplex access interference (MAI). This makes wireless transmission difficult and destroys the orthogonality of the CDMA code sequences transmitted by different users. The overall aim of this thesis is to design multiuser equalisers to mitigate the effects of the dispersive channel.

A wide variety of equalisation schemes can be found in the literature [8, 9, 10], and can be divided into:

1. Trained equalisers necessitate the periodic transmission of training sequences to be known a priori to the receiver. Trained algorithms are reliable but the training sequences can be considered as a waste of available valuable bandwidth. Trained equalisers can also suffer from poor tracking performance in fast time-varying channels.

2. Blind equalisation algorithms do not require explicit knowledge of the training sequences and channel parameters, instead estimation is performed blindly i.e. without explicit knowledge of channel or training sequences. Blind equalisers require more data to adapt but have the advantage of maximising the bandwidth utilisation. The most popular blind approach is the constant modulus algorithm (CMA) which assumes that all points in the transmit constellation have the same modulus.

3. Hybrid equalisation includes decision-directed (DD) and semi-blind algorithms. DD means the equaliser uses a detected version of its output signal, based on a non-linear decision device, to update its weights. Semi-blind adaptation is used when the transmission of full training sequences is either infeasible or undesirable, this means the length of the training sequences is reduced — instead of suppressed — in order to optimise the data throughput. Hybrid algorithms are used when trained equalisation is not sufficient to minimise the difference between the transmitted and received sequences.

This thesis is concerned with developing new robust and low-complexity multiuser equalisers over frequency selective fading channels. The channels used throughout this thesis are time-varying (except where otherwise mentioned), which motivates the use of equalisation algorithms with good adaptation and tracking abilities. The remainder of this chapter presents the original contributions of this dissertation and outlines the subsequent chapters of the thesis.

1.2 Original Contributions

The main original contributions in this thesis are believed to be:

1. **Fast and Robust Multiuser Pilot-Assisted Equaliser for Downlink UMTS-TDD (Chapter 3)** [11]. A robust pilot-assisted equalisation strategy for the partially loaded time-division duplex (TDD) component of the universal mobile telecommunications system (UMTS) is derived. In addition to training-based equalisation performed using the midamble of a data packet, some of the unused spreading codes are exploited to upload pilots in order to perform an additional training-based adaptation over the payload of a packet. The latter ensures continuous adaptation and better tracking performance. The affine projection concept along with the concurrent constant modulus algorithm (CMA) and decision-directed (DD) mode are implemented to update the equaliser weights.
2. **A PDF Matching Blind Multiuser Equaliser (Chapter 4)** [12]. A new blind adaptive equalisation approach, the so-called PDF matching algorithm suitable for fully loaded DS-CDMA downlink systems, is derived. The proposed approach is based on fitting the probability density function (PDF) of the equaliser output to the desired PDF of the corresponding symbol alphabet. The underlying PDF at the equaliser output is estimated by means of the Parzen window method. A switch between blind and decision directed adaptation is possible by manipulating the kernel size of the Parzen window estimator. The cost function of the proposed technique can be optimised by a stochastic gradient approach.
3. **A PDF Matching Blind Multiuser Equaliser over frequency selective fading channels (Chapter 4)** [13]. A new frequency selective channel model based on Rayleigh fading is introduced. This time-varying channel model is used to test the

tracking performance of the PDF matching technique mentioned above. The performance of the proposed adaptation strategy is assessed by a number of simulations, and benchmarked against CMA under QPSK modulation in a doubly-dispersive environment.

4. **Fast converging implementation of the STBC receiver over dispersive channels (Chapter 5)** [14]. A new blind adaptive technique is derived for the equalisation of space-time block coded (STBC) signals transmitted over a dispersive MIMO channel. The adaptation is based on minimising the difference between the PDF of the equaliser output and a desired PDF based on the source symbols. In the proposed approach, the PDFs are estimated by means of the Parzen window method using Gaussian kernels. The cost function combines this PDF fitting with an orthogonality criterion derived from the STBC structure of the transmitted data in order to discourage the extraction of identical signals. This cost function motivates an effective and low-cost stochastic gradient descent algorithm for adapting the equaliser. The performance is demonstrated in a number of simulations and benchmarked against other blind schemes for the equalisation of STBC over broadband MIMO channels.
5. **Fast converging implementation of the TRSTBC receiver over dispersive channels (Chapter 5)** [15]. A new blind multiuser equalization strategy for time reversal STBC (TRSTBC) signals transmitted over dispersive MIMO channels is derived. Similar to the STBC receiver above, the cost function used here combines the PDF matching component with an orthogonality criterion derived from the TR-STBC structure. The performance is demonstrated in a number of simulations and benchmarked against other blind schemes. The proposed algorithm has a moderate computational complexity and can perform with higher adaptation rate.

1.3 Outline of Thesis

The following chapters of this thesis are organized as follows:

Chapter 2 is a brief survey of adaptive equalisation concepts in digital communications. The mean square error criterion is explained and the Wiener-Hopf solution is outlined. Then, the formulation of some training based equalisers is demonstrated, mainly: the least mean squares algorithm and recursive least squares algorithm. Blind equalisation schemes are then discussed. Specifically, properties of the most popular blind algorithm, the constant modulus algorithm, are highlighted and analysed. **Chapter 3** introduces a pilot-assisted equalisation approach for the downlink UMTS TDD system. First, a blind multiuser adaptive equaliser based on the affine projection (AP) filtered-R multiple error (FIRMER) concurrent constant modulus algorithm (CMA) and decision-directed (DD) algorithm, is briefly presented, then a suitable cost function for a pilot assisted scheme and an associated stochastic gradient algorithm are derived. We illustrate that the proposed semi-blind approach outperforms the basic equalisation scheme in terms of MSE and BER.

Chapter 4 presents a blind matched-PDF algorithm for multiuser equalisation over frequency selective fading channels. The algorithm operates in the chip rate and reduces the error by minimising the difference between the PDF of the equaliser output and the PDF of the corresponding constellation alphabet. Simulation results are shown to highlight the performance of the derived algorithm.

Chapter 5 starts by reviewing the STBC scheme, and presenting a non-block based approach to the blind equalisation of STBC over dispersive channels. The derived algorithm adds a new term to the PDF-matching criterion, whereby the output of the equaliser is forced to have the same structure as the transmitted STBC code word. Simulation results are presented to evaluate the performance of the new algorithm in time-varying channels.

Then, the block-based time reversal STBC (TRSTBC) scheme is introduced. A PDF-matching based receiver for TRSTBC is analysed and shown to achieve faster convergence than the CMA based receiver. This chapter investigates the performance gain of the proposed algorithm against added complexity.

Chapter 6 summarises the main results of this dissertation, and puts forward ideas and suggestions for future work and investigations.

Chapter 2

Algorithms for Adaptive Equalisation

This chapter introduces the general adaptive equalisation problem and reviews some adaptive equalisation techniques. Sec. 2.1 explains how an adaptive equaliser can alleviate inter-symbol interferences (ISI) introduced by a dispersive channel. The concept of mean square error (MSE) is explained in Sec. 2.2, while the derivation of the Wiener-Hopf solution is addressed in Sec. 2.3. Next in Sec. 2.4 and 2.5, the well known least mean squares (LMS) and recursive least squares (RLS) algorithms are briefly reviewed, respectively. Then, in Sec. 2.6 the affine projection algorithm is derived. In Sec. 2.8 and Sec. 2.9 the concepts of decision directed adaptation (DD) and constant modulus algorithm (CMA) are reviewed.

2.1 General Concept of Adaptive Equalisation

In digital communication systems, equalisers are mainly designed to combat the multipath effect of the channel, which causes inter-symbol interference (ISI). A simple model for such a system is illustrated in Fig. 2.1. The equaliser coefficient vector \mathbf{w} is assumed to be a linear tapped delay line filter with finite impulse response (FIR) of length L .

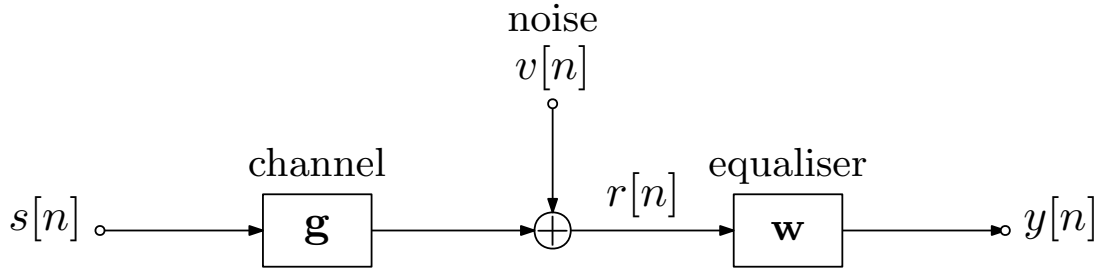


Figure 2.1: Basic communication system model with channel \mathbf{g} and equaliser \mathbf{w} operating on received signal $r[n]$; the aim of the equaliser is to approximate the transmit signal $s[n]$ at its output $y[n]$ in some optimal sense.

This structure has a linear relation between the equaliser output $y[n]$ and the equaliser vector \mathbf{w} . The linearity and FIR structure have in the past contributed to the popularity of this equaliser in practice [16, 17, 18]. In contrast, e.g. decision feedback equalisers (DFEs) do not have this property.

The propagation environment adopted here is a dispersive channel defined by its channel impulse response (CIR) $g[n]$ with sample index n . This channel is a linear tapped delay filter of length L_c with an associate coefficient vector

$$\mathbf{g} = [g_0 \ g_1 \ \cdots \ g_{L_c-1}]^T, \quad (2.1)$$

and contains any filtering at the transmitter such as pulse shaping which may or may not be known at the receiver.

2.2 Mean Square Error Criterion

Equalisers are mainly designed to combat the multipath effect of the channel, and hence the minimisation of the probability of the occurrence of incorrect decisions, or the bit error ratio (BER), is the main aim. In the past the BER have been found difficult to evaluate and it does

not level itself easily as a cost function for adapting an equaliser [19]. However, significant efforts have been made in implementing simple filtering and adaptation structures based on a minimum bit error ratio (MBER) criterion, that have shown outstanding performance at moderate computational complexity [20]. Nevertheless, the Wiener-Hopf or minimum MSE solution, which minimises the error between the transmitted signal $s[n]$ and the equaliser output $y[n]$, remains a popular equaliser, which forms an important benchmark to which other equalisers are frequently compared.

In the following we aim to derive the Wiener-Hopf equaliser coefficients and the corresponding MMSE solution, by minimising the expected squared magnitude of the error

$$e[n] = s[n - \delta] - y[n] \quad , \quad (2.2)$$

for a specific choice of delay δ . The source signal $s[n]$ is assumed to be an independent identically distributed (i.i.d.) sequence. With these quantities, the n th equaliser output can be calculated by

$$y[n] = \mathbf{w}^H \mathbf{r}_n \quad , \quad (2.3)$$

the discrete convolution between the coefficients $w[n]$ and the received signal $r[n]$. These signals can be expressed in vector notations: \mathbf{w} and \mathbf{r}_n ,

$$\mathbf{w} = [w_0^*, w_1^*, \dots, w_{L-1}^*]^T \quad (2.4)$$

For later convenience note that, the coefficients of vector \mathbf{w} are *complex conjugate* w_i^* .

$$\mathbf{r}_n = [r[n], r[n-1], \dots, r[n-L+1]]^T \quad (2.5)$$

By substituting (2.3) into (2.2) we obtain

$$e[n] = s_{n-\delta} - \mathbf{w}^H \mathbf{r}_n \quad , \quad (2.6)$$

Minimisation of the mean square error (MSE) for optimisation problems is widely used in practice due to the fact that its mathematical derivation is relatively straight-forward.

The mean squared error (MSE) criterion ξ_{MSE} is given by the statistical expectation of the squared error signal,

$$\begin{aligned} \xi_{\text{MSE}} &= \mathcal{E}\{e[n]e^*[n]\} = \mathcal{E}\{(s_{n-\delta} - \mathbf{w}^H \mathbf{r}_n)(s_{n-\delta}^* - \mathbf{r}_n^H \mathbf{w})\} \\ &= \mathcal{E}\{s_{n-\delta}s_{n-\delta}^*\} - \mathcal{E}\{\mathbf{w}^H \mathbf{r}_n s_{n-\delta}^*\} - \mathcal{E}\{s_{n-\delta} \mathbf{r}_n^H \mathbf{w}\} + \mathcal{E}\{\mathbf{w}^H \mathbf{r}_n \mathbf{r}_n^H \mathbf{w}\} \\ &= \sigma_s^2 - \mathbf{w}^H \mathcal{E}\{\mathbf{r}_n s_{n-\delta}^*\} - \mathbf{w}^T \mathcal{E}\{s_{n-\delta} \mathbf{r}_n^*\} + \mathbf{w}^H \mathcal{E}\{\mathbf{r}_n \mathbf{r}_n^H\} \mathbf{w} \\ &= \sigma_s^2 - \mathbf{w}^H \mathbf{p} - \mathbf{w}^T \mathbf{p}^* + \mathbf{w}^H \mathbf{R} \mathbf{w} \end{aligned} \quad (2.7)$$

where substitutions with the cross-correlation vector \mathbf{p} and the auto-correlation matrix (covariance matrix for zero-mean processes) \mathbf{R} have taken place. The cross-correlation vector \mathbf{p} is defined by

$$\mathbf{p} = \mathcal{E}\{\mathbf{r}_n s_{n-\delta}^*\} = \mathcal{E}\left\{ \begin{bmatrix} r_n s_{n-\delta}^* \\ r_{n-1} s_{n-\delta}^* \\ \vdots \\ r_{n-L+1} s_{n-\delta}^* \end{bmatrix} \right\} = \begin{bmatrix} r_{rs}[\delta] \\ r_{rs}[\delta-1] \\ \vdots \\ r_{rs}[\delta-L+1] \end{bmatrix} \quad (2.8)$$

where $r_{rs}[\tau]$ is the cross-correlation function between $r[n]$ and $s[n]$,

$$r_{rs}[\tau] = \mathcal{E}\{r[n + \tau]s^*[n]\} = r_{sr}^*[-\tau] \quad . \quad (2.9)$$

The entries of the auto-correlation matrix $\mathbf{R} \in \mathbb{C}^{L \times L}$

$$\mathbf{R} = \mathcal{E}\{\mathbf{r}_n \mathbf{r}_n^H\} = \mathcal{E} \left\{ \begin{bmatrix} r_n r_n^* & r_n r_{n-1}^* & \cdots & r_n r_{n-L+1}^* \\ r_{n-1} r_n^* & r_{n-1} r_{n-1}^* & \cdots & r_{n-1} r_{n-L+1}^* \\ \vdots & \vdots & \ddots & \vdots \\ r_{n-L+1} r_n^* & r_{n-L+1} r_{n-1}^* & \cdots & r_{n-L+1} r_{n-L+1}^* \end{bmatrix} \right\} \quad (2.10)$$

$$= \begin{bmatrix} r_{rr}[0] & r_{rr}[-1] & \cdots & r_{rr}[-L+1] \\ r_{rr}^*[-1] & r_{rr}[0] & \cdots & r_{rr}[-L+2] \\ \vdots & \vdots & \ddots & \vdots \\ r_{rr}^*[-L+1] & r_{rr}^*[-L+2] & \cdots & r_{rr}[0] \end{bmatrix} \quad (2.11)$$

are samples of the auto-correlation function $r_{rr}[\tau]$ defined by (2.9). \mathbf{R} is Töplitz, i.e each descending diagonal from left to right is identical, and is Hermitian, i.e is equal to its own conjugate transpose: $\mathbf{R}^H = \mathbf{R}$. These properties imply that the matrix \mathbf{R} is positive semi-definite and possesses real valued eigenvalues [10, 21].

The cost function ξ_{MSE} is quadratic in the filter coefficients, and because of the semi-definiteness of \mathbf{R} , the cost function (2.7) has a global minimum solution, which is unique if \mathbf{R} is full rank.

2.3 Wiener-Hopf Solution

Using the properties of covariance matrix \mathbf{R} mentioned in the previous section, minimising the cost function in (2.7) can be achieved by setting the derivative of ξ_{MSE} with respect to its coefficients to zero.

To optimise a convex function of complex parameters, the cost function has to be differentiated with respect to the unconjugated coefficients, i.e. the complex conjugate of the coefficient vector, to obtain the correct gradient, according to Wirtinger Calculus (Appendix A) equation (A.4), such that

$$\xi_{\text{MSE}}(\mathbf{w}) \stackrel{!}{=} \min \quad \longleftrightarrow \quad \nabla \xi_{\text{MSE}} = \frac{\partial \xi_{\text{MSE}}}{\partial \mathbf{w}^*} \stackrel{!}{=} 0 \quad . \quad (2.12)$$

Hence, to minimise the MSE cost function with respect to the coefficients requires

$$\frac{\partial \xi_{\text{MSE}}}{\partial \mathbf{w}^*} = -\mathbf{p} + \frac{\partial}{\partial \mathbf{w}^*} \mathbf{w}^H \mathbf{R} \mathbf{w} \stackrel{!}{=} 0. \quad (2.13)$$

Transposing the scalar quantity $(\mathbf{w}^H \mathbf{R} \mathbf{w})^T = \mathbf{w}^T \mathbf{R}^T \mathbf{w}^*$, the derivative of the second summand in (2.13) can be solved using the product rule,

$$\frac{\partial}{\partial \mathbf{w}^*} \mathbf{w}^H \mathbf{R} \mathbf{w} = \left(\frac{\partial}{\partial \mathbf{w}^*} \mathbf{w}^H \right) \mathbf{R} \mathbf{w} + \left(\frac{\partial}{\partial \mathbf{w}^*} \mathbf{w}^T \mathbf{R}^T \right) \mathbf{w}^*. \quad (2.14)$$

Therefore, using equations (A.11) and (A.12), (2.12) becomes

$$\frac{\partial \xi_{\text{MSE}}}{\partial \mathbf{w}^*} = -\mathbf{p} + \mathbf{R} \mathbf{w} \stackrel{!}{=} 0. \quad (2.15)$$

If the auto-correlation matrix \mathbf{R} is regular, (2.15) can be solved by inverting \mathbf{R} to give the

optimum vector \mathbf{w}_{opt} which is known as the Wiener-Hopf solution,

$$\mathbf{w}_{\text{opt}} = \mathbf{R}^{-1}\mathbf{p}. \quad (2.16)$$

If the auto-correlation matrix \mathbf{R} is not full rank, the optimum solution in (2.16) cannot be computed, and hence an infinite number of solutions exists. Even if \mathbf{R} is invertible, it can be ill-conditioned such that the inversion is prone to numerical errors. To avoid such problems, we will next explore iterative schemes which are numerically more robust, and also avoid the high computational cost that may be involved in the inversion of a matrix of considerable dimension.

2.4 Least Mean Square Algorithm

2.4.1 Method of Steepest Descent

Adaptive equalisation can be performed by means of several iterative algorithms to find the optimum solution. A popular search technique is the gradient descent algorithm, also known as steepest descent algorithm, which can be formulated as

$$\mathbf{w}_{n+1} = \mathbf{w}_n - \mu \nabla \xi_{\text{MSE}}[n], \quad (2.17)$$

where $\nabla(\cdot)$ is the gradient operator, $\xi_{\text{MSE}}[n]$ is the MSE cost function yielded by the coefficient vector \mathbf{w}_n at time n , and μ is referred to as the step size, loosely defining the length of the step. Assuming \mathbf{w}_n is the current weight vector at time n , a new improved weight vector \mathbf{w}_{n+1} can be achieved using (2.17) by taking a step μ towards the negative gradient of the cost function $\xi_{\text{MSE}}[n]$.

From (2.15), at time n the explicit term for the gradient can be phrased as

$$\nabla \xi_{\text{MSE}}[n] = \frac{\partial \xi_{\text{MSE}}}{\partial \mathbf{w}_n^*} = -\mathbf{p} + \mathbf{R}\mathbf{w}_n \quad . \quad (2.18)$$

Substituting (2.18) into (2.17) leads to an update equation famously known as the steepest descent algorithm [10, 22]. This update equation does not require any further inversion of the auto-correlation matrix \mathbf{R} , however a reliable estimation is needed for both the auto-correlation matrix \mathbf{R} and the cross-correlation vector \mathbf{p} .

2.4.2 Gradient Estimate

To lower the computational complexity and to avoid recursively involving very long data windows to estimate statistical parameters required of \mathbf{R} and \mathbf{p} , the gradient (2.18) is calculated by estimates of the auto-correlation matrix \mathbf{R} and the cross-correlation vector \mathbf{p} based only on the previous samples of $r[n]$ and $s[n]$, which is equivalent to minimising the instantaneous squared error, $e_n e_n^*$ rather than the MSE. Setting

$$\hat{\mathbf{p}} = \mathbf{r}_n s_n^* \quad (2.19)$$

$$\hat{\mathbf{R}} = \mathbf{r}_n \mathbf{r}_n^H, \quad (2.20)$$

and substituting (2.19) and (2.20) into (2.18) gives a gradient estimate

$$\begin{aligned} \hat{\nabla} \xi_n &= -\hat{\mathbf{p}} + \hat{\mathbf{R}}\mathbf{w}_n \\ &= -(\mathbf{r}_n s_n^*) + \mathbf{r}_n \mathbf{r}_n^H \mathbf{w}_n \\ &= -\mathbf{r}_n (s_n^* - \mathbf{r}_n^H \mathbf{w}_n) \\ &= -\mathbf{r}_n e_n^*. \end{aligned} \quad (2.21)$$

LMS Algorithm	
1:	$y[n] = \mathbf{w}_n^H \mathbf{r}_n$
2:	$e[n] = s[n] - y[n]$
3:	$\mathbf{w}_{n+1} = \mathbf{w}_n + \mu \mathbf{r}_n e^*[n]$

Table 2.1: Equations for channel equalisation by LMS adaptive algorithm at symbol rate n .

Substituting (2.21) into (2.17) yields the well known Least Mean Squares (LMS) algorithm [10, 22, 23, 24] as

$$\mathbf{w}_{n+1} = \mathbf{w}_n + \mu \mathbf{r}_n e_n^* . \quad (2.22)$$

Tab. 2.1 illustrates the main equations involved to update the equaliser coefficients by using the LMS adaptive algorithm.

2.4.3 Computational Complexity

The computational complexity of the LMS algorithm as listed in Tab. 2.1 results in

$$C_{\text{LMS}} = 1 + 2L \quad (2.23)$$

multiplications where L is the filter length. Clearly, the LMS algorithm has a low complexity which is in an order of $\mathcal{O}(L)$ compared to Wiener-Hopf equation, which generally required $\mathcal{O}(L^3)$ due to the matrix inversion, or $\mathcal{O}(L^2)$ of the method of steepest descent due to it involving a matrix-vector multiplication.

2.5 Least Squares Algorithm

In contrast to the LMS algorithm where the cost function is estimated by trying to reduce the expectation of the squared error, the least squares (LS) algorithm directly finds the

filter coefficients by minimising a sum of squared errors. In this section, the least squares formulation is introduced first, then a recursive structure of the least squares algorithm leads to the well known recursive least squares (RLS), which is followed by a discussion of the RLS complexity.

2.5.1 Least Squares Formulation

The cost function to be minimised in the least squares algorithm is the sum of squared errors over all previous samples up to current time, n , de-emphasizing each past contribution by an exponential time window,

$$\xi_{\text{LS},n} = \sum_{v=0}^n \beta^v e[n-v]e^*[n-v], \quad (2.24)$$

which is achieved by introducing a forgetting factor β , where $0 < \beta \leq 1$.

Similar to (2.12) the minimisation of this cost function requires

$$\nabla_{\xi_{\text{LS},n}} = \frac{\partial \xi_{\text{LS},n}}{\partial \mathbf{w}^*} \stackrel{!}{=} 0 \quad . \quad (2.25)$$

Similar to the derivations of the Wiener-Hopf solution in Sec. 2.3 [10], the minimisation of (2.25) leads to

$$\mathbf{R}_n \mathbf{w}_n = \mathbf{p}_n \quad (2.26)$$

By introducing the forgetting factor β to \mathbf{R}_n and \mathbf{p}_n we obtain

$$\mathbf{R}_n = \sum_{k=0}^n \beta^k \mathbf{r}[n-k] \mathbf{r}^H[n-k], \quad (2.27)$$

and

$$\mathbf{p}_n = \sum_{l=0}^n \beta^l s^*[n-l] \mathbf{r}[n-l]. \quad (2.28)$$

2.5.2 Recursive Least Squares Algorithm

The recursive least squares (RLS) is an algorithm which recursively finds an updated filter coefficients \mathbf{w}_{n+1} using the current \mathbf{w}_n and the auto-correlation matrix and the cross-correlation vector from previous samples,

$$\mathbf{R}_n = \beta \mathbf{R}_{n-1} + \mathbf{r}_n \mathbf{r}_n^H, \quad (2.29)$$

$$\mathbf{p}_n = \beta \mathbf{p}_{n-1} + s_n^* \mathbf{r}_n. \quad (2.30)$$

After recursively updating \mathbf{R}_{n-1} and \mathbf{p}_{n-1} , (2.25) can be solved for each time index n , which will involve inverting \mathbf{R}_n in (2.29) using the Matrix Inversion Lemma (also known as *Woodbury's identity*) [10, 22]. For a matrix \mathbf{A} ,

$$\mathbf{A} = \mathbf{U} + \mathbf{V} \mathbf{Z} \mathbf{V}^H, \quad (2.31)$$

according to the Matrix Inversion Lemma, the inverse of \mathbf{A} can be expressed as

$$\mathbf{A}^{-1} = \mathbf{U}^{-1} - \mathbf{U}^{-1} \mathbf{V} (\mathbf{Z}^{-1} + \mathbf{V}^H \mathbf{U}^{-1} \mathbf{V})^{-1} \mathbf{V}^H \mathbf{U}^{-1}. \quad (2.32)$$

The Matrix Inversion Lemma can be proven by multiplying \mathbf{A} (2.31) by \mathbf{A}^{-1} (2.32), and recognizing that the result of this product is the identity matrix [22]. With $\mathbf{U} = \beta \mathbf{R}_{n-1}$, $\mathbf{V} = \mathbf{r}_n$, $\mathbf{Z} = \mathbf{I}_1$, $(\mathbf{U} + \mathbf{V} \mathbf{Z} \mathbf{V}^H)$ becomes the right hand side of (2.29). Defining $\Phi_n = \mathbf{R}_n^{-1}$,

the matrix inversion can be performed iteratively using (2.32), giving

$$\Phi_n = \frac{1}{\beta} \left(\Phi_{n-1} - \frac{\Phi_{n-1} \mathbf{r}_n \mathbf{r}_n^H \Phi_{n-1}}{\beta + \mathbf{r}_n^H \Phi_{n-1} \mathbf{r}_n} \right), \quad (2.33)$$

where the initial Φ_0 is usually set to a small identity matrix weighted by a small factor to ensure regularity of the matrix Φ_n for small n . Introducing a gain vector

$$\lambda_n = \frac{\Phi_{n-1} \mathbf{r}_n}{\beta + \mathbf{r}_n^H \Phi_{n-1} \mathbf{r}_n}, \quad (2.34)$$

equation (2.33) can be formulated as

$$\Phi_n = \frac{1}{\beta} (\Phi_{n-1} - \lambda_n \mathbf{r}_n^H \Phi_{n-1}). \quad (2.35)$$

For later convenience, it is advantageous to simplify λ_n such that equation (2.34) becomes

$$\lambda_n \beta + \lambda_n \mathbf{r}_n^H \Phi_{n-1} \mathbf{r}_n = \Phi_{n-1} \mathbf{r}_n, \quad ,$$

and hence

$$\lambda_n = \frac{1}{\beta} (\Phi_{n-1} \mathbf{r}_n - \lambda_n \mathbf{r}_n^H \Phi_{n-1} \mathbf{r}_n) \quad (2.36)$$

$$\begin{aligned} &= \left\{ \frac{1}{\beta} (\Phi_{n-1} - \lambda_n \mathbf{r}_n^H \Phi_{n-1}) \right\} \mathbf{r}_n \\ &= \Phi_n \mathbf{r}_n. \end{aligned} \quad (2.37)$$

RLS Algorithm	
1:	$y[n] = \mathbf{w}_n^H \mathbf{r}_n$
2:	$\alpha[n] = s[n] - \mathbf{w}_{n-1}^H \mathbf{r}_n$
3:	$\mathbf{h} = \mathbf{r}_n^H \Phi_{n-1}$
4:	$k = \beta + \mathbf{h} \mathbf{r}_n$
5:	$\lambda_n = \Phi_{n-1} \mathbf{r}_n / k$
6:	$\mathbf{w}_n = \mathbf{w}_{n-1} + \lambda_n \alpha^*[n]$
7:	$\Phi_n = \frac{1}{\beta} (\Phi_{n-1} - \lambda_n \mathbf{h})$

Table 2.2: Equations for channel equalisation by RLS adaptive algorithm at symbol index n .

The weight vector update equation $\mathbf{w}_n = \Phi_n \mathbf{p}_n$ can be solved by substituting \mathbf{p}_n from (2.30) and then Φ_n from (2.35),

$$\mathbf{w}_n = \beta \Phi_n \mathbf{p}_{n-1} + s_n^* \Phi_n \mathbf{r}_n \quad (2.38)$$

$$= \Phi_{n-1} \mathbf{p}_{n-1} - \lambda_n \mathbf{r}_n^H \Phi_{n-1} \mathbf{p}_{n-1} + s_n^* \Phi_n \mathbf{r}_n \quad (2.39)$$

$$= \mathbf{R}_{n-1}^{-1} \mathbf{p}_{n-1} - \lambda_n \mathbf{r}_n^H \mathbf{R}_{n-1}^{-1} \mathbf{p}_{n-1} + s_n^* \Phi_n \mathbf{r}_n \quad (2.40)$$

$$= \mathbf{w}_{n-1} - \lambda_n \mathbf{r}_n^H \mathbf{w}_{n-1} + s_n^* \lambda_n \quad (2.41)$$

$$= \mathbf{w}_{n-1} + \lambda_n [s_n^* - \mathbf{r}_n^H \mathbf{w}_{n-1}] \quad (2.42)$$

$$= \mathbf{w}_{n-1} + \lambda_n \alpha_n^* \quad , \quad (2.43)$$

where

$$\alpha_n = s_n - \mathbf{r}_n^T \mathbf{w}_{n-1}^* \quad (2.44)$$

$$= s_n - \mathbf{w}_{n-1}^H \mathbf{r}_n \quad (2.45)$$

is the *a priori estimation error* which is a tentative value of e_n (2.6) before updating the weight vector. The complete RLS equations involved in updating the equaliser coefficients are listed in Tab. 2.2.

When analysing the convergence [10], in a stationary environment the forgetting factor β is set to 1 to consider previous samples' knowledge, and the RLS algorithm is affected equally by old and current memory. Overall, the convergence behaviour of the RLS is considered superior to the LMS.

In non-stationary environments, the forgetting factor is set to $\beta < 1$ to ensure the RLS algorithm puts more emphasis on the current data and is not biased by past, out-dated samples. This is a major factor in time varying environments [25] where in some situations the LMS has a performance advantage [26, 27, 28, 29].

2.5.3 Computational Complexity

Compared to the LMS algorithm, the recursive least squares algorithm exhibits fast convergence. However, the RLS comes at a high computational complexity. As listed in Tab. 2.2, the multiplications create a computational cost of order $\mathcal{O}(L^2)$,

$$C_{\text{RLS}} = 3L + 3L^2 . \quad (2.46)$$

Clearly the RLS complexity is higher than the LMS (2.23), therefore efforts have been undertaken to create variations of the RLS algorithm with lower computational cost.

2.6 Affine Projection Algorithm

In this section we consider the affine projection algorithm (APA) which is a popular algorithm within the acoustic echo cancellation schemes [30] and is included here because it links LMS and RLS algorithms [31]. The APA was first proposed by Ozeki and Umeda [32] with the aim to improve the slow convergence of the normalised LMS (NLMS) scheme which is a

variant of the LMS algorithm with a normalised step size with regards to the power of the transmitted signal. A more in-depth analysis of the convergence behaviour of the APA can be found in a number of articles [33, 34, 35]. The main idea behind APA is reusing data by exploiting previous regressor vectors to attain faster adaptation.

2.6.1 APA Formulation

Similar to the NLMS, APA can be seen as a solution to the following optimization problem:

Given the current coefficient vector \mathbf{w}_n , the received vector \mathbf{r}_n , and the current value of the desired signal s_n , calculate the new weight vector \mathbf{w}_{n+1} such that

$$\|\mathbf{w}_{n+1} - \mathbf{w}_n\|_2 \stackrel{!}{=} \min, \quad (2.47)$$

subject to

$$\mathbf{r}^H[n-i]\mathbf{w}_{n+1} \stackrel{!}{=} s^*[n-i], \quad i = 0, 1, \dots, P-1 \quad (2.48)$$

where P is the number of constraints and hence defines the order of the APA algorithm. This means that the new weight vector \mathbf{w}_{n+1} should be best fit to the new data as well as the previous $P-1$ past received signals and their matching desired signals. It is important to note that for the special case of $P=1$ the APA algorithm becomes the NLMS adaptive filter,

$$\begin{aligned} \mathbf{r}_n^H \mathbf{w}_{n+1} &\stackrel{!}{=} s_n^* \\ \mathbf{r}_{n-1}^H \mathbf{w}_{n+1} &\stackrel{!}{=} s_{n-1}^* \\ &\vdots \\ \mathbf{r}_{n-P+1}^H \mathbf{w}_{n+1} &\stackrel{!}{=} s_{n-P+1}^* \end{aligned} \quad (2.49)$$

For convenience of mathematical presentation, we introduce the definitions

$$\mathbf{X}_n^H = [\mathbf{r}_n^H, \mathbf{r}_{n-1}^H, \dots, \mathbf{r}_{n-P+1}^H] \quad (2.50)$$

$$\mathbf{s}_n^* = [s_n^*, s_{n-1}^*, \dots, s_{n-P+1}^*] \quad (2.51)$$

The system of equations (2.49) becomes

$$\mathbf{X}_n^H \mathbf{w}_{n+1} \stackrel{!}{=} \mathbf{s}_n^* \quad (2.52)$$

From equations (2.6) and (2.50) we can define the past error vector \mathbf{e}_n , whose complex conjugate is expressed by

$$\mathbf{e}_n^* = \mathbf{s}_n^* - \mathbf{X}_n^H \mathbf{w}_n \quad (2.53)$$

Using (2.52)

$$\mathbf{e}_n^* \stackrel{!}{=} \mathbf{X}_n^H \mathbf{w}_{n+1} - \mathbf{X}_n^H \mathbf{w}_n, \quad (2.54)$$

hence

$$\mathbf{w}_{n+1} = \mathbf{w}_n + (\mathbf{X}_n^H)^{-1} \mathbf{e}_n^* \quad (2.55)$$

Keeping in mind that the APA demands a minimum change in the weight vector coefficients (2.47), (2.55) can be solved by the pseudo-inverse $(\mathbf{X}_n^H)^\dagger$ of \mathbf{X}_n^H [21]. Either the left or right $(\mathbf{X}_n^H)^\dagger$ has to be used depending on whether (2.54) is underdetermined ($P < L$) or overdetermined ($P \geq L$). Here we only consider situations where ($P < L$), which means the left pseudo-inverse $(\mathbf{X}_n^H)^\dagger = \mathbf{X}_n (\mathbf{X}_n^H \mathbf{X}_n)^{-1}$ should be used to solve (2.55) [32],

$$\mathbf{w}_{n+1} = \mathbf{w}_n + \mathbf{X}_n (\mathbf{X}_n^H \mathbf{X}_n)^{-1} \mathbf{e}_n^*. \quad (2.56)$$

<i>p</i> th order APA Algorithm	
1:	update \mathbf{s}_n and \mathbf{X}_n
2:	$\mathbf{e}_n = \mathbf{s}_n - \mathbf{X}_n^T \mathbf{w}_n^*$
3:	$(\mathbf{X}_n^H)^\dagger = \mathbf{X}_n (\mathbf{X}_n^H \mathbf{X}_n + \eta \mathbf{I})^{-1}$
4:	$\mathbf{w}_{n+1} = \mathbf{w}_n + \mu (\mathbf{X}_n^H)^\dagger \mathbf{e}_n^*$.

Table 2.3: Equations for the filter update by the APA adaptive algorithm.

Introducing a relaxation factor μ into the right summand of (2.56) and a weighted identity matrix to $(\mathbf{X}_n^H)^\dagger$ for regularisation purposes the update equation of the P th order APA is formulated as

$$\mathbf{w}_{n+1} = \mathbf{w}_n + \mu \mathbf{X}_n (\mathbf{X}_n^H \mathbf{X}_n + \eta \mathbf{I})^{-1} \mathbf{e}_n^*. \quad (2.57)$$

Tab. 2.3 summarises the main equations involved to update the equaliser coefficients by using the APA adaptive algorithm.

2.6.2 Geometrical Interpretation

Assuming the hyperplane \mathbf{P}_{n-i+1} defines the solution space of the i th equation of the system of equations (2.49), then successive projections from the current coefficient vector \mathbf{w}_n onto the hyperplanes $\mathbf{P}_{n-p+2}, \mathbf{P}_{n-p+3}, \dots, \mathbf{P}_{n+1}$ will solve (2.52) if the system of equations (2.49) is consistent, i.e. all hyperplanes \mathbf{P}_{n-i+1} cross at least in one point [36], which is similar to requiring \mathbf{X}_n to be a full rank matrix.

2.6.3 Complexity Issues

According to the implementation steps summarised in Tab. 2.3, the computational complexity of the APA is noted as

$$\mathcal{C}_{\text{APA}} = (P^2 + \mathcal{O}(P^3)) + 2PL, \quad (2.58)$$

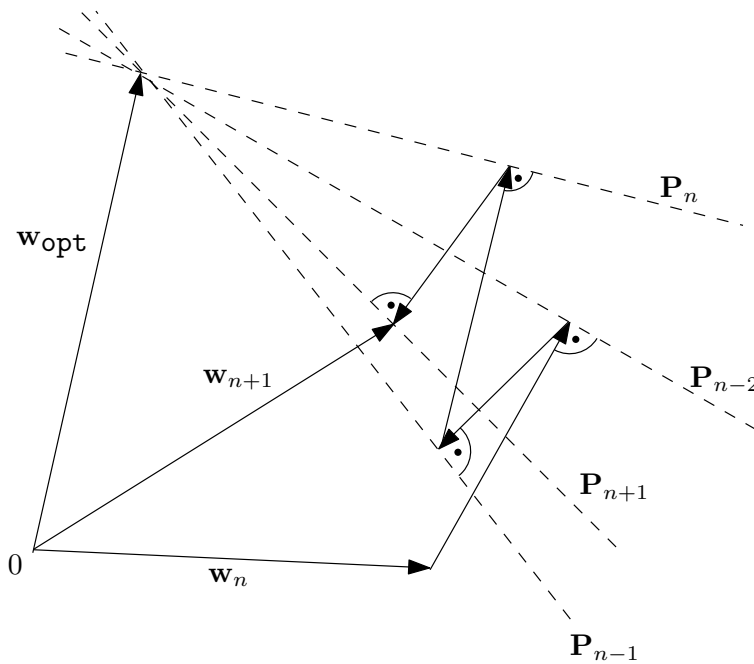


Figure 2.2: Geometrical interpretation of affine projection algorithm

where P is the order of projection. The term $\mathcal{O}(P^3)$ is related to the complexity of calculating the pseudo-inverse in step (3) of Tab. 2.3. Fast implementations of the APA (FAPA) claim to reduce this cost to $\mathcal{C}_{\text{FAPA}} = 2L + 20P$ [37].

2.7 Training versus Blind Equalisation

In most high speed high data rate applications the propagation channel is not known a priori and is very likely time varying, which requires adaptive solutions in the design of a receiver. A classical approach in an adaptive receiver is the transmission of the pre-arranged sequence, so-called training sequence, which is known a priori at the transmitter and receiver. A training sequence is typically a fixed portion of the source sequence which is known in advance at the transmitter and receiver, and therefore contains no information. Hence, training signals take up bandwidth which might be considered too costly for certain applications. In a time-

varying channel, constant training would be required, as any converged solution without tracking would be out-dated soon, therefore the need to operate without explicit training sequences arises. Such an approach is termed blind. Many blind algorithms have been proposed such as second order statistics (SOS), [38, 39], minimum output energy (MOE) [40, 41] and constant modulus (CMA) algorithms which will be discussed in more detail in Sec. 2.9. Next the semi-blind decision directed algorithm is presented.

2.8 Decision Directed Adaptation

In decision-directed (DD) updating, the equaliser output $y[n]$ is passed through a non-linear decision device $q(\cdot)$ which estimates the transmitted source symbol $s[n]$ by nearest neighbour decision. DD is usually used after the convergence of the LMS algorithm when training has ended, or after a successful convergence of a blind equalisation algorithm. Lucky [42] recognised if the decisions are correct “most of the time”, the reference sequence $s[n]$ in the LMS’ error can be replaced with its estimate $q(y[n])$. This blind scheme is thus termed decision directed adaptation. Tab. 2.4 illustrates the main equations involved to update the equaliser coefficients by using this DD approach.

DD has the ability to track slowly varying changes in the channel without explicit need of a training sequence, and converges to the optimal equaliser (2.16) when initialised at an open-eye setting [43]. However, reliability of DD depends on the reliability of the source estimate $q(y[n])$. Typically in blind equalisation scenarios another blind technique which operates from a cold start settings such as CMA is used to reduce the error rate sufficiently before switching to DD.

DD Algorithm	
1:	$y[n] = \mathbf{w}^H \mathbf{r}_n$
2:	$e[n] = q(y[n]) - y[n]$
3:	$\mathbf{w}_{n+1} = \mathbf{w}_n + \mu \mathbf{r}_n e^*[n]$

Table 2.4: Equations for channel equalisation by DD adaptive algorithm at symbol rate n .

2.9 Constant Modulus Algorithm

The constant modulus (CM) criterion was first proposed by Godard in [44] and developed independently by Treichler and Agee in [45]. CMA is a popular blind algorithm for cold start-up of a tapped-delay-line equaliser structure [16]. Godard's original intention was to develop an algorithm for phase and amplitude-modulated signals, for example QAM which decoupled equalisation and carrier recovery, so that carrier phase tracking could be accomplished at the equaliser output in DD mode [44]. Treichler and Agee's original intention was to develop a criterion which sensed multipath induced amplitude modulation (AM) on an otherwise constant envelope frequency modulation (FM) signal [45].

The CM criterion attempts to fit a power of the modulus of the equaliser output to a constant. This constant is chosen to essentially project all constellation points onto a circle of radius γ . Mathematically from [44] this criterion is expressed as

$$\mathcal{E}\{(|y[n]|^p - \gamma_p)^2\} \text{ ,} \quad (2.59)$$

with

$$\gamma_p = \frac{\mathcal{E}\{|s[n]|^{2p}\}}{\mathcal{E}\{|s[n]|^p\}} \text{ ,} \quad (2.60)$$

where γ_p is often called the dispersion constant of the constellation. The case $p = 1$ is usually attributed to Sato [46]. We study solely the case $p = 2$ in the sequel and henceforth CMA refers to the $p = 2$ case. Tab. 2.5 illustrates the main equations involved in updating the

CMA Algorithm	
1:	$y[n] = \mathbf{w}^H \mathbf{r}_n$
2:	$e[n] = (\gamma^2 - y[n]^2)y[n]$
3:	$\mathbf{w}_{n+1} = \mathbf{w}_n + \mu \mathbf{r}_n e^*[n]$

Table 2.5: Equations for channel equalisation by CMA at symbol rate n .

equaliser coefficients $\mathbf{w}[n]$ by using the CMA algorithm.

Godard shows that the value of the dispersion γ_p (2.60) minimises the CM cost function (2.59). The relation between CM and MSE criterion is strong: Treichler and Agee demonstrated that in terms of convergence, minimising the constant modulus performance function is equivalent to minimising the mean square error [45].

Due to the simplicity of the CMA and its independence of system and channel models [47], the CMA has shown robustness to many system and channel impairments, see e.g. [19, 48, 49]. Furthermore, since the CMA uses the absolute value of $y[n]$, the algorithm is insensitive to a phase error, which can be caused by carrier frequency offset or/and unknown channel phase [44]. Hence, carrier frequency offset estimation can be established separately after CMA equalisation.

2.9.1 Convergence Speed of CMA

The basic CMA discussed above as well as many other blind algorithms based on non-convex cost functions, exhibit local minima and slow convergence speed [47, 50]. There have been numerous attempts to improve the typical CMA slow convergence [48, 51, 52]. One can implement a CMA cost function for example with lattice filter equalisers [51], or with an affine projection algorithm (APA) [52] or simply use the recursive least squares (RLS) [48]. It is known that for trained equalisers, these approaches show faster convergence speed than LMS type algorithms [10, 22, 31], however they require higher precision than the LMS

as well as a higher computational complexity per iteration [47]. In order to obtain faster converging algorithms with CMA by using these algorithms, some modifications are needed. The Lattice CMA (LCMA), first proposed in [51] has shown faster convergence than the basic CMA. Similar modification has been adopted for RLS CMA where a simple version of this algorithm is presented in [10]. The APA CMA described in [52] has a simpler structure than the Lattice CMA and RLS CMA and it is known by its capability to escape from local minima as discussed in [52]. Note there are other approaches which aim to speed up the convergence rate of CMA and are not covered here such as the conjugate gradient search CMA [53], the Modified Constant Modulus Algorithm (MCMA) [54], Multi-Modulus Algorithm (MMA) [55], and normalised CMA [56, 57]. Basically, the above approaches try to apply already known fast converging algorithms to CMA, with the resulting convergence speeds usually being faster than that of the CMA. However, the increase in convergence speed is not as great as what may be expected from RLS or Lattice algorithms with training sequences [47]. This is likely because the CM cost function being minimised is not the MSE for which these algorithms are designed.

2.9.2 Ill-Convergence and Initialisation

Unlike MSE, the CM cost function is a non-convex multi-modality function [50, 58]. Yet, in addition to the global minima, other stationary points which includes saddle points, local minima and local maxima have been distinguished on the error surface of the CM cost function [58]. For example, since the CM criterion operates purely on the magnitude of the equaliser output, not the phase, we can easily recognise that any phase rotated versions of a CM-optimal solution are as well solutions themselves. In differentially encoded systems, the encoding scheme can remove some of the phase ambiguity. Other minima and saddles of the CM error surface can arise from the possible choices of system delay, additive noise and

insufficient equaliser length [19]. Note also the existence of a flat point of the cost function surface at the origin. It is shown that the origin is the only maximum of the CMA surface which according to Treichler et al. [45] can be avoided by proper equaliser initialisation; the traditional all zero initial vector should not be used [19]. A proper equaliser initialisation remains an open research issue, with various ideas discussed in the literature [58].

2.10 Concluding Remarks

This chapter has reviewed the general concept of adaptive equalisation in digital communication systems. The Wiener-Hopf solution, which is based on minimising the MSE, has been highlighted. In addition to the Wiener-Hopf solution, a number of popular adaptive algorithms have been reviewed, starting with training based adaptive filters such as the LMS algorithm, the least squares algorithm and the recursive least squares (RLS) algorithm, as well as the affine projection algorithm (APA). Finally, basics and characteristics of some blind algorithms have been discussed, mainly of the constant modulus algorithm (CMA) and the decision directed (DD) update scheme. The next chapter presents a more detailed implementation of the CMA algorithm for multi-user systems, and then discusses combining the CMA with the DD algorithm concurrently, as well as applying the APA to the resulting filter.

Chapter 3

Firmer-CMA and Variations

In this chapter we review a blind multiuser equalisation strategy for downlink DS-CDMA systems, the so-called filtered-R multiple error CM algorithm (FIRMER-CMA). We start by introducing the algorithm's cost function and deriving the corresponding stochastic gradient search in Sec. 3.1. The following Sec. 3.2 presents a concurrent FIRMER-CMA and decision directed algorithm for multiuser equalisation with an analysis and assessment of the convergence behaviour of both FIRMER-CMA and the concurrent algorithm. In Sec. 3.3, an affine projection algorithm is applied to the concurrent scheme to further accelerate the convergence speed. Finally, partially loaded systems are considered in Sec. 3.4, whereby three different algorithms which exploit inactive users' codes are implemented and compared.

3.1 Blind Multiuser FIRMER-CMA Equaliser

Transmission over a dispersive channel destroys the mutual orthogonality of the codes which are used to multiplex the various users in downlink DS-CDMA system. As a result, the received and code-demultiplexed user signals are subject not only to ISI due to channel

dispersion but also to multiple access interference (MAI) due to the loss of code orthogonality. In order to re-establish orthogonality of the codes, a chip level equaliser can be utilised [59, 60]. In fact, by introducing an equaliser in front of the matched code filter, optimum detection with zero ISI and MAI can be achieved in case of perfect equalisation. Furthermore, unlike the uplink (UL) where different users are subject to different dispersive channels, in the downlink (DL) transmission all users signals are synchronous and propagate through the same medium which makes equalisation a simpler task. Various blind equalisation techniques, which can simultaneously suppress MAI and ISI and improve bandwidth efficiency, have been proposed [40, 61, 62]. The constant modulus (CM) algorithm (CMA) based multiuser equaliser is by far the most popular scheme. It has a very simple computational requirement and readily meets the real-time computational constraint. In [61, 62], blind schemes have been performed using the CM criterion, whereby additional orthogonality constraints or mutual decorrelation of the recovered user sequence are required. In response to this scenario, we propose a simple and robust blind multiuser strategy, based on exploiting the CM criterion of all active users of the system, whereby neither explicit constraints nor mutual decorrelation are required. In the following, the main derivations of the proposed algorithm are presented.

In a multi-user communications system where many users share a common channel, interference from various users may distort the detection of a single user. Therefore in the receiver the respective signals require to be separated in a manner such that interference is reduced.

3.1.1 Demultiplexed User Signals

We consider the DS-CDMA downlink system in Fig. 3.1. The blocks p/s and s/p refer to parallel-to-serial and serial-to-parallel procedures, respectively. Here, we are concerned

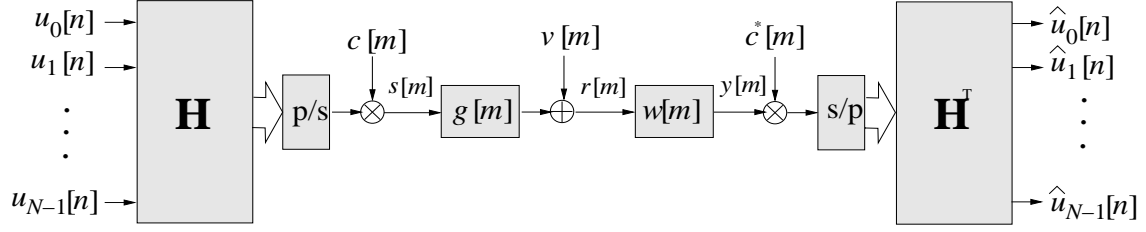


Figure 3.1: Signal model of DS-CDMA downlink with a Firmer-CMA equaliser

about blindly adapting the equaliser coefficients, where the system is fully loaded with $K = N$ multiple synchronous users' signals, which for simplicity are assumed to have the same rate. First we derive the detected signal $\hat{u}_l[n]$ as a function of the chip rate equaliser \mathbf{w} . Then, we state a suitable cost function based on which the equaliser can be adapted.

The sequence for decoding the l th user, contained in a vector \mathbf{h}_l , can be taken from an $N \times N$ Hadamard matrix \mathbf{H} . Therefore, the l th user is decoded as

$$\begin{aligned} \hat{u}_l[n] &= \mathbf{h}_l^T \cdot \begin{bmatrix} c^*[nN] & \mathbf{0} \\ c^*[nN-1] & \\ & \ddots \\ \mathbf{0} & c^*[nN-N+1] \end{bmatrix} \cdot \begin{bmatrix} y[nN] \\ y[nN-1] \\ \vdots \\ y[nN-N+1] \end{bmatrix} \\ &= \tilde{\mathbf{h}}_l^T[nN] \cdot \begin{bmatrix} \mathbf{w}^H & \mathbf{0} \\ & \mathbf{w}^H \\ & \ddots \\ \mathbf{0} & \mathbf{w}^H \end{bmatrix} \cdot \begin{bmatrix} r[nN] \\ r[nN-1] \\ \vdots \\ r[nN-L-N+2] \end{bmatrix}, \end{aligned} \quad (3.1)$$

where the descrambling code $c^*[m]$ has been absorbed into a modified and now time-varying code vector $\tilde{\mathbf{h}}_l[nN]$, and $\mathbf{w} \in \mathbb{C}^L$ contains the equaliser's L chip-spaced complex conjugate weights. Rearranging \mathbf{w} and $\tilde{\mathbf{h}}_l[nN]$ yields

$$\begin{aligned}
\hat{u}_l[n] &= \mathbf{w}^H \begin{bmatrix} \tilde{\mathbf{h}}_l^T[nN] & \mathbf{0} \\ & \tilde{\mathbf{h}}_l^T[nN] \\ & & \ddots \\ \mathbf{0} & & & \tilde{\mathbf{h}}_l^T[nN] \end{bmatrix} \begin{bmatrix} r[nN] \\ r[nN-1] \\ \vdots \\ r[nN-L-N+2] \end{bmatrix} \\
&= \mathbf{w}^H \mathbf{H}_l[nN] \mathbf{r}_{nN} ,
\end{aligned} \tag{3.2}$$

with $\mathbf{H}_l[nN] \in \mathbb{Z}^{L \times (L+N-1)}$ being a convolutional matrix comprising the l th user's modified code vector $\tilde{h}^T[n]$, and $\mathbf{r}_{nN} \in \mathbb{C}^{N+L-1}$ is the received signal. Note that $\mathbf{H}_l[nN]$ only addresses the decoding of the l th user signal.

3.1.2 Cost Function

Since the modulation scheme used for downlink UMTS-TDD is mainly quadrature phase shift keying (QPSK) and in some exceptions 8PSK [63], the user signals $u_l[n]$ consist of symbols with a constant modulus γ . By forcing all received user symbols $\hat{u}_l[n]$ onto γ , a blind cost function ξ_{CM} can be proposed to adapt the weights \mathbf{w} . Therefore, a suitable cost function ξ_{CM} can be formulated as

$$\xi_{\text{CM}} = \mathcal{E} \left\{ \sum_{l=0}^{N-1} (\gamma^2 - |\hat{u}_l[n]|^2)^2 \right\} \tag{3.3}$$

which penalises the deviation of each of the N users' decoded symbols from the desired modulus. The optimum equaliser coefficient vector $\mathbf{w}_{\text{CM,opt}}$ is obtained from

$$\mathbf{w}_{\text{CM,opt}} = \arg \min_{\mathbf{w}} \xi_{\text{CM}} . \tag{3.4}$$

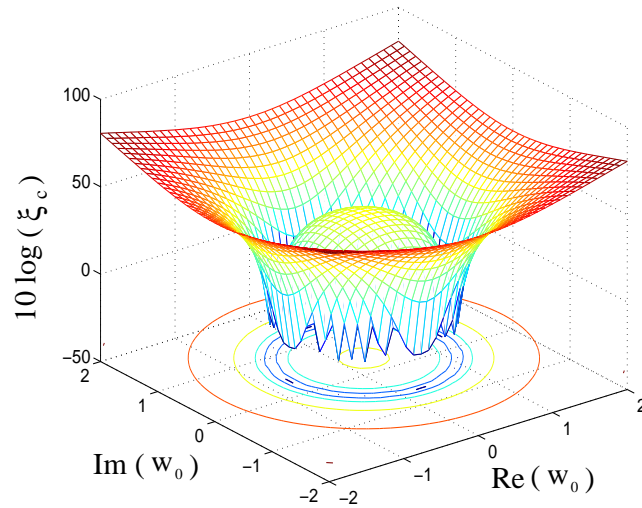


Figure 3.2: Cost function ξ_c in dependency of a single complex valued coefficient w_0 .

There is no unique solution to (3.4), since minimising (3.3) is ambiguous with a manifold of solutions due to an indeterminism in phase rotation. However, any member of this manifold is a suitable solution for the equaliser \mathbf{w} , and can be used in combination with a differential modulation scheme to recover $u_l[n]$.

Example. The cost function ξ_{CM} is plotted in Fig. 3.2 in dependency of an equaliser with a single complex coefficient w_0 . The system adopted here is a fully loaded UMTS TDD system with $N = 16$ users transmitting their signals over an ideal AWGN channel with 30 dB SNR. The modulation scheme employed here is QPSK with $\gamma = 1$. Fig. 3.2 shows that ξ_{CM} exhibits a manifold of optimum solutions satisfying $|w_0| = \gamma$. Also, note the flat point at $w_0 = 0$ which forbids this coordinate as an initialisation point.

3.1.3 Blind Adaptation

A simple stochastic gradient descent update rule for $\mathbf{w}[m]$ can be found by calculating the gradient of an instantaneous cost function, i.e. omitting the expectation operator in (3.3)

$$\hat{\xi}_{\text{CM}} = \sum_{l=0}^{N-1} (\gamma^2 - |\hat{u}_l[n]|^2)^2 . \quad (3.5)$$

The resulting terms are then minimised with regard to \mathbf{w} to obtain instantaneous estimates of the cost function gradient $\nabla \hat{\xi}(\mathbf{w}_n)$, leading to the stochastic gradient update

$$\mathbf{w}_{n+1} = \mathbf{w}_n - \mu \nabla \hat{\xi}_{\text{CM}}(\mathbf{w}_n) \quad (3.6)$$

where μ is the step size. The introduction of gradient noise through inaccurate estimates of the true underlying statistics into the update routine can assist in avoiding the adaptation to remain in flat points of the cost function. However, we will later see that this does not apply to $\mathbf{w} = \mathbf{0}$.

To determine $\nabla \hat{\xi}_{\text{CM}}$, we apply complex vector calculus [64] to (3.6), yielding

$$\begin{aligned} \frac{\partial \hat{\xi}_{\text{CM}}}{\partial \mathbf{w}^*} &= -2 \sum_{l=0}^{N-1} \left[(\gamma^2 - |\hat{u}_l[n]|^2) \frac{\partial}{\partial \mathbf{w}^*} \hat{u}_l[n] \hat{u}_l^{\text{H}}[n] \right] \\ &= -2 \sum_{l=0}^{N-1} [(\gamma^2 - |\hat{u}_l[n]|^2) \mathbf{H}_l[nN] \mathbf{r}_{nN} \cdot \mathbf{r}_{nN}^{\text{H}} \mathbf{H}_l^{\text{H}}[nN] \mathbf{w}] \\ &= -2 \sum_{l=0}^{N-1} (\gamma^2 - |\hat{u}_l[n]|^2) \mathbf{H}_l[nN] \mathbf{r}_{nN} \hat{u}_l^*[n]. \end{aligned} \quad (3.7)$$

This algorithm differs from the standard CM algorithm [50] in the inclusion of a code filtered term $\mathbf{H}_l[nN] \mathbf{r}_{nN}$ rather than just the equaliser input tap delay line vector \mathbf{r}_{nN} . This is structurally similar to a multiple-error filtered-X LMS algorithm [65], where the transfer functions appearing in the paths between the adaptive filter output and the error formations have to be accounted for by modifying the LMS updating scheme. Hence, the proposed scheme in (3.7) is referred to as filtered-R multiple error CM algorithm (FIRMER-CMA).

FIRMER-CMA Algorithm	
1:	$\mathbf{x}_l[nN] = \mathbf{H}_l \mathbf{r}_{nN}$, for $l = 0(1)N - 1$
2:	$\hat{u}_l[n] = \mathbf{w}_n^H \mathbf{x}_l[nN]$, for $l = 0(1)N - 1$
3:	$e_l[n] = (\gamma^2 - \hat{u}_l[n] ^2) \hat{u}_l[n]$, for $l = 0(1)N - 1$
4:	$\mathbf{w}_{n+1} = \mathbf{w}_n + \mu \sum_{l=0}^{N-1} \mathbf{x}_l[nN] e_l^*[n]$

Table 3.1: Equations for multiuser channel equalisation by FIRMER-CMA adaptive algorithm at symbol index n .

Tab. 3.1 illustrates the main equations involved to update the equaliser coefficients $\mathbf{w}[m]$ by using the resulting FIRMER-CMA algorithm. Regarding the earlier comment to avoid initialisation with $\mathbf{w} = 0$, this would lead to a zero output from step 2 of the algorithm in Tab. 3.1, and subsequently null the error and innovations in steps 3 and 4, leading to the CMA algorithm remaining trapped at $\mathbf{w} = 0$.

3.2 Concurrent FIRMER-CMA and Decision Directed Updating

The previously proposed blind multiuser FIRMER-CMA equaliser improves system bandwidth efficiency by avoiding the use of a training sequence and can readily meet the real-time computational constraint. However, since the latter algorithm is a CMA based equaliser, slow convergence and the moderate levels of steady-state MSE are the main drawbacks of such a scheme, which may limit its implementation in practical wireless communication systems. Therefore, this section introduces some fast and robust blind multiuser equalisation alternatives. In order to increase the convergence speed of the FIRMER-CMA a concurrent FIRMER-CMA and decision directed (DD) algorithm capable of achieving a low steady-state MSE is derived.

Since FIRMER-CMA is based on the CM criterion, it is prone to achieve only moder-

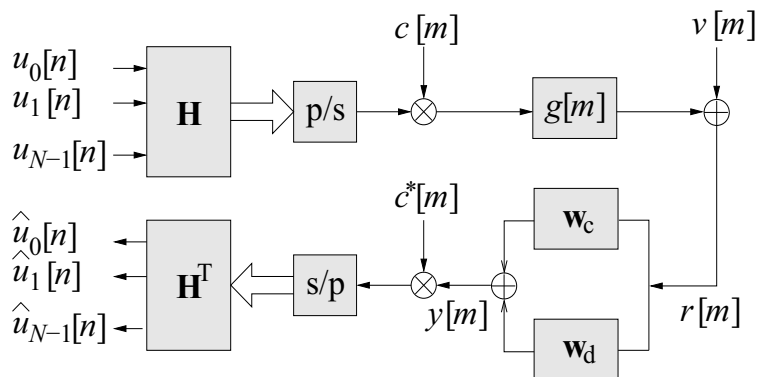


Figure 3.3: Signal model with a concurrent equaliser

ate levels of steady-state mean square error (MSE) performance after convergence, which may not be sufficiently low for the system to attain adequate bit error ratio (BER) performance. A possible solution to the latter problem is to switch to a decision-directed (DD) mode in order to minimise the residual CMA steady state MSE [43]. In order to avoid error propagation due to incorrect decisions, the CMA residual MSE should be sufficiently low. In practice such a low level of MSE may not always be achievable by the CMA [20, 66]. Consequently, a promising solution, suitable for single user transmission, has been proposed in [66], whereby a DD equaliser is concurrently operating with a CMA rather than switching to a DD adaptation after the CMA has converged. This concurrent CMA+DD equaliser is reported to achieve a significant enhancement in equalisation performance over the CMA [66].

Based on [66], a concurrent FIRMER-CMA+DD algorithm which is suitable for synchronous DS-CDMA systems is derived. Adaptation is performed by concurrently minimising two cost functions based on either a CM criterion or a DD scheme for all active users.

3.2.1 Concurrent Cost Function

We consider the downlink DS-CDMA system with an equaliser \mathbf{w} which consists of a CMA part \mathbf{w}_c and a DD branch \mathbf{w}_d operated in parallel, such that $\mathbf{w} = \mathbf{w}_c + \mathbf{w}_d$, as depicted in Fig. 3.3. The weights \mathbf{w}_c and \mathbf{w}_d are updated by minimising the two cost functions ξ_c and ξ_d respectively which are given by

$$\xi_c = \mathcal{E} \left\{ \sum_{l=0}^{N-1} (\gamma^2 - |\hat{u}_l[n]|^2)^2 \right\}, \quad (3.8)$$

$$\xi_d = \mathcal{E} \left\{ \sum_{l=0}^{N-1} (|q(\hat{u}_l[n]) - \hat{u}_l[n]|^2) \right\}, \quad (3.9)$$

with $q(\cdot)$ mapping its input onto the closest constellation point. The optimum vectors $\mathbf{w}_{c,\text{opt}}$ and $\mathbf{w}_{d,\text{opt}}$ are therefore obtained from

$$\mathbf{w}_{c,\text{opt}} = \arg \min_{\mathbf{w}_c} \xi_c, \quad (3.10)$$

$$\mathbf{w}_{d,\text{opt}} = \arg \min_{\mathbf{w}_d} \xi_d. \quad (3.11)$$

There are no unique solutions to either equations (3.10) or (3.11), since both (3.8) and (3.9) are closely coupled. The phase indeterminism of (3.8) is somewhat reduced by (3.9) to possible phase rotation, by $\frac{\pi}{2}$, π and $\frac{3\pi}{2}$. Therefore, by operating DD and CMA concurrently the phase ambiguity found in FIRMER-CMA case can be mitigated to some degree by locking the solution onto the prescribed constellation pattern.

Example. In this example the two cost functions ξ_c and ξ_d are plotted in Figs. 3.4 and 3.5 respectively, in dependency of an equaliser \mathbf{w} with a single complex coefficient w_0 . The

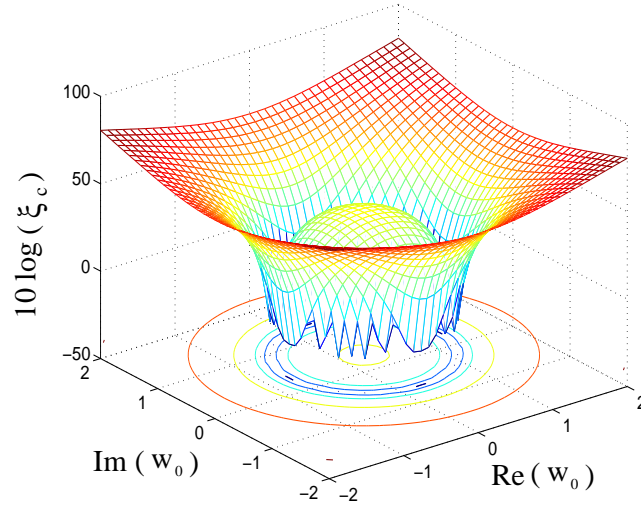


Figure 3.4: Cost function ξ_c in dependency of a single complex valued coefficient w_0 .

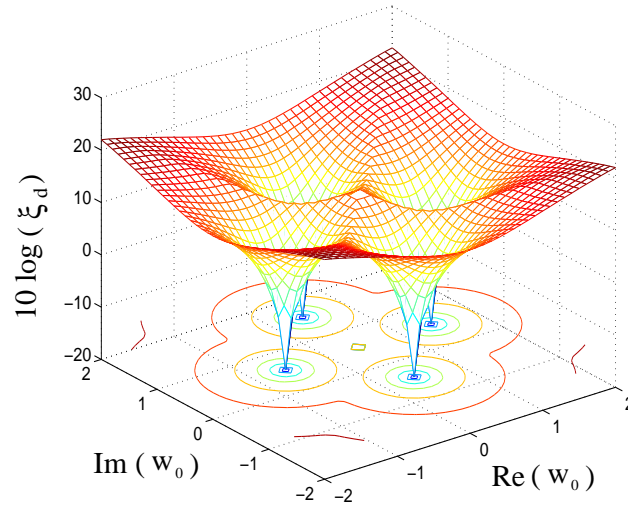


Figure 3.5: Cost function ξ_d in dependency of a single complex valued coefficient w_0 .

system adopted here is a fully loaded DS-CDMA system with $N = 16$ users transmitting their signals over a distortionless and delayless channel with an SNR of 30 dB. The modulation scheme employed here is QPSK with $\gamma = 1$. Fig. 3.4 shows that ξ_c exhibits a manifold of optimum solutions satisfying $|w_0| = \gamma$. Yet, only four solutions can be seen in ξ_d due to the four possible QPSK decisions, Fig. 3.5.

3.2.2 Concurrent Adaptation

In the following, we derive the concurrent FIRMER-CMA+DD algorithm which updates the multiuser equaliser vector \mathbf{w} , similarly to the single-user concurrent CMA+DD described in [66]. The main idea is to update the CMA part \mathbf{w}_c , which is followed by a DD adaptation step only if the previous CMA adaptation step is deemed successful. The proposed algorithm, which is updated at the symbol rate with symbol time index n , can be described by the following steps:

1. The decoded signals $\hat{u}_l[n]$ are calculated for all users according to

$$\hat{u}_l[n] = \mathbf{w}_c^H[n] \mathbf{x}_l[n] + \mathbf{w}_d^H[n] \mathbf{x}_l[n], \text{ for } l = 0(1)N - 1. \quad (3.12)$$

whereby $\mathbf{x}_l[n]$ represents a vector of filtered received signal samples,

$$\mathbf{x}_l[n] = \mathbf{H}_l[nN] \mathbf{r}_{nN}. \quad (3.13)$$

2. The CMA part w_c is adapted according to the rule

$$\mathbf{w}_c[n+1] = \mathbf{w}_c[n] + \mu_c \sum_{l=0}^{N-1} e_{l,c}^* \mathbf{x}_l[n] \quad (3.14)$$

where $e_{l,c} = \hat{u}_l[n](\gamma^2 - |\hat{u}_l[n]|^2)$ and μ_c is the CMA step size. This stochastic gradient adaptation is identical to the FIRMER-CMA and it is based on optimising an instantaneous cost function derived from (3.8) by dropping the expectation operator.

3. Intermediate signals $\tilde{u}_l[n], l = 0(1)N - 1$, are evaluated by exploiting the previously

calculated $\mathbf{w}_c[n + 1]$ such that

$$\tilde{u}[n] = \mathbf{w}_c^H[n + 1]\mathbf{x}_l[n] + \mathbf{w}_d^H[n]\mathbf{x}_l[n]. \quad (3.15)$$

4. Finally, the DD part of the algorithm adjusts \mathbf{w}_d as

$$\mathbf{w}_d[n + 1] = \mathbf{w}_d[n] + \mu_d \sum_{l=0}^{N-1} \delta(q(\tilde{u}_l[n]) - q(\hat{u}_l[n]))e_{l,d}^*\mathbf{x}_l[n], \quad (3.16)$$

where $e_{l,d} = q(\hat{u}_l[n]) - \hat{u}_l[n]$, and μ_d is the DD step size. The indicator $\delta(\cdot)$ is defined as

$$\delta(\alpha) = \begin{cases} 1 & \text{if } \alpha = 0 \\ 0 & \text{if } \alpha \neq 0, \end{cases} \quad (3.17)$$

and therefore disables the DD adaptation step for a specific user if the CMA adaptation step leads to altering the decision.

The convergence of this concurrent scheme is governed by the step sizes in the algorithm. In practice, the DD step size μ_d can often be chosen much larger than the CMA step size μ_c . However, choosing too large a value can cause serious error propagation due to incorrect decisions. Tab. 3.2 summarises the main equations of the proposed concurrent FIRMER-CMA+DD. The potential drawback of DD adaptation is that if the hard decision is incorrect, error propagation occurs which subsequently degrades the equaliser performance. It has been shown that if the equaliser hard decisions before and after the CMA adaptation are the same then the decision is likely to be correct [20]. For this reason, \mathbf{w}_d is only updated in the latter case, similar to [66]. Hence, by employing the concurrent FIRMER-CMA+DD, a considerably enhanced convergence speed and a lower steady state MSE can be achieved compared to the standard FIRMER-CMA.

Concurrent FIRMER-CMA+DD algorithm		
1:	update $\mathbf{x}_l[n] = \mathbf{H}_l[nN]\mathbf{r}_{nN}$,	for $l = 0(1)N - 1$
2:	$\hat{u}_l[n] = \mathbf{w}^H[n]\mathbf{x}_l[n]$,	for $l = 0(1)N - 1$
3:	$e_{l,c} = \hat{u}_l[n](\gamma^2 - \hat{u}_l[n] ^2)$,	for $l = 0(1)N - 1$
4:	$\mathbf{w}_c[n+1] = \mathbf{w}_c[n] + \mu_c \sum_{l=0}^{N-1} e_{l,c}^* \mathbf{x}_l[n]$	
5:	$\tilde{u}_l[n] = \mathbf{w}_c^H[n+1]\mathbf{x}_l[n] + w_d^H[n]\mathbf{x}_l[n]$	
6:	$e_{l,d} = (q(\tilde{u}_l[n]) - \hat{u}_l[n])$,	for $l = 0(1)N - 1$
7:	$\mathbf{w}_d[n+1] = \mathbf{w}_d[n] + \mu_d \sum_{l=0}^{N-1} \delta(q(\tilde{u}_l[n]) - q(\hat{u}_l[n]))e_{l,d}^* \mathbf{x}_l[n]$	
8:	$\mathbf{w}[n+1] = \mathbf{w}_c[n+1] + \mathbf{w}_d[n+1]$	

Table 3.2: Concurrent FIRMER-CMA+DD algorithm.

3.2.3 Simulation Results

For the simulations below, we consider a fully loaded synchronous DS-CDMA system, where the modulation scheme adopted is QPSK. We apply the FIRMER-CMA+DD to two different channel impulse responses, a short $g_1[m]$ and a more dispersive $g_2[m]$, as characterised by their chip rate transfer functions

$$G_1(z) = 0.89 + (0.36 - 0.27j)z^{-1} + 0.09z^{-3} , \quad (3.18)$$

$$G_2(z) = 0.67 + (0.54 - 0.27j)z^{-4} + (0.41 - 0.07j)z^{-7} - 0.20jz^{-11} . \quad (3.19)$$

In the following, we first demonstrate the convergence behaviour and the steady state MSE over noise-free channels, and thereafter characterise the evolution of the received constellation in a noisy environment.

Experiment 1: In order to demonstrate the convergence behaviour of the proposed algorithm, we transmit $N = 16$ QPSK user signals over $g_1[m]$ in the absence of channel noise. The length of the equaliser is $L = 10$, and the relaxation factors are chosen to be $\mu_c = 10^{-4}$ and $\mu_d = 10^{-2}$. After multiple simulations, these step sizes are the largest values

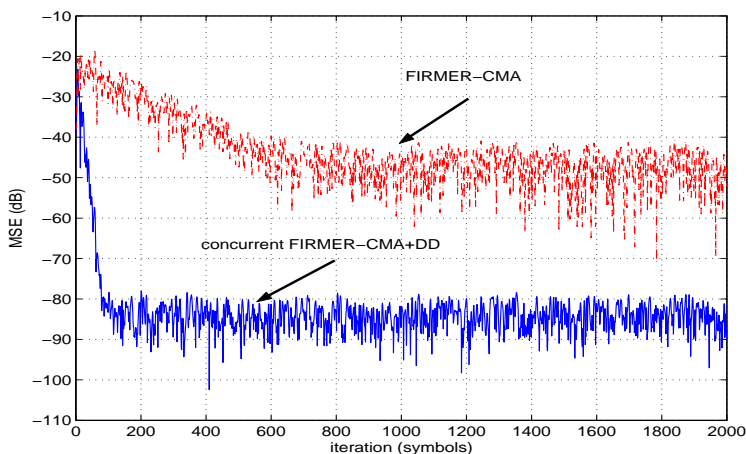


Figure 3.6: Comparison of convergence speed and steady state MSE between the concurrent FIRMER-CMA+DD algorithm and the standard FIRMER-CMA.

for which all simulations provided fast stable convergence. The adaptation is initialised with both first coefficients in the weight vectors \mathbf{w}_c and \mathbf{w}_d set to $1/2$ and zeroing all remaining taps. The MSE performances of the proposed concurrent FIRMER-CMA+DD and the standard FIRMER-CMA algorithms are shown in Fig. 3.6. Evidently a faster convergence and lower steady state can be achieved by the proposed concurrent algorithm compared to an adaptation based on FIRMER-CMA.

Experiment 2: For $N = 16$ QPSK users, we have adapted the concurrent FIRMER-CMA under $\text{SNR} = 10\text{dB}$ over the dispersive channel $g_2[m]$. The length of the equaliser is $L = 64$, and the relaxation factors are chosen to be $\mu_c = 10^{-6}$ and $\mu_d = 10^{-4}$. Again the selected step sizes are the largest values for which all simulations provided fast stable convergence. Fig. 3.7 depicts the decoded signal constellations of user $l = 0$ after adaptation of 5×10^3 symbols with (a) no equalisation performed (b) a standard FIRMER-CMA equaliser, and (c) the concurrent FIRMER-CMA+DD. The results clearly show that the concurrent algorithm overcomes the phase ambiguity encountered in the CMA scheme by locking onto the constellation pattern prescribed by $q(\cdot)$.

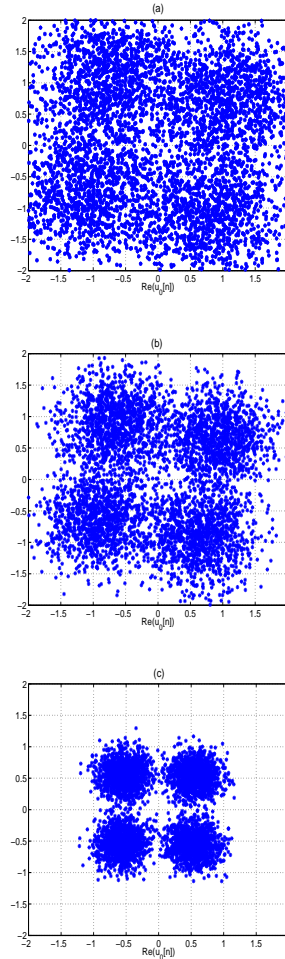


Figure 3.7: The decoded signal constellations of user $l = 0$ after adaptation of 5×10^3 symbols with (a) no equalisation (b) standard FIRMER-CMA equaliser and (c) concurrent FIRMER-CMA+DD.

3.3 Concurrent FIRMER-CMA+DD with Affine Projection

In the previous section, the FIRMER-CMA+DD algorithm has provided a significant performance enhancement in terms of steady-state MSE and convergence speed over the standard FIRMER-CMA. The latter improvement is mainly due to the contribution of the DD branch operating concurrently with CMA. However, the DD part is only updated if this step

is considered secure. Therefore, the adaptation is generally governed by CMA rather than DD especially in initially closed-eye systems. Thus, a slow convergence may still persist in the proposed algorithm's performance. A possible solution to this problem is to accelerate FIRMER-CMA+DD by adopting the concept of the affine projection algorithm (APA) scheme presented in Sec. 2.6. In this section, we derive a combined AP-FIRMER-CMA+DD structure in order to gain benefits from both FIRMER-CMA+DD and APA algorithms.

The APA was first proposed by Ozeki and Umeda [32]. Initially, it was developed to improve the perceived slow convergence of the NLMS scheme. A more in-depth analysis of the convergence behaviour of the APA can be found in a number of articles [33, 34, 35]. The main idea behind APA is reusing data by exploiting previously received signal vectors to perform a faster adaptation.

3.3.1 Modified Cost Function

The CM term in (3.8) can be further reformulated as [52]

$$\mathcal{E} \left\{ \sum_{l=0}^{K-1} |d_{l,c}[n] - \hat{u}_l[n]|^2 \right\} \quad (3.20)$$

$$\text{with} \quad d_{l,c}[n] = \gamma \frac{\hat{u}_l[n]}{|\hat{u}_l[n]|}. \quad (3.21)$$

This alternative CM philosophy suggests to enforce the detected symbol $\hat{u}_l[n]$ to its nearest symbol $d_{l,c}[n]$ from the circle which has the radius γ and the centre at the origin, as illustrated in Fig. 3.8. The new form has a structure similar to an MMSE criterion, whereby the only difference lies in the value of the desired symbol $d_{l,c}[n]$. Defining the DD decision function as

$$d_{l,d}[n] = q(\hat{u}_l[n]), \quad (3.22)$$

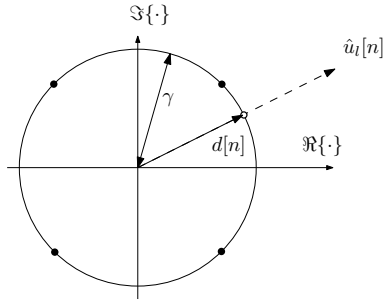


Figure 3.8: Configuration of the desired response for the CM criterion, assuming a QPSK constellation.

both ξ_c and ξ_d can be written as

$$\xi_m = \mathcal{E} \left\{ \sum_{l=0}^{N-1} |d_{l,m}[n] - \hat{u}_l[n]|^2 \right\}, \quad (3.23)$$

with $m \in \{c, d\}$ indicating the operational mode as either CM or DD.

Next, we are concerned with minimising both ξ_c and ξ_d concurrently based on the affine projection scheme.

3.3.2 Formulation

The following steps present how the AP-FIRMER-CMA+DD is formulated.

1. We split (3.2) for the l th user's decoded symbol $\hat{u}_l[n]$ into a scalar product between the weight vector and an input vector,

$$\hat{u}_l[n] = \mathbf{w}^H \mathbf{x}_l[n], \quad (3.24)$$

whereby $\mathbf{x}_l[n]$ represents a vector of filtered received signal samples,

$$\mathbf{x}_l[n] = \mathbf{H}_l[nN] \mathbf{r}_{nN}. \quad (3.25)$$

2. We retain a record of the past P input vectors $\mathbf{x}_l[n-p]$, and $d_{l,c}[n-p]$ and $d_{l,d}[n-p]$ which are the the corresponding desired signal values for the CMA and DD parts respectively, such that $p = 0 \cdots (P-1)$,

$$\mathbf{X}_l[n] = [\mathbf{x}_l[n] \quad \mathbf{x}_l[n-1] \quad \cdots \quad \mathbf{x}_l[n-P+1]], \quad (3.26)$$

$$\mathbf{d}_{l,c}[n] = [d_{l,c}[n] \quad d_{l,c}[n-1] \quad \cdots \quad d_{l,c}[n-P+1]]^T, \quad (3.27)$$

$$\mathbf{d}_{l,d}[n] = [d_{l,d}[n] \quad d_{l,d}[n-1] \quad \cdots \quad d_{l,d}[n-P+1]]^T. \quad (3.28)$$

3. We define the error vector according to the CMA part $\mathbf{e}_{l,c}[n]$ at time instance n ,

$$\mathbf{e}_{l,c}^*[n] = \mathbf{d}_{l,c}^*[n] - \mathbf{X}_l^H[n] \mathbf{w}[n], \quad l = 0(1)N-1, \quad (3.29)$$

Based on this error vector, we want to perform a CMA weight update such that

$$\mathbf{X}_l[n]^H \mathbf{w}_c[n+1] = \mathbf{d}_{l,c}^*[n], \quad l = 0(1)N-1. \quad (3.30)$$

4. Inserting (3.29) in (3.30), we can update the CMA part of the equaliser weights

$$\mathbf{w}_c[n+1] = \mathbf{w}_c[n] + \mathbf{X}_l^\dagger[n] \mathbf{e}_{l,c}^*[n], \quad (3.31)$$

where $\mathbf{X}_l^\dagger[n]$ is the pseudo-inverse of the data matrix $\mathbf{X}_l[n]$

$$\mathbf{X}_l^\dagger[n] = \mathbf{X}_l[n] (\mathbf{X}_l[n]^H \mathbf{X}_l[n] + \alpha \mathbf{I})^{-1}, \quad (3.32)$$

where α is a small number used for weighting the identity matrix \mathbf{I} . Adding a relaxation factor μ_c to the update and taking the contributions of all N users into account, (3.31)

becomes

$$\mathbf{w}_c[n+1] = \mathbf{w}_c[n] + \mu_c \sum_{l=0}^{N-1} \mathbf{X}_l^\dagger[n] \mathbf{e}_{l,c}^*[n]. \quad (3.33)$$

5. We calculate the l th user's intermediate symbol $\tilde{u}_l[n]$ where only the CMA part is updated

$$\tilde{u}_l[n] = \mathbf{X}_l^T[n] \mathbf{w}_c^*[n+1] + \mathbf{X}_l^T[n] \mathbf{w}_d^*[n]. \quad (3.34)$$

6. Making the decision of updating the DD part

$$\Lambda_l[n] = \text{diag}(\delta\{\mathbf{q}(\tilde{\mathbf{u}}_l[n]) - \mathbf{q}(\mathbf{w}^H \mathbf{X}_l[n])\}). \quad (3.35)$$

The indicator $\delta(\cdot)$ is a vectorial decision function that compares the l th intermediate symbol $\tilde{u}_l[n]$ with l th user's decoded symbol $\hat{u}_l[n]$, where $\delta(\cdot)$ behaves similarly to (3.17).

7. Similar to (3.33) we update the DD part of the equaliser weights

$$\mathbf{w}_d[n+1] = \mathbf{w}_d[n] + \mu_d \sum_{l=0}^{N-1} \Lambda_l[n] \mathbf{X}_l^\dagger[n] \mathbf{e}_{l,d}^*[n], \quad (3.36)$$

where $\mathbf{e}_{l,d}^*[n] = \mathbf{d}_{l,d}^*[n] - \mathbf{X}_l^T[n] \mathbf{w}[n]$ for $l = 0(1)N-1$, and μ_d is a relaxation factor. Therefore, $\Lambda_l[n]$ disables the DD adaptation step for a specific user if the CMA adaptation step leads to an alteration in the decision (3.35).

8. The final equaliser coefficients are updated through combination of the CM and DD weights according to

$$\mathbf{w}[n+1] = \mathbf{w}_c[n+1] + \mathbf{w}_d[n+1]. \quad (3.37)$$

9. Increment n and to return to step 1.

<i>p</i> th order concurrent affine projection algorithm	
1:	update, $\mathbf{X}_l[n]$, $\mathbf{d}_{l,c}[n]$ and $\mathbf{d}_{l,d}[n]$ for $l = 0(1)N - 1$
2:	$\mathbf{X}_l^\dagger[n] = \mathbf{X}_l[n](\mathbf{X}_l[n]^H \mathbf{X}_l[n] + \alpha \mathbf{I})^{-1}$
3:	$\mathbf{e}_{l,c}[n] = \mathbf{d}_{l,c}[n] - \mathbf{X}_l^T[n] \mathbf{w}^*[n]$
4:	$\mathbf{w}_c[n+1] = \mathbf{w}_c[n] + \mu_c \sum_{l=0}^{N-1} \mathbf{X}_l^\dagger[n] \mathbf{e}_{l,c}^*[n]$
5:	$\tilde{\mathbf{u}}_l[n] = \mathbf{X}_l^T[n] \mathbf{w}_c^*[n+1] + \mathbf{X}_l^T[n] \mathbf{w}_d^*[n]$
6:	$\Lambda_l[n] = \text{diag}(\delta\{\mathbf{q}(\tilde{\mathbf{u}}_l[n]) - \mathbf{w}^H \mathbf{X}_l[n]\})$
7:	$\mathbf{e}_{l,d}[n] = \mathbf{d}_{l,d}[n] - \mathbf{X}_l^T[n] \mathbf{w}^*[n]$
8:	$\mathbf{w}_d[n+1] = \mathbf{w}_d[n] + \mu_d \sum_{l=0}^{N-1} \Lambda_l[n] \mathbf{X}_l^\dagger[n] \mathbf{e}_{l,d}^*[n]$
9:	$\mathbf{w}[n+1] = \mathbf{w}_c[n+1] + \mathbf{w}_d[n+1]$

Table 3.3: Concurrent affine projection algorithm (AP-FIRMER-CMA+DD) for pilot-assisted multiuser equalisation.

Similar to the convergence of the concurrent scheme, AP-FIRMER-CMA+DD is governed by the step sizes μ_c and μ_d . In practice, the DD step size μ_d can often be chosen much larger than the CMA step size μ_c . However, choosing too large values can cause serious error propagation due to incorrect decisions [66].

The potential drawback of DD adaptation is the probability of error propagation occurring in case of a wrong hard decision, which subsequently degrades the performance. It has been shown that if the equaliser's hard decision before and after the CM adaptation are the same then the decision is likely to be correct [66]. For this reason, \mathbf{w}_d is only updated in the latter case, similar to [66]. Hence, by employing the APA scheme alongside the concurrent approach, a considerably enhanced convergence speed and a lower steady state MSE could be achieved compared to the standard FIRMER-CMA and FIRMER-CMA+DD. Hence, the implementation of the *p*th order algorithm could be summarised as shown in Tab. 3.3,

3.3.3 Performance

In this section, we show by computer simulations that a considerable improvement in performance has been achieved compared to FIRMER-CMA and FIRMER-CMA+DD. We first

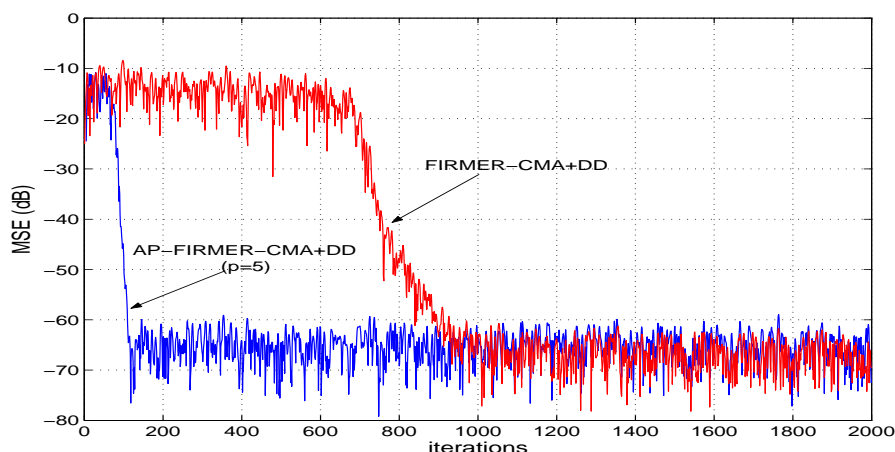


Figure 3.9: MSE curves of the FIRMER-CMA+DD ($p = 1$) and AP-FIRMER-CMA+DD ($p = 5$).

demonstrate the convergence behaviour and the steady state MSE over noise-free channels, and thereafter characterise the bit error rate performance of the proposed algorithm.

Simulation 1: In this computer simulation we demonstrate the convergence behaviour of the proposed scheme. We consider a QPSK constellation and transmit $N = 16$ user signals over a dispersive channel $g_1[m]$ with a chip rate transfer function

$$G_1(z) = 0.89 + (0.36 - 0.27j)z^{-1} + 0.09z^{-3} . \quad (3.38)$$

The length of the equaliser is $L = 10$, we choose the relaxation factors to be $\mu_c = 5 \times 10^{-3}$ and $\mu_d = 2 \times 10^{-2}$ and the projection order to be $p = 5$. These step sizes have been selected after numerous simulations and are the largest values for which all simulations provided fast stable convergence. We set the second tap in the weight vector to unity in the initial adaptation step. The MSE performances of the proposed AP-FIRMER-CMA+DD and the standard concurrent FIRMER-CMA+DD algorithms are shown in Fig. 3.9. The results clearly show that the convergence speed of the proposed scheme is faster compared to the standard FIRMER-CMA+DD.

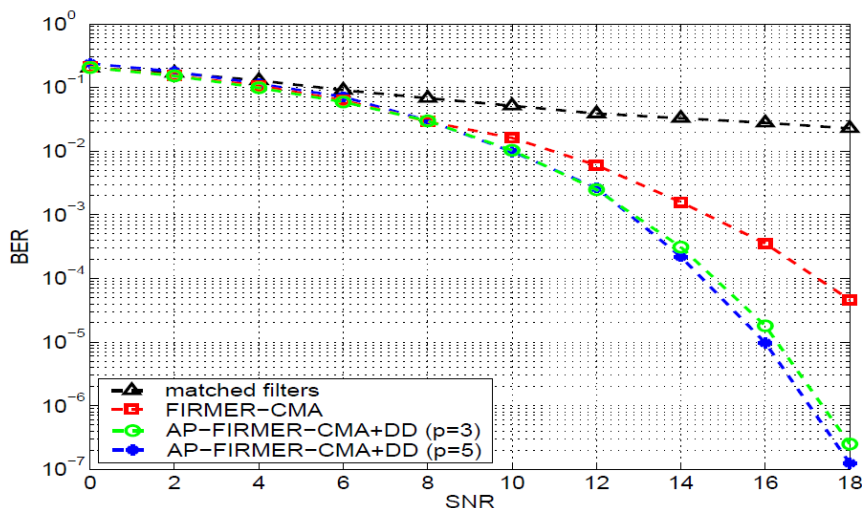


Figure 3.10: BER curves of the matched filter receiver, FIRMER-CMA ($p = 1$), and AP-FIRMER-CMA+DD equalisers for two different projection orders with $p = 3$ and $p = 5$.

Simulation 2: For $N = 4$ QPSK users, we have considered the matched filters [16, 40], FIRMER-CMA ($p = 1$), and the proposed AP-FIRMER-CMA+DD (with $p = 3$ and $p = 5$, retrospective justification in discussion later) for adaptation under different Signal-to-Noise-Ratio circumstances over the same channel $g_1[m]$. The length of the equaliser is $L = 10$, whereby the first coefficient in the weight vector is set to unity and the remaining coefficients set to zero, and we adjust the step sizes μ_c and μ_d until an adequate BER is achieved. The algorithms have always been given 10^3 symbol periods to converge prior to correction of the phase rotation and BER measurement.

Discussion: The BER curves are given in Fig. 3.10. It is evident from the simulation results that the proposed algorithm exhibits a large improvement in BER performance when going from $p = 1$ to $p = 3$ and outperforms both the standard FIRMER-CMA and matched filter receiver, but for $p > 3$, the improvement is small compared to the cost increase.

3.4 Semi-Blind Adaptation

In this section, we explore a semi-blind channel equalisation scheme for the downlink time-division duplex (TDD) component of the universal mobile telecommunication system (UMTS). In addition to the basic MSE chip rate equalisation performed over the training field of each UMTS TDD time burst, a semi-blind adaptation is adopted over data fields. In a partially loaded scenario, a number of inactive users are exploited to load pilot signals in order to enhance the system tracking performance and eliminate the typical CMA phase ambiguity problem. The performance of the proposed scheme in terms of MSE in partially loaded systems and the effect of various loading conditions on the proposed algorithm behaviour are illustrated in this section through various simulations. A new UMTS TDD burst structure will be introduced, which is more suitable for the proposed pilot-assisted scheme, and provides better spectrum efficiency than the standard UMTS data bursts.

3.4.1 UMTS TDD Physical channel

In the UMTS TDD physical channel, 15 time slots form one frame, whereby each frame has a duration of 10 ms [63] as shown in Fig. 3.11(a). Within every time slot a maximum of $N = 16$ users can transmit their signals simultaneously by means of different spreading codes. The contribution of each user is called a burst, which is a combination of two data fields, a midamble and a guard period as depicted in Fig. 3.11(b). There are two burst types proposed in [63], namely burst type 1 and burst type 2. As illustrated in Fig 3.11(b), both types have the same length of 2560 chips, concluded by a guard period of 96 chips in order to avoid overlapping of consecutive time slots. Burst type 1 has a longer midamble (512 chips), suitable for channel conditions where long training periods are required for adaptation and tracking of an equaliser.

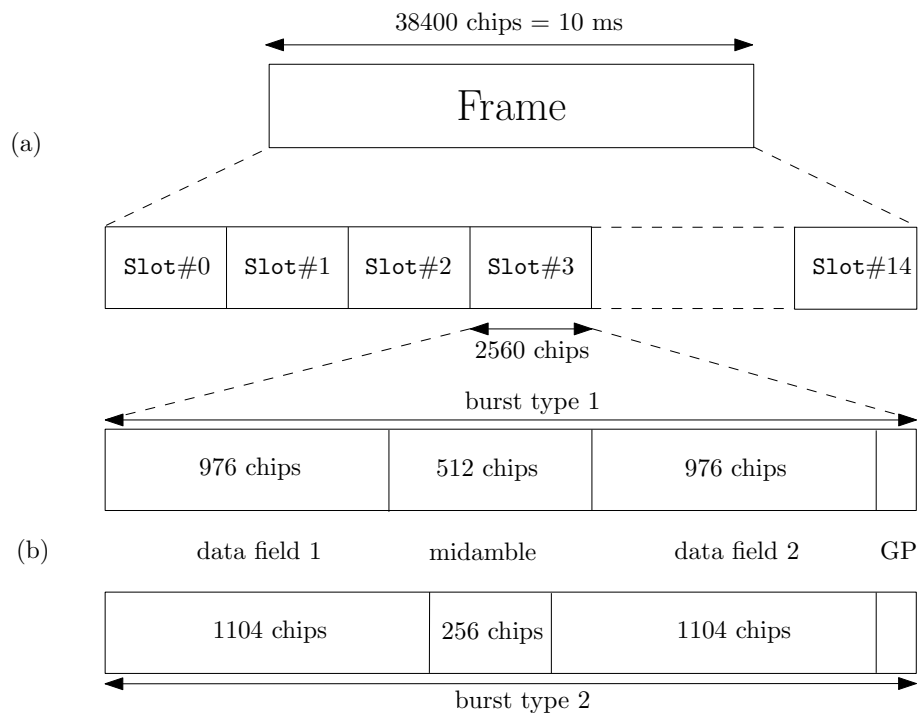


Figure 3.11: Time structure in UMTS TDD: (a) basic frame structure, and (b) burst structure.

3.4.2 Signal Model

We consider the UMTS-TDD downlink model in Fig. 3.12 with a maximum of N (assumed 16 in the following) symbol-synchronous active users, which for simplicity are assumed to have the same rate. In the case of a partially loaded system with $K \leq N-1$, we assume the first K users with signals $u_l[n]$, $l = 0(1)K-1$, to be active, and the next $N_p \leq N-K$ to be pilots with signals $p_l[n]$, $l = 0(1)N_p-1$ while the remaining $N-K-N_p$ inactive user signals $z_l[n]$ are assumed to be zero. The signals $u_l[n]$ and $p_l[n]$ are code multiplexed using Walsh sequences of length N extracted from a Hadamard matrix \mathbf{H} . The resulting chip rate signal, running at N times the symbol rate, is further scrambled by $c[m]$ prior to transmission over a channel with dispersive impulse response $g[m]$ and corruption by additive white Gaussian noise $v[m]$, which is assumed to be independent of the transmitted signal $s[m]$.

The dispersive channel $g[m]$ destroys the orthogonality of the Walsh codes, such that

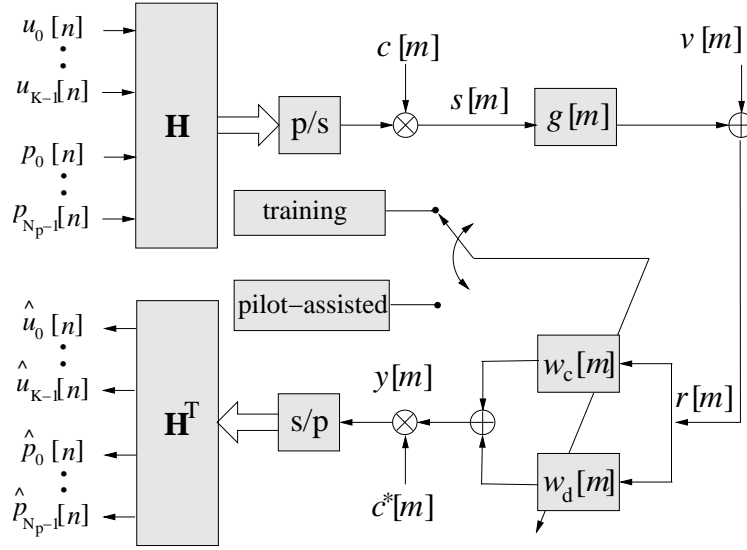


Figure 3.12: Signal model of DS CDMA downlink with a concurrent equaliser for a partially loaded system

direct decoding of the received signal $r[m]$ with descrambling by $c^*[m]$ and code-matched filtering by \mathbf{H}^T will lead to both multiple access interference and inter-symbol interference of the decoded user signals $\hat{u}_l[n]$, $l = 0(1)K - 1$. In order to re-establish orthogonality of the codes, a chip level equaliser $w[m]$ can be utilised. The equalisation is performed in both midamble period and data fields; in the former by means of the training sequence at the chip rate in the minimum mean-squared error (MMSE) sense [60], in the latter by using a blind or semi-blind scheme [67].

3.4.3 Semi-Blind Equalisation Criterion

We first derive the detected user signals $\hat{u}_l[n]$ and the pilot signals $\hat{p}_l[n]$ as a function of the equaliser $w[m]$. Based on this, we state a suitable cost function based on which the equaliser can be adapted.

3.4.4 Demultiplexed User and Pilot Signals

The DS-CDMA downlink model shown in Fig. 3.12 is fairly similar to the system which has been addressed in Sec. 3.1.1. Hence, based on (3.1), the l th user is decoded as

$$\hat{u}_l[n] = \mathbf{w}^H \mathbf{H}_l[nN] \mathbf{r}_{nN}, \quad (3.39)$$

and with similar analysis, the l th pilot's demultiplexed signal can be given as

$$\hat{p}_l[n] = \mathbf{w}^H \mathbf{H}_l[nN] \mathbf{r}_{nN} \quad (3.40)$$

where $\mathbf{H}_l[nN] \in \mathbb{C}^{L \times (N+L-1)}$ is a convolutional matrix comprising of the l th either user's or pilot's modified code vector $\tilde{\mathbf{h}}^T[n]$ and $\mathbf{r}_{nN} \in \mathbb{C}^{N+L-1}$ is the received signal.

3.4.5 Cost Functions

The equaliser $w[n]$ consists of an equaliser with a CM component $w_c[n]$ and a DD component $w_d[n]$ operated in parallel, such that $w[n] = w_c[n] + w_d[n]$. In the following, we are concerned with concurrently updating $w[n]$.

The CM term: The K active user signals $u_l[n]$ consist of symbols with a constant modulus γ . By forcing all received user symbols $\hat{u}_l[n]$ onto γ and the received pilot symbols $\hat{p}_l[n]$ onto the known transmitted sequences $p_l[n]$, a semi-blind cost function ξ_c is proposed to adapt w_c weights. Note that the remaining $N - K - N_p$ inactive users $\hat{z}_l[n]$ should be taken into consideration, otherwise the equalisation problem is underdetermined. Accordingly, the signals $\hat{z}_l[n]$ are forced to zeros in the MSE sense to ensure that the overall system is fully determined. Therefore, the proposed cost function ξ_c consists of three terms and is formulated as

$$\xi_c = \mathcal{E} \left\{ \sum_{l=0}^{K-1} (\gamma^2 - |\hat{u}_l[n]|^2)^2 \right\} + \mathcal{E} \left\{ \sum_{l=0}^{N_p-1} |p_l[n] - \hat{p}_l[n]|^2 \right\} + \mathcal{E} \left\{ \sum_{l=0}^{N-K-N_p-1} |\hat{z}_l[n]|^2 \right\}, \quad (3.41)$$

where $\mathcal{E}\{\cdot\}$ denotes the expectation operator. The optimum equaliser coefficient vector w_c in the CM sense is obtained from

$$\mathbf{w}_{c,\text{opt}} = \arg \min_{\mathbf{w}_c} \xi_c. \quad (3.42)$$

The DD term: By employing a non-linearity $q(\cdot)$ that maps its input onto the the closest constellation point, the multiuser decision directed cost function ξ_d for the DD part can be formulated as

$$\xi_d = \mathcal{E} \left\{ \sum_{l=0}^{K-1} |q(\hat{u}_l[n]) - \hat{u}_l[n]|^2 \right\} + \mathcal{E} \left\{ \sum_{l=0}^{N_p-1} |p_l[n] - \hat{p}_l[n]|^2 \right\} + \mathcal{E} \left\{ \sum_{l=0}^{N-K-N_p-1} |\hat{z}_l[n]|^2 \right\} \quad (3.43)$$

The optimum equaliser coefficient vector w_d in the mean square error sense based on the assumption of correct decisions is obtained from

$$\mathbf{w}_{d,\text{opt}} = \arg \min_{\mathbf{w}_d} \xi_d. \quad (3.44)$$

In case where no pilot is loaded there are no unique solutions to either (3.42) or (3.44), since minimising (3.41) or (3.43) is ambiguous due to an indeterminism in phase rotation. Also, note that erroneous decisions are possible in (3.43) and therefore affect (3.44).

3.4.6 Phase ambiguity

Since an ambiguity with respect to a complex rotation $e^{j\varphi}$ ($\varphi \in [0; 2\pi]$) cannot be resolved by the CM criterion, this rotation invariance could be overcome by the use of the inactive codes to load pilot signals.

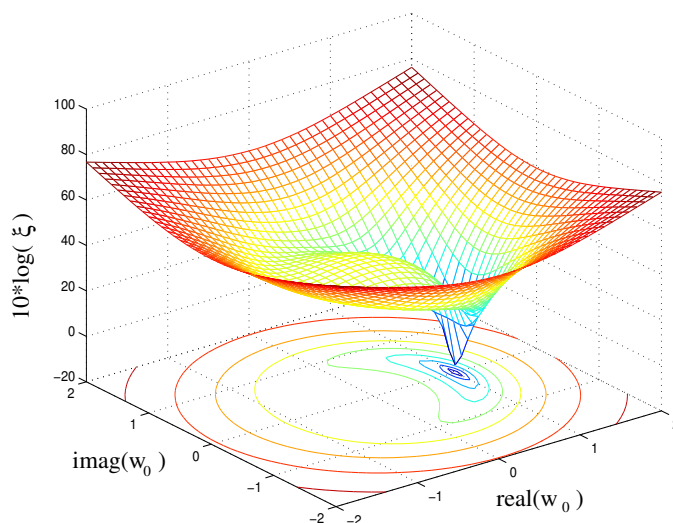


Figure 3.13: Cost function ξ_c in dependency of a single complex valued coefficient w_0 , for a partially loaded system with 10 active users and 6 pilots.

Example. To show how pilots overcome the phase ambiguity, the following example is presented. We assume a system with $K = 10$ active users and $N_p = 6$ pilots, over a distortion-less and delayless channel $g[n] = \delta[n]$. Thus, as shown in Fig. 3.13, the cost function ξ_c has one unique optimum solution $w_0 = 1$. By comparison, the cost functions ξ_c and ξ_d plotted in Figs. 3.2 and 3.5 respectively, implemented in a fully loaded system with $N = 16$, ξ_c exhibited a manifold of solutions while ξ_d showed four solutions corresponding to the four QPSK decisions. Hence, in partially loaded systems, exploiting inactive users to load pilot signals has successfully resolved the rotation invariance problem and prevented the phase ambiguity from manifesting itself.

3.4.7 Modified Cost Function

The alternative CM philosophy suggested in Sec. 3.3.1 is used to reformulate the CM term in (3.41), whereby the detected symbol $\hat{u}_l[n]$ is mapped to its nearest symbol $d_{l,c}[n]$ from the circle which has the radius γ and the centre at the origin. Both ξ_c and ξ_d can simply be

	Active user	Pilot	Inactive user
$b_l[n]$	$\hat{u}_l[n]$	$\hat{p}_l[n]$	$\hat{z}_l[n]$
$d_{l,c}[n]$	$\gamma \frac{\hat{u}_l[n]}{ \hat{u}_l[n] }$	$p_l[n]$	0
$d_{l,d}[n]$	$q(\hat{u}_l[n])$	$p_l[n]$	0

Table 3.4: Parameter values of the generalised cost function ξ_m .

written as

$$\xi_m = \mathcal{E} \left\{ \sum_{l=0}^{N-1} |d_{l,m}[n] - b_l[n]|^2 \right\}, \quad (3.45)$$

with $m \in \{c, d\}$ indicating the operational mode as either CM or DD. The index $l = 0(1)N-1$ represents either active users for $l \leq K-1$, pilots for $K \leq l \leq K+N_p-1$, or inactive users for $K+N_p \leq l \leq N-1$. Tab. 3.4 shows the various parameter values of the modified cost function ξ_m .

Next, we are concerned with minimising both ξ_c and ξ_d concurrently based on the affine projection scheme.

3.4.8 Concurrent Affine Projection Adaptation

In this section we consider applying the affine projection algorithm on the concurrent-CMA+DD in a partially loaded system. It is convenient to define:

$$\mathbf{x}_l[n] = \mathbf{H}_l[nN] \mathbf{r}_{nN}, \quad (3.46)$$

$$\mathbf{x}_j[n] = \mathbf{H}_j[nN] \mathbf{r}_{nN}, \quad (3.47)$$

$$\mathbf{x}_i[n] = \mathbf{H}_i[nN] \mathbf{r}_{nN}. \quad (3.48)$$

In the p th order of the APA algorithm, the current and last P data, pilot, and inactive vectors are taken into account for updating:

$$\mathbf{X}_l[n] = [\mathbf{x}_l[n] \ \mathbf{x}_l[n-1] \ \cdots \ \mathbf{x}_l[n-P+1]] \ , \quad (3.49)$$

$$\mathbf{X}_j[n] = [\mathbf{x}_j[n] \ \mathbf{x}_j[n-1] \ \cdots \ \mathbf{x}_j[n-P+1]] \ , \quad (3.50)$$

$$\mathbf{X}_i[n] = [\mathbf{x}_i[n] \ \mathbf{x}_i[n-1] \ \cdots \ \mathbf{x}_i[n-P+1]] \ . \quad (3.51)$$

The implementation of the p th order algorithm has been previously summarised in Tab. 3.3. The following steps briefly describe how the AP-FIRMER-CMA+DD is applied to partially loaded systems.

1. The l th active user and j th pilot decoded symbols, $\hat{u}_l[n]$ and $\hat{p}_j[n]$, have been defined in (3.39) and (3.40), respectively as

$$\hat{u}_l[n] = \mathbf{w}^H \mathbf{H}_l[nN] \mathbf{r}_{nN}, \quad (3.52)$$

$$\hat{p}_j[n] = \mathbf{w}^H \mathbf{H}_j[nN] \mathbf{r}_{nN}.$$

2. We define the error e_p according to the pilot signals at time instance n ,

$$e_p[n] = p_j[n] - \hat{p}_j[n]. \quad (3.53)$$

3. We retain a record of the past P pilot errors $e_p[n-p]$ and inactive user signals $\hat{u}_i[n-p]$, such that $p = 0 \cdots (P-1)$,

$$\mathbf{e}_p[n] = [e_p[n] \ e_p[n-1] \ \cdots \ e_p[n-P+1]], \quad (3.54)$$

$$\hat{\mathbf{u}}_i[n] = [\hat{u}_i[n] \ \hat{u}_i[n-1] \ \cdots \ \hat{u}_i[n-P+1]]. \quad (3.55)$$

4. We obtain the gradient of ξ_c (3.41) with regards to \mathbf{w} using the CMA update equation defined in (3.33) with K active users. Taking into consideration the N_p pilots and the remaining $N - K - N_p$ inactive signals [68], the CMA update equation for partially loaded systems becomes

$$\mathbf{w}_c[n+1] = \mathbf{w}_c[n] + \mu_c \left[\sum_{l=0}^{K-1} \mathbf{X}_l^\dagger[n] \mathbf{e}_{l,c}^*[n] - \sum_{j=K}^{K+N_p-1} \mathbf{X}_j[n] \mathbf{e}_p[n]^* + \sum_{i=K+N_p}^{N-1} \mathbf{X}_i[n] \hat{\mathbf{u}}_i^* \right]. \quad (3.56)$$

5. Using equations (3.34) and (3.35) the DD part is updated (3.36). Similar to (3.56), the gradient of ξ_d (3.43) is calculated

$$\mathbf{w}_d[n+1] = \mathbf{w}_d[n] + \mu_d \left[\sum_{l=0}^{K-1} \Lambda_l[n] \mathbf{X}_l^\dagger[n] \mathbf{e}_{l,d}^*[n] - \sum_{j=K}^{K+N_p-1} \mathbf{X}_j[n] \mathbf{e}_p[n]^* + \sum_{i=K+N_p}^{N-1} \mathbf{X}_i[n] \hat{\mathbf{u}}_i^* \right], \quad (3.57)$$

where $\Lambda_l[n]$ disables the DD adaptation step for a specific user if the CMA adaptation step leads to an alteration in the decision (3.35).

6. Combining the CM and DD weights leads to the final equaliser update equation

$$\mathbf{w}[n+1] = \mathbf{w}_c[n+1] + \mathbf{w}_d[n+1]. \quad (3.58)$$

7. After incrementing the symbol index n , the next iteration would recommence with step 1 of the algorithm.

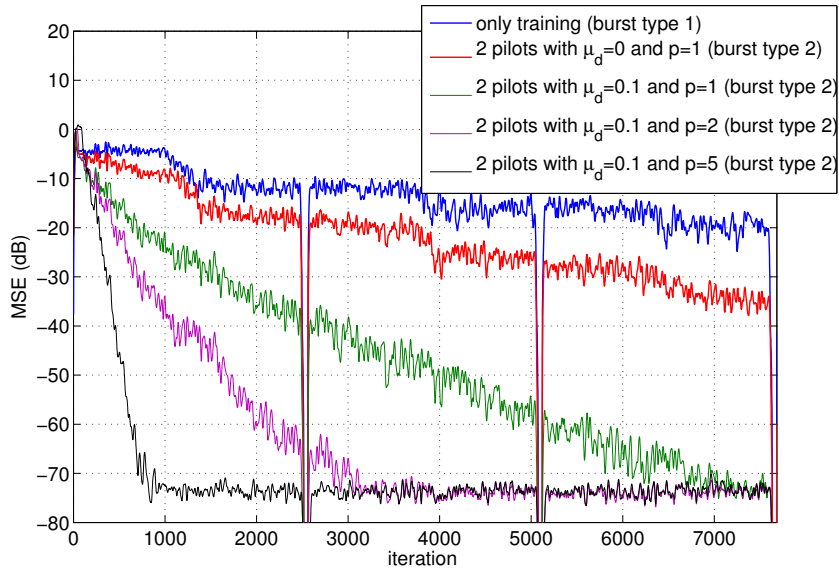


Figure 3.14: MSE curves of the FIRMER-CMA, FIRMER-CMA+DD, and AP-FIRMER-CMA+DD with $p = \{2, 5\}$ in partially loaded scenario.

3.4.9 Simulation Results

In order to demonstrate the convergence behaviour of the proposed algorithm, we transmit $K = 14$ QPSK active user signals and $N_p = 2$ pilots over a noise-free but dispersive channel $g_3[m]$, represented by its transfer function

$$G_3(z) = 0.84 + (0.42 - 0.34j)z^{-1} + 0.09z^{-2}. \quad (3.59)$$

The length of the equaliser is $L = 20$, and the relaxation factors are set to $\mu_c = 0.05$ and $\mu_d = 0.1$. The adaptation is initialised with the first coefficients in both weight vectors \mathbf{w}_c and \mathbf{w}_d set to 0.5, with the remaining coefficients set to zero. The MSE curves of the proposed algorithm operating in different scenarios over two UMTS TDD bursts are shown in Fig. 3.14.

As evident from Fig. 3.14, by operating the proposed algorithm with $\mu_d = 0$ (only CM

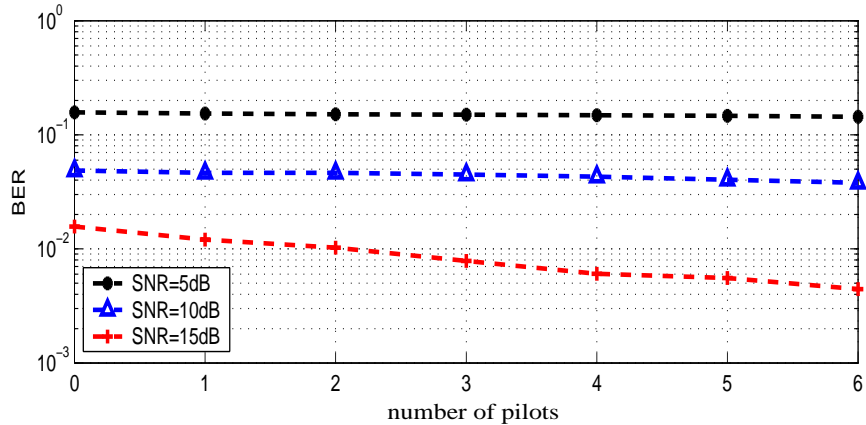


Figure 3.15: Effect of the number of pilots on the BER performance.

branch is active) over bursts of type 2 (short training period), a better MSE performance is reached as compared to the case where only training is performed in type 1 with its larger midamble. The shortening of the midamble at no performance loss is equivalent to an increase in data throughput by 13%. Furthermore, faster convergence is obtained by either activating the DD equaliser or increasing the algorithm's projection order to $p = 2$ and $p = 5$. The AP-FIRMER-CMA+DD ($p = 5$) reaches a steady state MSE in one tenth of the time required by the FIRMER-CMA+DD.

3.4.10 Effect of Pilot Loading on BER Performance

Loading more pilots enhances the quality of the transmission, however that comes at a cost as all transmissions are subject to power constraints. Increasing the number of pilots will consume more of the allocated power. In CDMA systems, the optimal power ratio of pilot and data channels was obtained in [69].

To show the effect of various loading scenarios on the BER performance of the proposed algorithm we perform two experiments. In the first experiment, we consider a UMTS TDD system with $K = 10$ active users and N_p pilots with $0 \leq N_p \leq 6$ where we calculate the BER

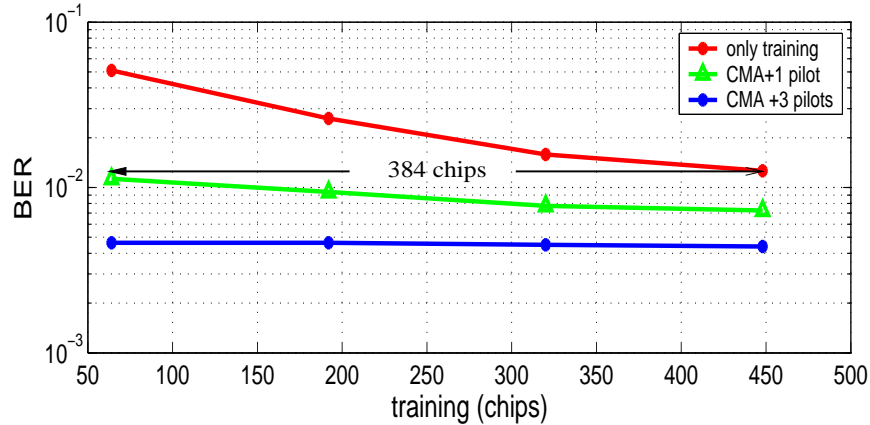


Figure 3.16: Effect of the training sequence length and pilot loading on the BER performance.

for different number of loaded pilots and various SNRs. As shown in Fig. 3.15, loading more pilots enhances the BER performance of the system for relatively medium to high SNRs, and nearly no improvement in BER performance is noticed for low SNRs.

In the second experiment, the BER is calculated for different midamble sizes, which we aim to shorten with respect to the values proposed in [70]. The length of the equaliser is $L = 10$, and the propagation environment used is a 3 paths quasi-time-varying channel, whereby it is assumed to be constant over each time slot with $\text{SNR} = 20\text{dB}$. The BER is averaged over 1000 time slots, for various loading conditions. As depicted in Fig. 3.16, the performance of the pilot-assisted algorithm is dramatically better than the classical training equalisation. A considerable reduction in BER and significant increase in data rate are achieved by loading pilots. For example, by loading only one pilot over a small midamble of size 64 chips, we obtain almost similar BER performance to the classical scheme where the adaptation is only performed over a seven times longer midamble, as shown in Fig. 3.16. Hence, 384 chips could be saved and used for data transmission. This means around 16% of data rate is gained. Moreover, by loading more pilots the BER could be reduced. For example, a reduction of at least 63% is obtained by loading three pilots for the previous short midamble, as presented in Fig. 3.16. However, we have noticed no further improvement in BER by adding further

pilots to the scheme.

3.4.11 Summary

A concurrent affine projection algorithm for pilot-assisted multiuser equalisation, suitable for the UMTS TDD downlink scenario, has been derived. The algorithm provides continuous channel tracking and presents better convergence behaviour over the basic training equalisation even with longer midambles, whereby advantages in terms of data rate and spectrum efficiency can be achieved. The convergence can be accelerated by either activating the DD equaliser or increasing the affine projection algorithm's order.

3.5 Concluding Remarks

Firmer-CMA: A blind equalisation approach for a DS-CDMA downlink scenario has been presented, which aims to enforce CM conditions on the various user signals. A stochastic gradient algorithm has been derived, which differs from previous CM algorithms by a code-prefiltering of its input. This algorithm has been extensively tested and demonstrated itself as very stable. Representative simulations have been presented, highlighting the convergence behaviour as well as its BER performance. It has been shown how this algorithm can be readily implemented in different modes and operating with various alternative algorithms.

Concurrent FIRMER-CMA+DD: A concurrent FIRMER-CMA+DD algorithm which is suitable for synchronous DS-CDMA systems has been derived. Adaptation is performed by concurrently minimising two cost functions based on the CM criterion and the DD scheme. The potential drawback of DD adaptation is the probability of error propagation occurring in case of a wrong hard decision, which subsequently degrades the performance. For this reason, the concurrent scheme is designed to update the DD part only if the equaliser's

hard decision before and after the CM adaptation are the same, and in doing so the DD adaptation is more likely to be successful.

By employing the concurrent FIRMER-CMA+DD, the convergence speed has been considerably enhanced and a lower steady state MSE has been achieved compared to the standard FIRMER-CMA, as demonstrated in simulations.

AP-FIRMER-CMA+DD: A consolidated AP-FIRMER-CMA+DD structure which combines advantages of both the AP-FIRMER-CMA and FIRMER-CMA+DD has been introduced. The proposed AP-FIRMER-CMA+DD provides a further increase in convergence speed over the FIRMER-CMA+DD and a lower BER than the FIRMER-CMA.

Pilot-Assisted AP-FIRMER-CMA+DD: A semi-blind AP-FIRMER-CMA+DD for pilot-assisted multiuser equalisation for a UMTS-TDD downlink scenario has been presented. The algorithm provides continuous channel tracking and presents better convergence behaviour over basic trained equalisation even with longer training periods, whereby a gain of data rate and spectrum efficiency can be achieved. It has been shown through various simulations that the implementation of pilots enhances the system performance in terms of MSE and BER and resolves the typical CM phase ambiguity. A burst structure with a shortened training field, which is suitable for the above pilot-assisted strategy, has been presented. The new burst offers a considerable gain in data rate and spectrum efficiency and ensures a continuous adaptation. The convergence can be accelerated by either activating the DD equaliser or by increasing the affine projection algorithm's order.

Chapter 4

Fast Adaptation for Time-Varying Channels

The previously proposed blind multiuser FIRMER-CMA equaliser improves system bandwidth efficiency by avoiding the use of a training sequence and can readily meet real-time computational constraints even for low cost commercial systems. However, since the latter algorithm is a CMA based equaliser, the slow convergence and the moderate levels of steady-state MSE are the main drawbacks of such a scheme, which may limit its implementation in any commercial wireless communication systems. This chapter introduces a fast and robust blind multiuser equalisation alternative based on a strategy called the PDF Matching Algorithm (also known as Matched-PDF or PDF Fitting Algorithm). We start by introducing the algorithm's cost function and deriving the corresponding stochastic gradient search in Sec. 4.1. The following Sec. 4.2 is dedicated to analysing and assessing the convergence behaviour and the BER performance of the proposed algorithm. We simulate a Rayleigh time-varying channel model in Sec. 4.3 to demonstrate the tracking performance of the proposed algorithm. Last, we conclude with some remarks in Sec. 4.4.

4.1 PDF Matching Algorithm

Recovering several users blindly, based on the constant modulus (CM) criterion, has been proposed in [67]. The latter approach was labelled as FIRMER-CMA, which utilises the CDMA user codes to implicitly impose the orthogonality constraint on the detected sequences, resulting in a simple and efficient CM algorithm. However, the adaptation in [67] is performed at relatively slow rate, and has a computational complexity that depends quadratically on the number of active users. These drawbacks render this algorithm inefficient for heavily loaded systems. An interesting alternative consists of trying to force the probability density at the output of the equaliser to match the known constellation PDF. In [71], the authors have proposed a method where the cost function is the quadratic distance between the current PDF at the output of the equalizer and the target PDF, based on statistical knowledge of the input sequence. Other PDF matching approaches have been proposed in the literature for QAM modulations [72, 73], however the so-called stochastic quadratic distance (SQD) has a computational burden which increases with the order of the QAM modulation scheme. The authors in [74] introduced a low cost stochastic quadratic distance (LC-SQD) PDF matching algorithm by only considering neighbouring values of the symbol constellation PDFs instead of using the whole constellation as in the SQD algorithm. The LC-SQD decreases the SQD complexity and outperforms it, however, at low signal-to-noise ratio (SNR), it may diverge in some cases. To avoid this drawback, the authors in [75] proposed a new method, also based on SQD, but that is more efficient than LC-SQD in terms of complexity, convergence speed and residual ISI. More recently, the PDF fitting algorithm was used to equalize QAM constellations by measuring the distance error between observed and assumed PDFs for the real and imaginary parts of the equalizer output separately [76, 77]. The only multiuser PDF matching approach was applied in [78] on space division multiple access (SDMA) systems for uplink scenarios with high computational complexity. In this

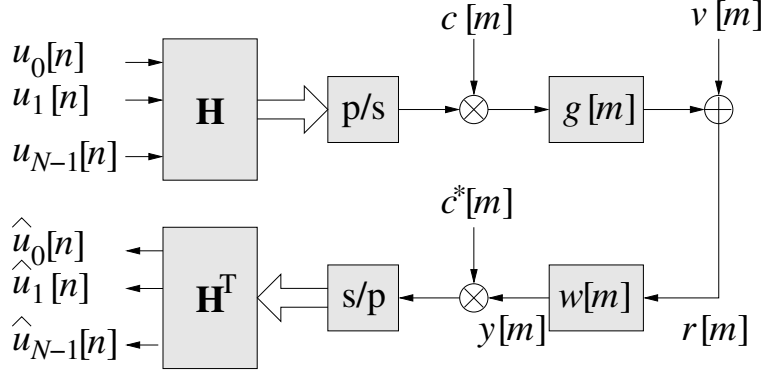


Figure 4.1: Signal model of DS-CDMA downlink with a PDF-Matching equaliser $\mathbf{w}[m]$

chapter, we investigate a simple but efficient blind adaptive multiuser equaliser applied in DS-CDMA systems.

4.1.1 Demultiplexed User Signals

Similar to Chap. 3, we consider the DS-CDMA downlink system in Fig. 4.1. Using the same derivations as in Sec. 3.1.1, the l th user can be decoded as

$$\hat{u}_l[n] = \mathbf{w}^H \mathbf{H}_l[nN] \mathbf{r}_{nN}, \quad (4.1)$$

with $\mathbf{H}_l[nN] \in \mathbb{Z}^{L \times (L+N-1)}$ (3.2) containing the decoding process of only the l th user's signal, $\mathbf{r}_{nN} \in \mathbb{C}^{N+L-1}$. In the following, we are concerned with blindly updating the equaliser vector \mathbf{w} .

The FIRMER-CMA assumes that the user signals $u_l[n]$ consist of symbols with a constant modulus γ , such as QPSK. The system model for the new proposed algorithm is the same model used for the FIRMER-CMA, only with a new cost function.

4.1.2 Cost Function

The proposed cost function is based on the idea of blindly equalising several signals, leading to a cost term which is here related to fitting the PDFs of the equaliser outputs to a desired PDF according to [73]. The idea of this approach is to measure the difference between two PDFs, $p_A(z)$ and $p_B(z)$, using the quadratic distance between them, which is defined as

$$\xi_{\text{PDF}} = \int_{-\infty}^{\infty} (p_A(z) - p_B(z))^2 dz \quad . \quad (4.2)$$

In the following, the PDF-matching criterion for the extraction of signals at the equaliser outputs $\hat{u}[n]$ is outlined. The variable whose PDF is measured at the equaliser output is the squared magnitude value $|\hat{u}[n]|^2$, in close relation to the constant modulus algorithm. The estimation of this PDF is based on the Parzen window method [79, 80], whereby a smooth PDF estimate is achieved by replacing a sample $|\hat{u}[n]|^2$ by a kernel function centred at its location. We here select a Gaussian kernel $K_\sigma(z)$ with variance σ ,

$$K_\sigma(z) = \frac{1}{\sqrt{2\pi}\sigma} e^{-\frac{z^2}{2\sigma^2}}, \quad (4.3)$$

such that the PDF estimate over a window of L_w output samples is given by

$$\hat{p}_{|\hat{u}[n]|^2}(z) = \frac{1}{L_w} \sum_{l=0}^{L_w-1} K_\sigma(z - |\hat{u}[n-l]|^2) \quad . \quad (4.4)$$

The larger the window length L_w , the more confident the PDF estimate will be. However, a trade-off exists, as during adaptation the output statistics are not stationary, and therefore it is advantageous to limit L_w to an interval within which the statistics can be assumed quasi-stationary. Therefore, the PDF of the original constellation must be convolved with the kernel of the Parzen estimator being used for $\hat{p}_{|\hat{u}[n]|^2}(z)$.

The PDF estimate at the equaliser output, $\hat{p}_{|\hat{u}[n]|^2}(z)$, will be compared to the PDF of the squared moduli of the transmitted signals, $|u[n]|^2$, subject to the same Gaussian kernel $K_\sigma(z)$ [72]. For consistency, the target PDF $\hat{p}_{|u[n]|^2}(z)$ must consider the effect of the estimator to guarantee the cost function is zero for perfect equalisation. Another advantage of convolving the discrete PDF of $|u[n]|^2$ defined by the constellation points of $u[n]$ with the Gaussian kernel in (4.3) is that the resulting PDF exhibits a spread around constellation points akin to the influence of channel noise. Given the model of AWGN, the PDF of squared moduli would be a superposition of chi-square distributions, which subsequently might provide a more appropriate kernel. However, we here follow the suggestion of a Gaussian kernel in [72] as this will lead to simplifications that are required for a solution with low computational cost.

Therefore, the convolution with the Gaussian kernel yields the desired PDF

$$\hat{p}_{|u_i|^2}(z) = \frac{1}{M} \sum_{m=1}^M K_\sigma(z - |s_m|^2) \quad , \quad (4.5)$$

where s_m , $m \in \{1, 2, \dots, M\}$, are the M constellation points of the i^{th} transmitted signal. By exploiting the fact that for Gaussian kernels [72]

$$\int_{-\infty}^{\infty} K_\sigma(z - z_1) K_\sigma(z - z_2) dz = K_{\sqrt{2}\sigma}(z_1 - z_2) \quad , \quad (4.6)$$

the cost function of the matched-PDF algorithm for the equaliser output becomes

$$\begin{aligned} \xi_{\text{PDF}}[n] = & \frac{1}{L_w^2} \sum_{m=0}^{L_w-1} \sum_{l=0}^{L_w-1} K_{\sigma\sqrt{2}}(|\hat{u}[n-l]|^2 - |\hat{u}[n-m]|^2) \\ & + \frac{1}{M^2} \sum_{m=1}^M \sum_{l=1}^M K_{\sigma\sqrt{2}}(|s_l|^2 - |s_m|^2) \\ & - \frac{2}{L_w M} \sum_{m=1}^M \sum_{l=0}^{L_w-1} K_{\sigma\sqrt{2}}(|\hat{u}[n-l]|^2 - |s_m|^2) \quad . \end{aligned} \quad (4.7)$$

Analysing this cost function, it can be observed that the first term on the right hand side is the estimator of the information potential associated with Renyi's entropy of the second order [81], except in our case the cost function must be minimised, whereas in [81] the information potential must be maximised. The second term on the right hand side does not depend on \mathbf{w} and can be neglected in the optimisation process. Finally, the third term pulls the PDF of the equaliser output towards the desired PDF. The third term is responsible for measuring the distance between PDFs while the first two act as normalisation for different PDFs. It has been argued in [73] that because these terms are used in a cost function which is meant to find an extremum, it is logical to use only the cross term, hoping that the minima of the two criteria occur at the same parameter value. Some evidence for this behaviour was highlighted in [82], where a similar cost function provides outstanding results in an application of information theory to clustering.

In any case, the first term of the cost function can be ignored for $L_w = 1$ while the second term can be considered spurious for constant modulus constellations [73]. Hence the matched-PDF cost function simplifies to

$$\xi_{\text{PDF}}[n] = -\frac{2}{M} \sum_{m=1}^M K_{\sigma\sqrt{2}}(|\hat{u}[n]|^2 - |s_m|^2) \quad . \quad (4.8)$$

The cost function in (4.8) is depicted in Figure 5.3. Similar to the CMA, the cost function

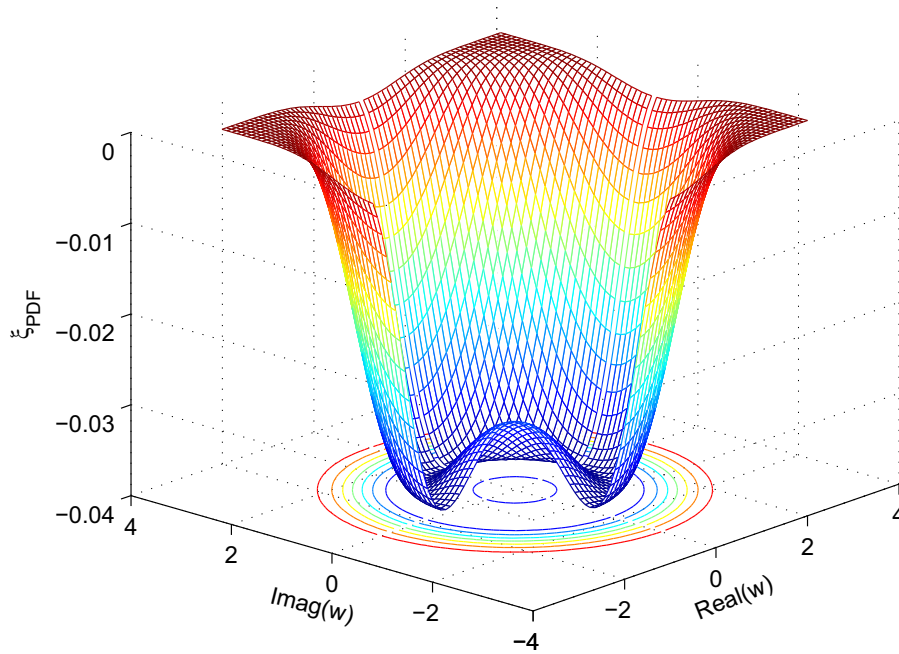


Figure 4.2: The PDF-matching cost function for one output. A segment of the surface is removed.

at hand exhibits a manifold of optimum solutions due to its phase ambiguity.

4.1.3 Stochastic Gradient Algorithm

Based on the cost function in (4.8), this section addresses the problem of adjusting the equaliser. The coefficients of the equaliser are updated using the stochastic gradient method,

$$\mathbf{w}_{n+1} = \mathbf{w}_n - \mu_{\text{PDF}} \nabla_{\mathbf{w}^*} \hat{\xi}_n, \quad (4.9)$$

where $\nabla_{\mathbf{w}^*}$ denotes the gradient with regard to \mathbf{w}^* , and μ_{PDF} is the step size. The derivative of the cost function with respect to \mathbf{w}^* can be calculated as

$$\frac{\partial}{\partial \mathbf{w}^*} \xi_{\text{PDF}}[n] = -\frac{2}{M} \sum_{m=1}^M K'_{\sqrt{2}\sigma}(|\hat{u}[n]|^2 - |s_m|^2) \hat{u}^*[n] \mathbf{r}_n, \quad (4.10)$$

where

$$K'_{\sqrt{2}\sigma}(z) = \frac{\partial}{\partial z} K_{\sqrt{2}\sigma}(z) = -\frac{1}{4\sigma^2} K_{\sqrt{2}\sigma}(z) \quad (4.11)$$

is the derivative of the Gaussian kernel in (4.3). In order to simplify the derivative, we assume that all the points in the transmit constellation have the same modulus, i.e. $|s_m|^2 = \gamma^2$, for $m = 1, \dots, M$. Thus, the summation and division by M drop out from (5.24). Evaluating the derivative K'_σ in (5.24) and rearranging terms leads to

$$\frac{\partial}{\partial \mathbf{w}^*} \xi_{\text{PDF}}[n] = 2K_{\sqrt{2}\sigma}(|\hat{u}[n]|^2 - \gamma^2) e^*[n] \mathbf{r}_n, \quad (4.12)$$

where,

$$e^*[n] = \frac{1}{4\sigma^2} (|\hat{u}[n]|^2 - \gamma^2) \hat{u}^*[n], \quad (4.13)$$

and $K_{\sqrt{2}\sigma}(z)$ is the Gaussian kernel used for the Parzen estimator as defined in (4.3). It is the addition of this kernel term that distinguishes the cost function gradient shown in (4.12) from a standard CM algorithm. The constants arising e.g. from the differentiation of the kernel can be absorbed into the step size μ .

4.2 PDF Algorithm Performance

In this section, we show by computer simulations that a considerable improvement can be achieved by the PDF matching algorithm compared to FIRMER-CMA.

4.2.1 Implementation Details

For the simulations below, we consider a fully loaded synchronous DS-CDMA system, where the adopted modulation scheme is QPSK. We apply the Matched-PDF algorithm and FIRMER-CMA to the same short channel with impulse responses $g_4[m]$ characterised by its chip rate transfer function

$$G_4(z) = 1 + (0.3 + 0.5j)z^{-1} + 0.2z^{-2}. \quad (4.14)$$

White Gaussian noise with an SNR of 30dB has been added at the output of the channel. The length of the equaliser is $L = 21$. The adaptation is initialised with the first coefficient in both weight vectors for the FIRMER-CMA and the Matched-PDF set to 1 and the remaining coefficients set to zero.

Step sizes $\mu_{\text{CMA}} = 1e^{-2}$ and $\mu_{\text{PDF}} = 5e^{-2}$ have been chosen for FIRMER-CMA and Matched-PDF, respectively. After numerous simulations, these step sizes are the largest values for which all simulations provided fast stable convergence. A kernel size $\sigma = 10$ have been chosen for the Matched-PDF approach. This large kernel size has been chosen because the main goal here is to maximise the convergence speed. The MSE curves are ensemble averaged over a window of 1000 data samples.

4.2.2 Results

The MSE curves of the proposed algorithm compared to the FIRMER-CMA algorithm are shown in Figure 4.3. It is clear from the MSE curves that the MSE performance of the Matched-PDF is much faster than FIRMER-CMA, where the Matched-PDF reaches its steady-state MSE of approximately -55dB almost twice as fast as the FIRMER-CMA. Figure 4.4 shows the BER performance for both FIRMER-CMA and Matched-PDF, where

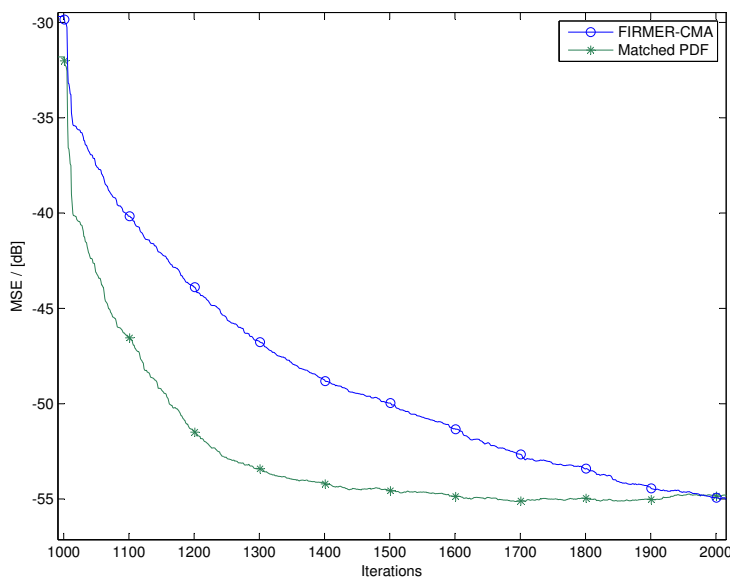


Figure 4.3: MSE curves of the proposed Matched-PDF Algorithm and the standard FIRMER-CMA.

it is clearly shown that the superior convergence rate of Matched-PDF comes at no cost in terms of BER degradation. In fact, the BER curves of both algorithms are almost identical, with an exception at low SNRs where the PDF-Matching has a slight edge over the FIRMER-CMA. A potential reason for this could be insufficient convergence time to reach the steady state for the slower CMA for some members of the ensemble average shown on Fig. 4.4.

In the presence of phase ambiguity, the inter-symbol-interference (ISI)

$$\text{ISI}_n = 10 \log_{10} \frac{\sum_n |\theta[n]|^2 - \max_n |\theta[n]|^2}{\max_n |\theta[n]|^2}, \quad (4.15)$$

provides a more accurate measure of system performance than the MSE, where $\theta[n]$ is the convolution of the channel and equaliser block. The ISI performance has been measured with the step sizes $\mu_{\text{CMA}} = 1e^{-3}$ and $\mu_{\text{PDF}} = 5e^{-3}$. The step sizes which have been selected are the largest values for which all simulations provided maximally fast and stable convergence.

Figure 4.5 indicates that the Matched-PDF algorithm offers convergence in terms of ISI

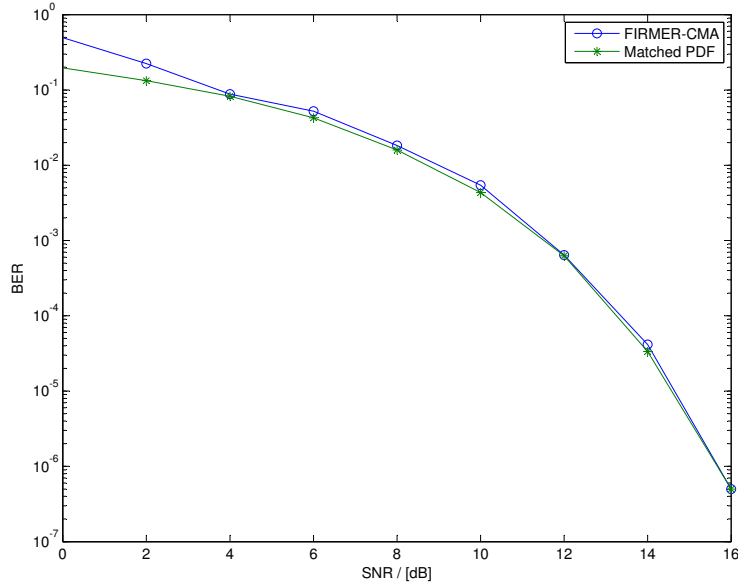


Figure 4.4: BER vs SNR curves of the Matched-PDF Algorithm and FIRMER-CMA.

performance that is approximately twice as fast as the FIRMER-CMA. By comparing the MSE and ISI performances, it is evident that the proposed algorithm converges much faster than the FIRMER-CMA, without any degradation in BER performance.

4.2.3 Summary

A new adaptive algorithm for blind multiuser equalisation has been derived. The new cost function of this method is based on minimising the distance between the actual PDF of the equaliser output and the desired PDF. The proposed method showed faster convergence speed compared to the FIRMER-CMA using QPSK constellation. Furthermore, the kernel size of the Parzen window estimator could be increased to accelerate the convergence speed, and once the ISI is sufficiently reduced the kernel size can be reduced to achieve higher accuracy.

So far in our simulations we have considered a stationary channel which gives a good measure in terms of convergence speed; however, in real life not all channels can be considered

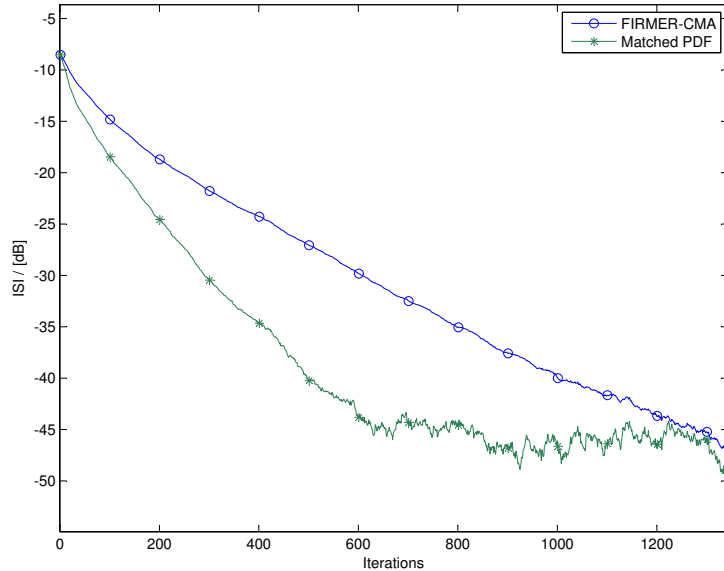


Figure 4.5: ISI curves of the Matched-PDF Algorithm and FIRMER-CMA.

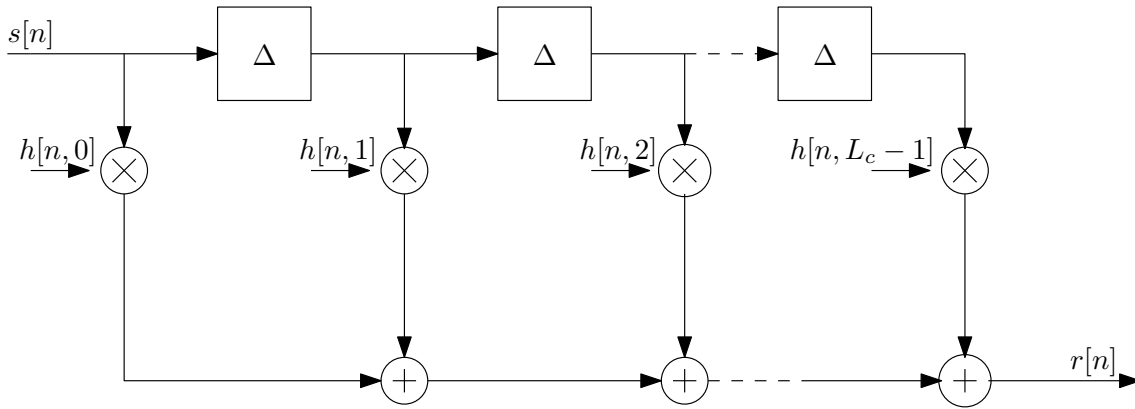
stationary but will vary in time. Therefore, in the next section we will test the proposed algorithm under time-varying channel conditions.

4.3 Time-Varying Channels and Tracking Performance

This section first introduces a time-varying channel model. Thereafter, this channel model is used to test how well the Matched-PDF algorithm can cope with changes in the channel, i.e. measure the tracking performance.

4.3.1 Time-Varying Channel Model

In order to demonstrate the tracking behaviour of the proposed algorithm, we run multiple computer simulations under various scenarios from transmitting a single user to $N = 16$ QPSK active user signals over a doubly-dispersive channel $h[n, \nu]$ which is frequency selec-

Figure 4.6: Channel Impulse Response at time n

tive and time-varying, where L_c is the length of the channel, n is the time index and ν is the coefficient index. The finite impulse response (FIR) filter of channel $h[n, \nu]$ with L_c coefficients is depicted in Fig. 4.6, where Δ is a delay of one symbol period.

Considerable contributions have been published previously to define a realistic and sensible representation of a time-varying channel [83, 84]. Clarke assumed isotropic scattering leading to a uniformly distributed angle of arrival (AoA) [84]. For reasons of simplicity, Clarke's representation with a Rayleigh distribution has been chosen to model time-varying channels.

Time variation of the channel is normally associated with mobility of a terminal, being the transmitter, the receiver or any reflecting object in the propagation environment. In wireless communication systems, multiple copies of the transmitted signal arrive at the receiver with different delays and phases creating the multipath phenomenon. Furthermore, due to mobility of a terminal, the signal experiences a random frequency modulation on each of the multipath components due to Doppler shifts.

When a signal is transmitted in a free-space propagation environment where there is no multipath propagation, the relative motion between the transmitter and receiver results in an apparent change in the frequency of the received signal. This apparent frequency change is called Doppler shift. To analyse this phenomenon, consider the simple scenario shown in

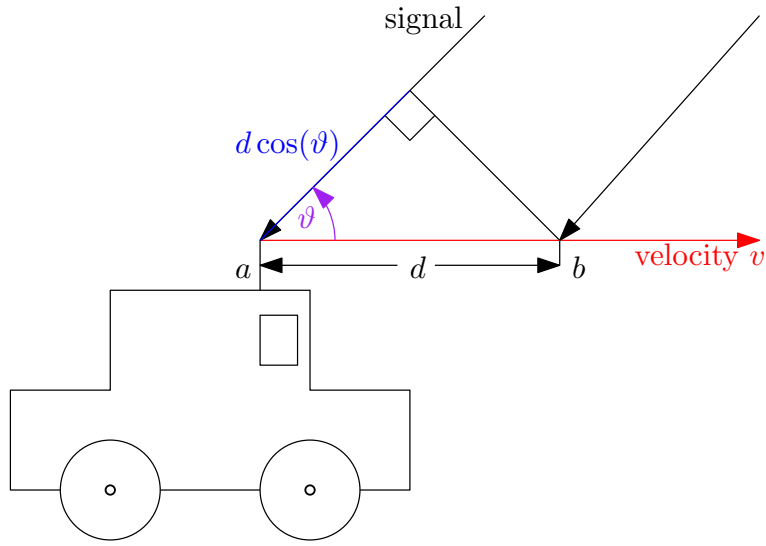


Figure 4.7: Mobility of a terminal causes Doppler Shift.

Fig. 4.7. Assuming the receiver is moving at a constant velocity v along a direction that forms an angle of arrival ϑ with the received signal, then it can be seen that the difference in path lengths travelled by the signal from the transmitter to the mobile receiver at points a and b is given by

$$\Delta l = d \cos(\vartheta), \quad (4.16)$$

$$= v \Delta t \cos(\vartheta), \quad (4.17)$$

where Δt is the time required for the mobile to travel from a to b . The phase change in the received signal due to the difference in path lengths is therefore

$$\Delta\phi = \frac{2\pi \Delta l}{\kappa}, \quad (4.18)$$

$$= \frac{2\pi v \Delta t}{\kappa} \cos(\vartheta), \quad (4.19)$$

where κ is the wavelength of the transmitted signal. Hence, the apparent change in received frequency, or Doppler shift, is given by:

$$\Omega_D = \frac{1}{2\pi} \frac{\Delta\phi}{\Delta t} , \quad (4.20)$$

$$= \frac{v}{\kappa} \cos(\vartheta) , \quad (4.21)$$

$$= \frac{v}{c} f_c \cos(\vartheta) . \quad (4.22)$$

using $c = f_c \kappa$, where c is the speed of light and f_c is the frequency of the transmitted signal.

It can be seen from (4.22) that the Doppler shift is a function of, among other parameters, the angle of arrival of the transmitted signal. In an environment with multipath propagation, in which multiple signal copies propagate to the receiver with different angles of arrival, different propagation paths experience different Doppler shifts. The resulting signal is the sum of the multipath components. Consequently, the frequency spectrum of the received signal will in general be ‘wider’ than that of the transmitted signal, i.e. it contains more frequency components than were transmitted. This phenomenon is referred to as Doppler spread.

The Doppler spread can be quantitatively characterised by the Doppler spectrum [85]. The Doppler spectrum is the power spectral density of the received signal when a single-frequency sinusoid is transmitted over a multipath propagation channel. In a static environment in which the reflectors stay immobile, the Doppler spectrum is simply an impulse located at the frequency of the transmitted sinusoid when there is no relative motion. When there is relative motion, the Doppler spectrum occupies a finite bandwidth. The exact shape of the Doppler spectrum depends on the configuration of the reflectors. It can be shown [85] that when the mobile receiver moves at a constant speed v and the signal power received by the receiver antenna arrives uniformly from all incident angles in $[0 : 2\pi]$, the Doppler power spectrum takes the form of:

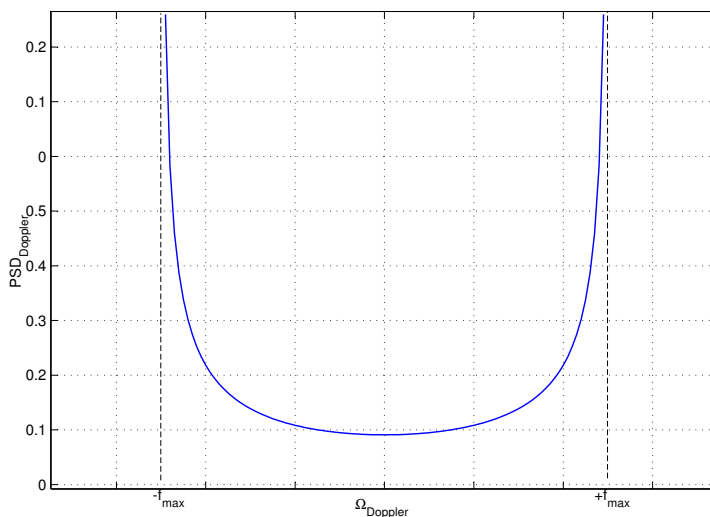


Figure 4.8: Magnitude response of the Doppler filter or PSD of a channel coefficient.

$$S(f) = \begin{cases} \frac{1.5}{\pi f_{\max} \sqrt{1 - (\frac{f-f_c}{f_{\max}})^2}} & |f - f_c| < f_{\max} \\ 0 & |f - f_c| \geq f_{\max}. \end{cases}$$

where $f_{\max} = \frac{v}{\kappa}$ is the maximum Doppler shift. This Doppler spectrum is plotted in Fig.4.8.

The implementation of a Rayleigh fading channel for simulation is based on the filtered Gaussian noise model and is performed in the frequency domain and then transformed into the time domain. As illustrated in Fig. 4.9, two Gaussian noise sources are generated and then multiplied by the frequency response of the Doppler filter (equivalent to time domain convolution). The resulting signals are transformed into the time domain by the inverse discrete Fourier transform. Taking the first output as it is, and multiplying the second by the imaginary unit $j = \sqrt{-1}$ provides the real and imaginary parts of the time domain coefficient trajectories of channel $h[n, \nu]$.

In the following computer simulations, the channel is implemented in overlap-save mode [86]. The length of the output data segment will be in the length of a block. If more data is re-

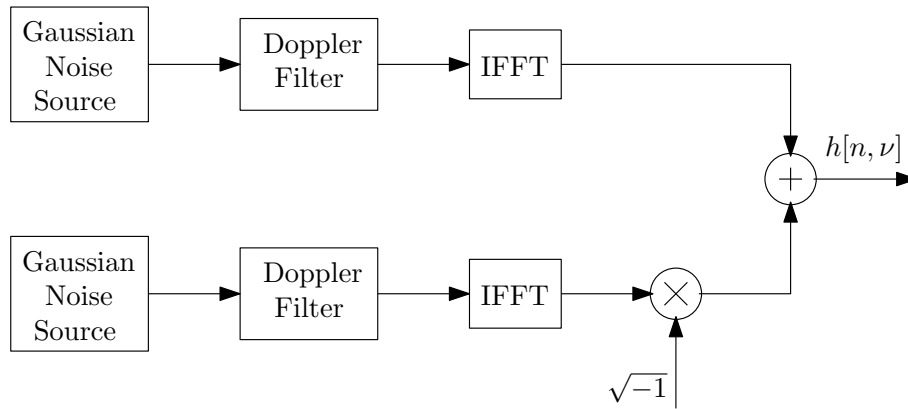


Figure 4.9: Implementation of a single Rayleigh fading coefficient

quired, further blocks can be produced without violating the smoothness constraint. The smooth continuation is achieved by overlap-save, whereby instead of saving an entire segment of random data points, only the seed value generating this data segment has to be remembered and passed to the next generation of coefficients.

Fig. 4.3.1(a) shows the Rayleigh time-varying channel used in our simulation, where the channel is changing for every transmitted symbol. Fig. 4.3.1(b) shows a zoomed version to enable a closer look at the first 100 coefficients, where you can clearly see the Rayleigh channel changing over time.

4.3.2 Implementation Details

White Gaussian noise with signal to noise ratio (SNR) of 30dB has been added at the output of the channel. The length of the equaliser is $L_w = 21$. The adaptation is initialized with the first coefficient in both weight vectors for the CMA and the Matched-PDF set to 1. A step size $\mu_{\text{PDF}} = 1e^{-3}$ and a kernel size $\sigma = 10$ have been selected for the Matched-PDF approach. The step size of the FIRMER-CMA Algorithm was set to $\mu_{\text{CMA}} = 1e^{-3}$. Again, both step sizes which have been selected for FIRMER-CMA and the Matched-PDF are the largest values for which all simulations provided stable convergence.

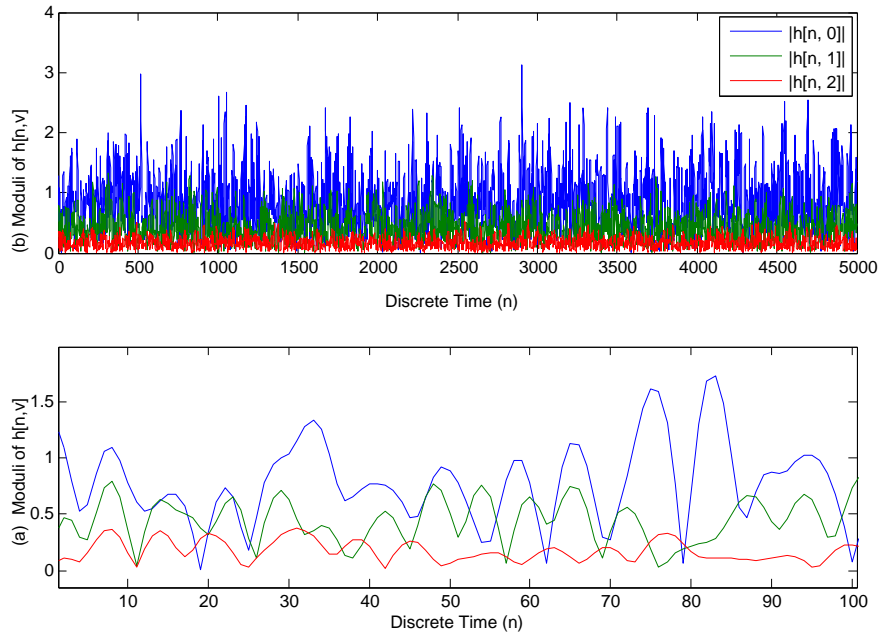


Figure 4.10: Trajectories of moduli of Rayleigh fading channel coefficients, with (a) a series of 5000 sampling periods and (b) a shorter detail.

4.3.3 Simulation Results

The MSE curves of the proposed algorithm compared to the CMA algorithm are shown in Fig. 4.11, under (a) a single user scenario, and (b) a multiuser scenario. The simulation result shows clearly the tracking behaviour in a time-varying environment. Starting from the optimum solution, both techniques track the changes in the channel and hence equalise the signal accordingly.

To enable a better comparison in the performance of the CMA and Matched-PDF algorithm under time-varying channels, in both single user and multiuser systems, we average the resulting MSE over a moving window of symbols, with the results shown in Fig. 4.12.

Unlike the performance of the CMA and Matched-PDF Algorithm in constant environments Fig. 4.3 [12], it was expected that a lower MSE performance would be obtained under

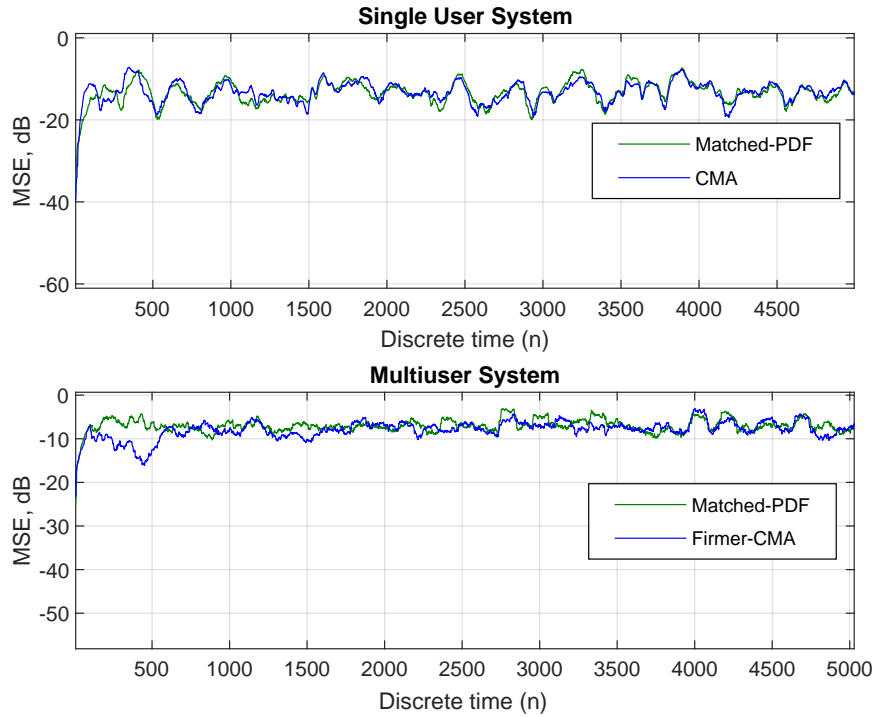


Figure 4.11: MSE curves of Matched-PDF and CMA with averaging for a single user system (top) and a multiuser system (bottom).

time-varying channels Fig. 4.11 and Fig. 4.12 [13]. It is also worth noting that the Matched-PDF algorithm has lost its advantage over the CMA under fast time-varying channels. In constant environments the Matched-PDF's MSE performance reached -55dB while Fig. 4.12 shows that its best MSE performance in time-varying environments reaches -12dB . However, the convergence speed of the Matched-PDF is still relatively faster than that of the CMA algorithm in both single and multiuser systems.

Fig. 4.12 also demonstrates that both algorithms reach a lower MSE level in the multiuser system; about 5dB lower than that of the single user system, this is due to the orthogonality of the Walsh codes used in multiplexing the users.

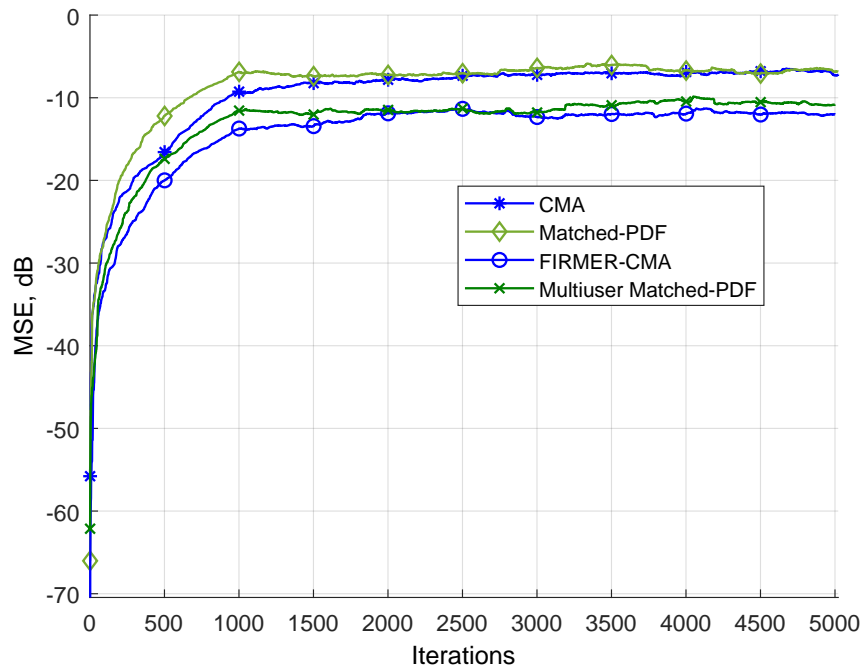


Figure 4.12: MSE curves of Matched-PDF and CMA with Averaging

4.3.4 Summary

Both Matched-PDF and FIRMER-CMA have been tested under Rayleigh time-varying channel conditions, which was designed based on the filtered Gaussian noise model, but implemented in overlap-save mode which ensures smooth continuation of the channel.

The Matched-PDF algorithm for blind adaptive equalisation under fast time-varying channels has been tested under a fast time-varying environment. The proposed algorithm showed a promising tracking performance, but could only be demonstrated to yield comparable tracking performance to FIRMER-CMA.

4.4 Concluding Remarks

A new adaptive algorithm for blind multiuser equalisation has been derived. The new cost function of this method is based on minimizing the distance between the actual PDF of the equalizer output and the desired PDF. The proposed method showed faster convergence speed compared to the FIRMER-CMA using QPSK constellation. Furthermore, the kernel size of the Parzen Window Estimator can be increased to accelerate the convergence speed, and once the ISI is sufficiently reduced the kernel size can be reduced to achieve higher accuracy.

The Matched-PDF algorithm has been reviewed under fast time-varying channels. The proposed method showed faster convergence speed compared to the classical CMA in constant environments. In a fast time-varying systems, the proposed algorithm yields comparable performance to the FIRMER-CMA but showed a promising robustness to noise and the double dispersiveness of the channel which was frequency selective and time-varying.

It can be concluded that the proposed algorithm provides advantages over the FIRMER-CMA in constant environments while it provides a similar tracking performance when the channels are fast time-varying.

Chapter 5

Case Studies: PDF Matching Algorithm for MIMO Systems

In the previous chapter we introduced a new adaptive algorithm for blind multiuser equalisation, which shows faster convergence speed compared to Firmer-CMA in stationary environments, and exhibits a promising robustness to noise and channel dispersiveness in time-varying scenarios. However, all algorithms considered so far are designed for the case of a single transmit and receive antenna. With many future communication systems relying on multiple-input multiple-output (MIMO) configurations of antennas, in this chapter we test the new scheme as an example on MIMO Space Time Block Coding (MIMO STBC) and Time Reversal Space Time Block Coding (MIMO TR-STBC), and we compare these against state-of-the-art algorithms. We also look at the computational cost of these algorithms.

This chapter is organised as follows. In Sec. 5.1 a description of the MIMO channel and signal model is given for MIMO-STBC. The proposed cost function for the equaliser is then derived. It also includes some simulation results benchmarked against existing approaches to mitigate ISI in broadband MIMO STBC systems. The following Sec. 5.2 is dedicated to

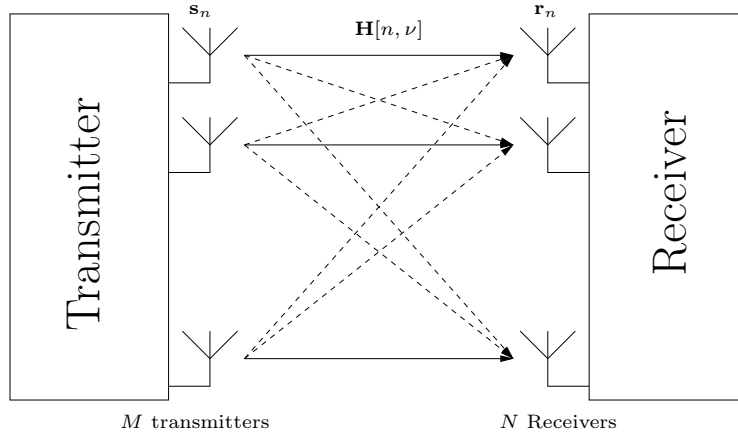


Figure 5.1: A Multiple-Input Multiple-Output system with M transmit and N receive antennas analysing and assessing the convergence behaviour and the BER performance of the proposed algorithm under MIMO TR-STBC system. Finally, conclusions are drawn in Sec. 5.3.

5.1 MIMO STBC Based on PDF Matching

Multiple-Input Multiple-Output (MIMO) systems use more than one antenna at both ends of the transmission in order to increase the performance of such systems. Figure 5.1 illustrates a typical MIMO system with M transmit and N receive antennas as given by

$$\begin{bmatrix} r_1[n] \\ r_2[n] \\ \vdots \\ r_n[n] \end{bmatrix} = \sum_{\nu=0}^{N-1} \mathbf{H}_{n,\nu} \begin{bmatrix} s_1[n-\nu] \\ s_2[n-\nu] \\ \vdots \\ s_m[n-\nu] \end{bmatrix}. \quad (5.1)$$

The use of multiple transmit and receive antennas has been shown to increase the capacity of the transmission link [87]. This extra capacity can be exploited to increase either the

multiplexing gain or the diversity gain of the system [87, 88], whereby we here focus on the latter using space-time coding schemes. The work in [88] proposed a STBC transmit diversity scheme, which is capable of maximising the diversity over frequency-flat MIMO channels, whose responses between pairs of transmit and receive antennas can be characterised by complex gain factors.

For high data rate services, most channels cannot be considered frequency-flat but are dispersive, causing inter-symbol interference. In order to exploit diversity in such an environment, a number of variations on the classical STBC encoding have been proposed. OFDM can decompose a frequency-selective channel into a number of subcarriers, which represent individual narrowband transmission channels, that can each be STBC encoded [89, 90]. The drawback of OFDM systems is in general the sensitivity to synchronisation errors and their large peak-to-average power ratio [91]. Single-carrier time domain approaches were first proposed by [90], whereby the STBC structure was applied to a window of symbols, which is, after a guard interval, repeated as a complex conjugate and time reversed version [92]. However, time-reversal (TR) STBC is sensitive if the channel is doubly-dispersive, i.e. frequency selective and time-varying [93].

A recently proposed blind equalisation scheme for STBC [93] overcomes this problem and shows a higher robustness towards time-variations of the channel than TR-STBC. In order to increase the convergence speed of the STBC-CMA algorithm, various algorithmic variations have been evaluated, of which the most successful is the recursive quasi-Newton (RQN) approach, [94]. Unfortunately, the RQN method requires a considerable computational effort, which even a fast version of this algorithm cannot entirely alleviate.

In [73] a cost function that minimises the difference between a measured PDF at the equaliser output and a target PDF has been proposed, assuming a simple Gaussian model for the desired PDF. The technique has been successfully applied for SISO equalisation [72, 73]

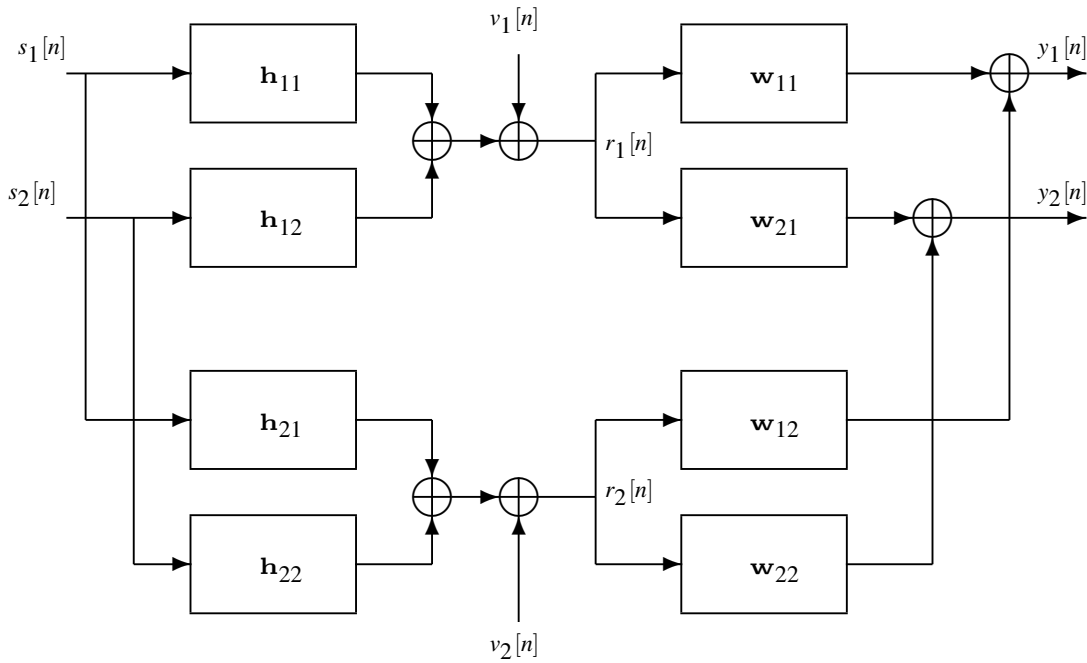


Figure 5.2: Channel and signal model with transmit STBC signals $s_i[n]$, a 2×2 MIMO channel with CIRs $h_{j,i}[n, \nu]$, received signals $r_j[n]$, equaliser components $\mathbf{w}_{i,j}[n]$ and equaliser outputs $y_i[n]$ which should adhere to the STBC structure.

and multiuser detection [12]. In this chapter we intend to apply Matched-PDF to target the equalisation of an STBC MIMO system. Based on the STBC-CMA approach [93], the aim of this chapter is to investigate a PDF fitting based cost function for the equalisation of STBC over a broadband MIMO channel.

5.1.1 Channel and Signal Model

The general setup of channel and equaliser is outlined in Fig. 5.2, and the individual system blocks are described below.

Space-Time Block Coding

Assuming transmission from two antennas, the transmit signal $s[n]$ is STB encoded to provide two antenna signals $s_i[n]$, $i \in \{1, 2\}$ for the i th antenna, computed according to [88],

$$\begin{bmatrix} s_1[n] & s_1[n+1] \\ s_2[n] & s_2[n+1] \end{bmatrix} = \begin{bmatrix} s[n] & -s^*[n+1] \\ s[n+1] & s^*[n] \end{bmatrix} . \quad (5.2)$$

This produces two orthogonal signals with a characteristic STBC structure, which will later be exploited in the equaliser.

MIMO Channel Model

The receiver requires a minimum of two receive antennas in order to equalise the MIMO system characterised above. Assuming the availability of two sufficiently spaced receive antennas, the signals $r_j[n]$, $j \in \{1, 2\}$, received at the j th receive antenna over a dispersive and noise-corrupted channel are given by

$$\begin{bmatrix} r_1[n] \\ r_2[n] \end{bmatrix} = \sum_{\nu=0}^{N-1} \mathbf{H}_{n,\nu} \begin{bmatrix} s_1[n-\nu] \\ s_2[n-\nu] \end{bmatrix} + \mathbf{v}_n . \quad (5.3)$$

The channel is characterised by the matrices

$$\mathbf{H}_{n,\nu} = \begin{bmatrix} h_{1,1}[n,\nu] & h_{1,2}[n,\nu] \\ h_{2,1}[n,\nu] & h_{2,2}[n,\nu] \end{bmatrix} , \quad (5.4)$$

whereby $h_{j,i}[n,\nu]$ is the ν th coefficient of the channel impulse response between the i th

transmit and the j th receive antenna, at time n . The vector

$$\mathbf{v}_n = \begin{bmatrix} v_1[n] \\ v_2[n] \end{bmatrix} \quad (5.5)$$

represents spatially and temporally uncorrelated Gaussian noise with zero mean and covariance $\mathcal{E}\{\mathbf{v}[n]\mathbf{v}^H[n]\} = \sigma_v^2\mathbf{I}$. The parameter N in (5.3) is the length of the MIMO channel in (5.4) such that $\mathbf{H}_{n,\nu} = \mathbf{0} \quad \forall n \geq N$.

MIMO Equaliser

For equalisation, we group the four subequalisers shown in Fig. 5.2 into two equalisers \mathbf{w}_i , $i \in \{1, 2\}$, each responsible for the i th output of the MIMO equaliser,

$$\mathbf{w}_i = \begin{bmatrix} \mathbf{w}_{i,1} \\ \mathbf{w}_{i,2} \end{bmatrix} \quad (5.6)$$

with

$$\mathbf{w}_{i,j}^H = [w_{i,j}[0] \quad \cdots \quad w_{i,j}[L-1]], \quad \{i, j\} \in \{1, 2\}. \quad (5.7)$$

Similarly, the received samples from the j th receive antenna sitting in the tap delay line of the subequaliser,

$$\mathbf{r}_j^T[n] = [r_1[n] \quad \cdots \quad r_1[n-L+1]] \quad , \quad (5.8)$$

are concatenated into

$$\mathbf{r}[n] = \begin{bmatrix} \mathbf{r}_1[n] \\ \mathbf{r}_2[n] \end{bmatrix} \quad . \quad (5.9)$$

With this notation, the outputs $y_i[n]$, $i \in \{1, 2\}$, of the equaliser in Fig. 5.2 over two successive symbol periods n and $n + 1$ can be written as

$$\begin{bmatrix} y_1[n] & y_1[n + 1] \\ y_2[n] & y_2[n + 1] \end{bmatrix} = \begin{bmatrix} \mathbf{w}_1^H \\ \mathbf{w}_2^H \end{bmatrix} \cdot [\mathbf{r}[n] \quad \mathbf{r}[n + 1]]. \quad (5.10)$$

For successful equalisation, the equaliser output should match the channel input in an appropriate sense, and also reflect the STBC structure in (5.2). We will use these properties to construct a suitable cost function next.

5.1.2 PDF-Matching Based Cost Function

Cost Function Structure

The proposed cost function is based on the idea of blindly equalising several signals, leading to a cost term which is here related to fitting the PDFs of the equaliser outputs to a desired PDF according to [73, 82]. The danger of applying a blind criterion to every equaliser output $y_i[n]$ is that the strongest received signal can be extracted multiple times to the detriment of weaker signals. In order to discourage multiple signal extraction, in [62] a cross-correlation criterion is added to the cost function which enforces the recovery of uncorrelated data streams. For STBC-CMA [93], this cross-correlation can be translated into an orthogonality condition ξ_{\perp} of the two transmitted STBC signals. A similar approach is taken with the proposed algorithm (STBC-PDF), resulting in a combined cost function

$$\xi = \alpha \sum_{i=1}^{N_{\text{Tx}}} \xi_{\text{PDF},i} + (1 - \alpha)\xi_{\perp}, \quad (5.11)$$

where $\xi_{\text{PDF},i}$ is the criterion to force the i th output to attain a specific desired PDF, with $N_{\text{Tx}} = 2$ the number of transmitted symbols within the period of one STBC block. The

parameter $0 \leq \alpha \leq 1$ controls the weighting between the two cost terms.

In the following, the PDF-fitting criterion for the extraction of signals at the equaliser outputs $y_i[n]$ is outlined, followed by comments on the orthogonality condition to discourage multiple signal extraction.

PDF-Fitting Cost Function Component

The idea of this approach is to measure the difference between the PDFs $p_A(z)$ and $p_B(z)$ [73] of two random variables A and B ,

$$\xi_{\text{PDF}} = \int_{-\infty}^{\infty} (p_A(z) - p_B(z))^2 dz \quad . \quad (5.12)$$

Applying this method below requires us to replace the true PDFs with estimates. Here, the variable whose PDF is estimated at the equaliser output is the squared magnitude value $|y_i[n]|^2$, in close relation to the constant modulus algorithm. The estimation of this PDF is based on the Parzen window method, whereby a smooth PDF estimate is achieved by replacing a sample $|y_i[n]|^2$ by a kernel function centred at its location. We here select a Gaussian kernel $K_\sigma(z)$ with variance σ ,

$$K_\sigma(z) = \frac{1}{\sqrt{2\pi}\sigma} e^{-\frac{z^2}{2\sigma^2}}, \quad (5.13)$$

such that the PDF estimate over a window of L output samples is given by

$$\hat{p}_{|y_i[n]|^2}(z) = \frac{1}{L} \sum_{l=0}^{L-1} K_\sigma(z - |y_i[n-l]|^2) \quad . \quad (5.14)$$

The larger the window length L , the more confident the PDF estimate will be. However, a trade-off exists, as during adaptation the output statistics may not be stationary, therefore

limiting L to an interval within which the statistics can be assumed quasi-stationary.

The PDF estimate $\hat{p}_{|y_i[n]|^2}(z)$ will be compared to the PDF of the squared moduli of the transmitted signals, $|s_i[n]|^2$, subject to the same Gaussian kernel $K_\sigma(z)$ [72]. An advantage of convolving the discrete PDF of $|s_i[n]|^2$ defined by the constellation points of $s_i[n]$ with the kernel is that the resulting PDF exhibits a spread around constellation points akin to the influence of channel noise. Given the model of AWGN as outlined above, the PDF of squared moduli would be a superposition of chi-square distributions, which subsequently might provide a more appropriate kernel. However, we here follow the suggestion of a Gaussian kernel in [72] as this will lead to simplifications that are required for a solution with low computational cost. Therefore, the convolution with the Gaussian kernel yields the desired PDF

$$\hat{p}_{|s_i|^2}(z) = \frac{1}{M} \sum_{m=1}^M K_\sigma(z - |s_{i,m}|^2) \quad , \quad (5.15)$$

where $s_{i,m}$, $m \in \{1, 2, \dots, M\}$, are the M constellation points of the i th transmitted signal.

By exploiting the fact that for Gaussian kernels [72]

$$\int_{-\infty}^{\infty} K_\sigma(z - z_1) K_\sigma(z - z_2) dz = K_{\sqrt{2}\sigma}(z_1 - z_2) \quad , \quad (5.16)$$

the matched-PDF component of the cost function for the i th equaliser output simplifies for $L = 1$ [73], such that

$$\xi_{\text{PDF},i}[n] = -\frac{1}{M} \sum_{m=1}^M K_{\sqrt{2}\sigma}(|y_i[n]|^2 - |s_{i,m}|^2) \quad . \quad (5.17)$$

The cost function component in (5.17) is depicted in Figure 5.3 in dependency of a single complex valued coefficient. Similar to the CMA, the cost function exhibits a manifold of

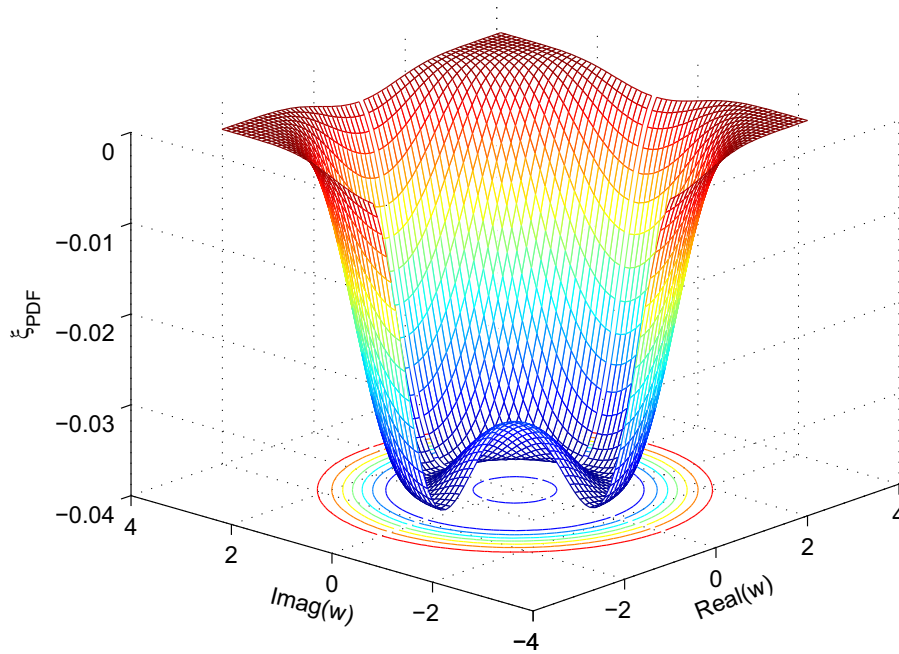


Figure 5.3: The PDF-matching cost function for one output. Part of the surface has been removed to visualise the shape near the origin.

optimum solutions due to its phase ambiguity.

Orthogonality Condition

Applying the PDF matching criterion to both equaliser outputs could potentially lead to the multiple extraction of only the strongest signal. Therefore, an additional constraint such as the minimisation of the cross-correlation between the equaliser outputs needs to be included into the cost function [62]. The orthogonality of the STBC structure provides a good condition which does not require the approximation of the cross-correlation over a window of data, but can be directly applied to data collected over two consecutive time slots [93].

Based on (5.2), in the absence of noise and for perfect equalisation we have $y_1[n] =$

$y_2^*[n+1] = s[n]$ and $y_2[n] = -y_1^*[n+1] = s[n+1]$. Thus the vector

$$\mathbf{a}_n = \begin{bmatrix} y_1[n] & -y_2^*[n+1] \\ y_2[n] & +y_1^*[n+1] \end{bmatrix} \quad (5.18)$$

provides a suitable measure of orthogonality, such that

$$\xi_{\perp} = \mathbf{a}_n^H \mathbf{a}_n \quad . \quad (5.19)$$

If two orthogonal sequences are extracted, then the measure in (5.19) will be zero. As the PDF-matching criterion is insensitive to the phase of the signals, the outputs $y_i[n]$ can be subject to an arbitrary rotation commonly found with constant modulus-type algorithms. If we introduce a rotation angle φ_i for the i th equaliser output

$$\mathbf{a}_n = \begin{bmatrix} y_1[n]e^{j\varphi_1} & -y_2^*[n+1]e^{-j\varphi_2} \\ y_2[n]e^{j\varphi_2} & +y_1^*[n+1]e^{-j\varphi_1} \end{bmatrix}, \quad (5.20)$$

and assume perfect equalisation $y_i[n] = s_i[n]$, then

$$\mathbf{a}_n^H \mathbf{a}_n = 0 \quad \iff \quad \varphi_1 = -\varphi_2 + 2\pi k \quad (5.21)$$

with $k \in \mathbb{Z}$. Thus, if the total cost function is minimised, the phase ambiguity of the PDF fitting cost function component is complemented by (5.21), enforcing the orthogonality component such that the equaliser outputs can be expected to match the transmitted signals save of opposite phase shifts.

Overall Cost Function

With the PDF fitting and orthogonality condition defined, the complete cost function outlined in (5.11) can be approximated as

$$\hat{\xi}_n = -\frac{\alpha}{M} \sum_{i=1}^2 \sum_{\nu=0}^1 \sum_{m=1}^M K_{\sqrt{2}\sigma} (|y_i[n+\nu]|^2 - |s_{i,m}|^2) + (1-\alpha) \mathbf{a}_n^H \mathbf{a}_n \quad . \quad (5.22)$$

The PDF fitting component has an additional summation over two contributions, as the STBC code as defined in (5.2) extends over two symbol periods.

5.1.3 Stochastic Gradient Algorithm

Based on the cost function in (5.22), this section addresses the problem of adjusting the equaliser. We choose a stochastic gradient approach whereby updating occurs for every STBC block spanning two symbol periods. The coefficients of the i th equaliser are updated using the stochastic gradient descent method,

$$\mathbf{w}_i[n+2] = \mathbf{w}_i[n] - \mu_{\text{PDF}} \nabla_{\mathbf{w}_i^*} \hat{\xi}_n, \quad (5.23)$$

where $\nabla_{\mathbf{w}_i^*}$ denotes the gradient with regard to \mathbf{w}_i^* , and μ_{PDF} is the step size. The gradient terms of $\hat{\xi}_n$ relating to the PDF and the orthogonality enforcing components are derived separately below.

PDF Term

The derivative of the PDF term with respect to \mathbf{w}_i^* is given by

$$\frac{\partial}{\partial \mathbf{w}_i^*} \xi_{PDF|i}[n] = \frac{1}{M} \sum_{m=1}^M K'_{\sqrt{2}\sigma}(|y_i[n]|^2 - |s_{i,m}|^2) y_i^*[n] \mathbf{r}_n, \quad (5.24)$$

where

$$K'_{\sqrt{2}\sigma}(z) = \frac{\partial}{\partial z} K_{\sqrt{2}\sigma}(z) = -\frac{1}{4\sigma^2} K_{\sqrt{2}\sigma}(z) \quad (5.25)$$

is the derivative of the Gaussian kernel (5.13). In order to simplify the derivative, we assume all the points in the transmit constellation to have the same modulus, i.e. $|s_{i,m}|^2 = \gamma^2$, for $m = 1, \dots, M$. Thus, the summation and division by M in (5.24) is spurious. Evaluating the derivative K'_σ in (5.24) and rearranging terms leads to

$$\frac{\partial}{\partial \mathbf{w}_i^*} \xi_{PDF|v}[n] = \begin{cases} K_{\sqrt{2}\sigma}(|y_i[n]|^2 - \gamma^2) e^*[n] \mathbf{r}_n & v = i \\ \mathbf{0} & v \neq i, \end{cases} \quad (5.26)$$

where

$$e^*[n] = \frac{1}{4\sigma^2} (|y_i[n]|^2 - \gamma^2) y_i^*[n], \quad (5.27)$$

and $K_{\sqrt{2}\sigma}(z)$ is the Gaussian kernel used for the Parzen estimator as defined in (5.13) [72, 98]. It is the addition of this kernel term that distinguishes this part of the cost function gradient shown in (5.26) from a standard CM algorithm.

Orthogonality Condition

Note that the second part of the cost function (5.11), ξ_\perp , has the same functionality as the orthogonality-enforcing term of the STBC-CMA cost function, as defined in (5.19), [93]. The gradient of the term with regard to the space-time equalisers \mathbf{w}_i , $i \in \{1, 2\}$, is given by

$$\begin{aligned} \frac{\partial}{\partial \mathbf{w}_1^*} \xi_\perp &= (y_1^*[n] - y_2[n+1]) \mathbf{r}_n + (y_2[n] + y_1^*[n+1]) \mathbf{r}_{n+1} \\ \frac{\partial}{\partial \mathbf{w}_2^*} \xi_\perp &= (y_2^*[n] + y_1[n+1]) \mathbf{r}_n + (y_2^*[n+1] - y_1[n]) \mathbf{r}_{n+1}. \end{aligned} \quad (5.28)$$

Inserting the combined terms (5.26) and (5.28) into (5.23) provides the update equation of the proposed algorithm. The constants arising e.g. from the differentiation of the kernel can be absorbed into the step size μ .

5.1.4 Algorithm Performance

This section provides details of the parameters of the algorithm and a comparison of its computational complexity, followed by simulations whose results are benchmarked against existing methods.

Computational Complexity

Tab. 5.1 lists the computational complexity of the STBC-PDF together with the STBC-CMA [93] and a fast converging, highly complex variant of the STBC-CMA based on a recursive Quasi-Newton update. The metric used here is to count complex multiply-accumulates (MAC) for every iteration n . The difference between the STBC-PDF and the STBC-CMA is the evaluation of the Gaussian kernel in the update equation. The Gaussian kernel can be approximated by a MacLaurin series [80] with only relatively few MACs but poor behaviour for larger arguments to the kernel. The best results we obtained by implementing the Gaussian function as a look-up table which requires memory and comparisons, but only one multiplication.

As shown in Table 5.1, the RQN equaliser's complexity is of the order $\mathcal{O}(L_w^2)$ whereas the

STBC-CMA	STBC-RQN-CMA	STBC-PDF
$24L_w + 4$	$36L_w^2 + 26L_w + 59$	$24L_w + 6$

Table 5.1: Complexity of the different equalisers, in number of complex multiply-accumulate (MAC) operations per iteration.

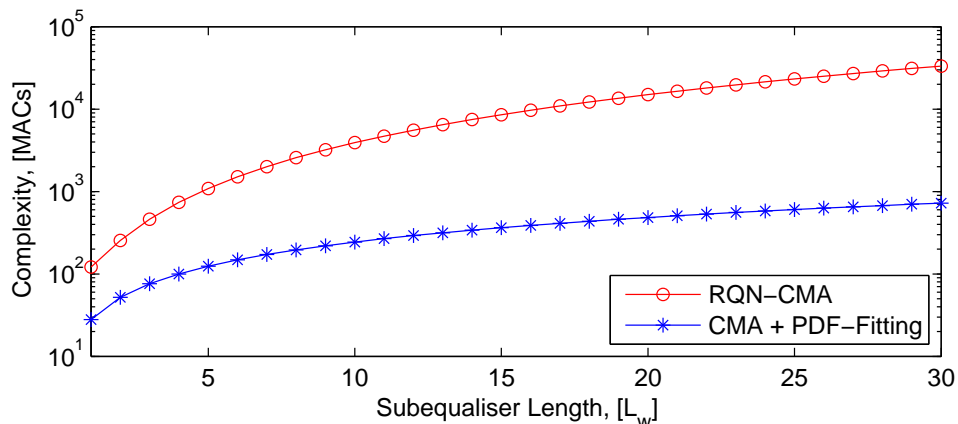


Figure 5.4: Complexity of the different equalisers, in number of complex multiply-accumulate (MAC) operations per iteration.

complexities of the STBC-CMA and the STBC-PDF schemes are of the order $\mathcal{O}(L_w)$. The complexity of the different equalisers is visualised in Fig. 5.4 as a function of the subequaliser length L_w . Both STBC-CMA and the STBC-PDF have very similar computational cost.

Channel Description and Transmission Parameters

A 2×2 MIMO model as indicated in Fig. 5.2 is used for simulations. It comprises of four dispersive channel impulse responses of length $L_h = 4$ obeying the delay-power profile characterised in Tab. 5.2. Simulations are performed over an ensemble of 100 MIMO channels whose coefficients are drawn from complex Gaussian distributions with variances defined by Tab. 5.2. QPSK modulation is used at the transmitter with a modulus equal to unity. At the receiver, signals are corrupted by AWGN at an SNR of 20dB. The length of the subequalisers $\mathbf{w}_{i,j}$, $i, j \in \{1, 2\}$ is set to $L_w = 11$, and they are initialised to zero with only the middle tap

delay	T_s	$2T_s$	$3T_s$	$4T_s$
strength [dB]	0	-3	-5	-7

Table 5.2: Delay-power profile of the MIMO system's channel impulse responses

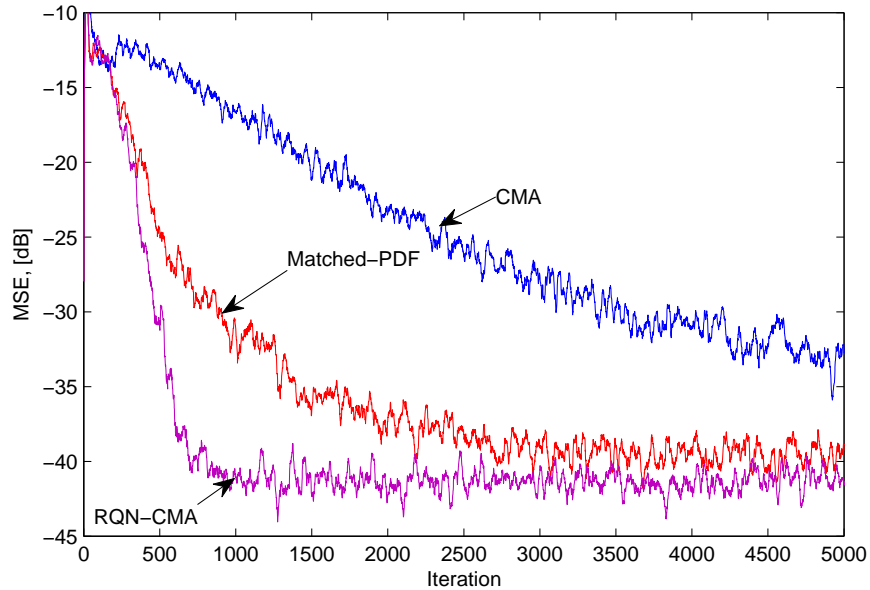


Figure 5.5: MSE curves of STBC-PDF and STBC-CMA

of each subequaliser set to unity. The step sizes for the various algorithms were selected such that they provided the approximately fastest yet still stable convergence across all channel realisations.

Simulation Results

Figure 5.5 shows the mean square error (MSE) curve of the STBC-PDF compared to those of the STBC-CMA and the RQN implementation at SNR = 20dB, whereby potential rotations as outlined in (5.21) have been compensated with respect to the steady-state performance. The results show that the MSE convergence of the PDF Matching Algorithm reaches the steady-state after fewer iterations compared to the STBC-CMA, while the RQN equaliser shows the fastest convergence but at the expense of a significantly higher computational complexity.

5.1.5 Summary

A novel algorithm has been derived for the blind adaptive equalisation of STBC over frequency selective channels. The proposed cost function is based on minimizing the distance between the estimated PDF of the equaliser output and a desired PDF, and is complemented by an additional term that ensures the STBC structure and hence orthogonality of the equaliser outputs. A low-cost stochastic gradient update was derived based on this cost function.

The complexity of the derived algorithm was found to be comparable to the STBC-CMA, but the proposed method exhibited a faster convergence close to the performance of the fast but very costly recursive quasi-Newton version of the STBC-CMA.

5.2 MIMO TR-STBC Based on PDF Matching

In order to achieve the maximum diversity in a doubly-dispersive environment, a number of variations on the classical STBC encoding have been proposed. OFDM can decompose a frequency-selective channel by introducing subcarriers and a cyclic prefix into a number of individual narrowband transmission channels, which can each be STBC encoded [89, 90]. The drawback of OFDM systems is in general the sensitivity to synchronization errors and their large peak-to-average power ratio [91]. The orthogonality of OFDM is also destroyed by time variations of the channel, such that the channel must be approximately stationary over the length of an OFDM symbol.

Single-carrier time domain approaches were first proposed in [90], whereby the STBC structure was applied to a window of symbols, which is, after a guard interval, repeated as a complex conjugate and time reversed version [92, 95]. However, time-reversal (TR) STBC is

sensitive if the channel is doubly-dispersive, e.g. frequency selective and time-varying [93].

The proposed blind equalisation scheme for TR-STBC in [96] showed slow convergence which might not be suitable for non-stationary channels. In order to increase the convergence speed of the TR-STBC-CMA algorithm, various algorithmic variations have been evaluated, including the conjugate gradient search method [97], and the fast Quasi-Newton (FQN) approach [22], which has been shown to be superior in terms of convergence speed compared to the conjugate gradient approach [22]. Unfortunately, both CG-TR-STBC and RQN-TR-STBC methods require a considerable computational effort, which hinders their application to TR-STBC.

In this section we intend to apply the low cost PDF matching algorithm to target the equalisation of a TR-STBC MIMO system, TR-STBC-PDF.

5.2.1 Channel and Signal Model

Burst Structure and TR-STBC Data Model

Considering a system with two transmit and two receive antennas, the transmitted data is divided into odd and even symbol sequences, depicted here in two sets of symbols $a_1[n]$ and $a_2[n]$, respectively. $a_1[n]$ and $a_2[n]$ are transmitted in blocks between preamble and postamble sequences $P[n]$; these guard periods are inserted in order to combat the effects of ISI. Data is transmitted in bursts as shown in Fig. 5.6, where L_s , L_a and L_p are the lengths of the burst, the source data and the guard period, respectively, which satisfy $L_a > L_p > 1$ and $L_p > L_h$, with L_h being the length of the longest multipath channel.

During the regular burst, $s_1[n]$ and $s_2[n]$ are transmitted from first and second antennas, respectively. During the reverse burst, the sequences are time reversed and conjugated, $-s_2^*[n]$ and $s_1^*[n]$. The data model is shown in Fig. 5.7, where $*$ is a non-linear function

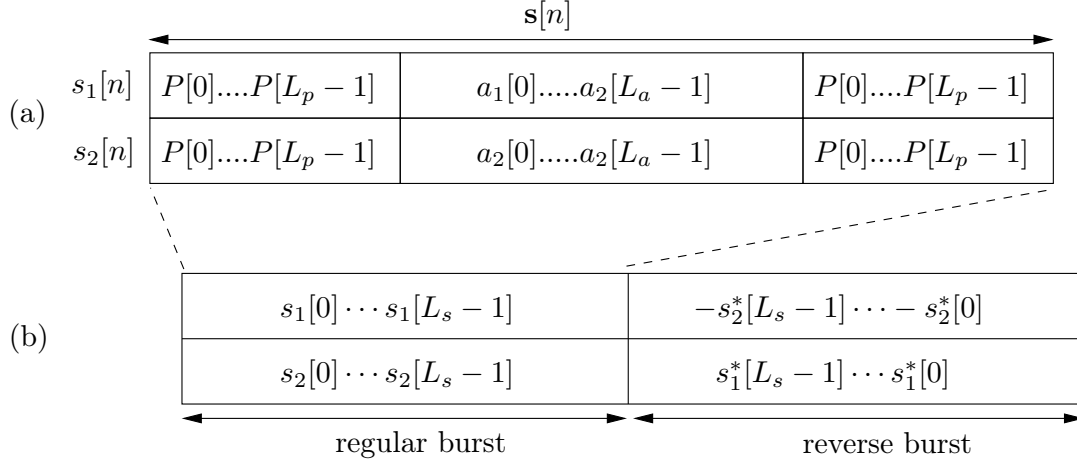


Figure 5.6: Block structure in Time-Reversal STBC: (a) regular burst, (b) regular and reverse bursts.

denoting complex conjugation and the TR is a linear but time varying function denoting time reversal.

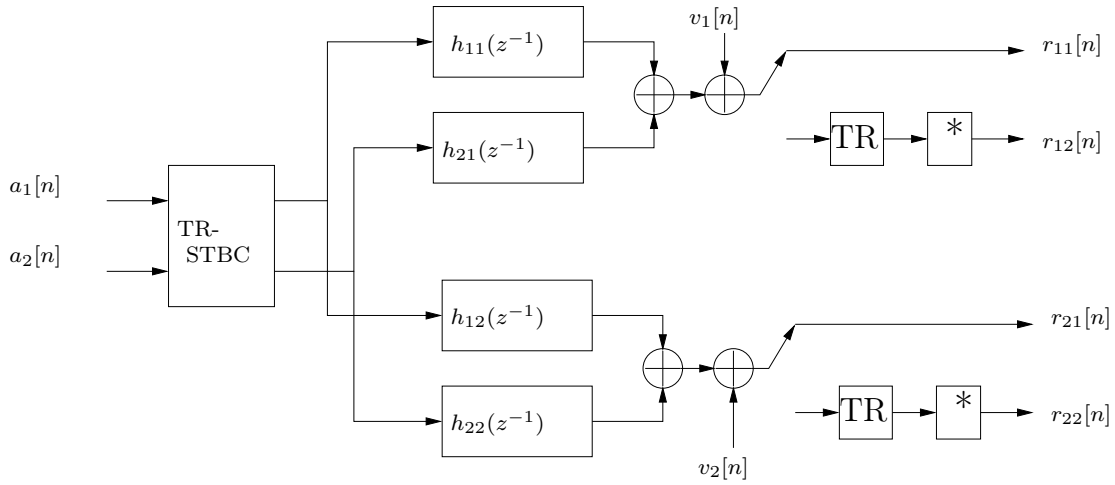
Let $\mathbf{r}[n]$ be the received signal of dimension 4×1 ,

$$\mathbf{r}[n] = [r_{11}[n] \quad r_{21}[n] \quad \tilde{r}_{12}[n] \quad \tilde{r}_{22}[n]]^T, \quad (5.29)$$

where $r_{i1}[n]$ and $r_{i2}[n]$ are the signals picked up by the i th antenna during the regular and reverse modes of transmission, respectively. It can be observed that the signals received during the second phase of transmission are conjugated and time reversed to produce $\tilde{r}_{12}[n]$ and $\tilde{r}_{22}[n]$ as depicted in the block diagram of Fig. 5.7. The vector $\mathbf{r}[n]$ can be written as

$$\mathbf{r}[n] = \sum_{\tau=0}^{L_h-1} \mathbf{H}[\tau] \mathbf{s}[n - \tau] + \mathbf{v}[n], \quad (5.30)$$

where $\mathbf{v}[n]$ is the additive white Gaussian noise vector, $\mathbf{s}[n] = [s_1[n] \quad s_2[n]]^T$. Note that the received signals contain contributions from both transmitted signals. In other words, the detection of $s_1[n]$ and $s_2[n]$ is coupled. Assuming the channel is stationary over the regular

Figure 5.7: Data model for a 2×2 TR-STBC system

and reverse bursts, $\mathbf{H}[\tau]$ is the τ th matrix valued coefficient of the polynomial channel matrix $\mathbf{H}(z)$,

$$\mathbf{H}(z) = \begin{bmatrix} \mathbf{h}_1(z) & \mathbf{h}_2(z) \\ \mathbf{h}_2^*(z^{-1}) & -\mathbf{h}_1^*(z^{-1}) \end{bmatrix}, \quad (5.31)$$

with,

$$\mathbf{h}_i(z) = \begin{bmatrix} h_{i1}(z) \\ h_{i2}(z) \end{bmatrix}, \quad (5.32)$$

where $h_{ij}(z)$ is the z-transform of the frequency selective channel from the j th transmit antenna to the i th receive antenna,

$$h_{ij}(z) \bullet \circ h_{ij}[n] \quad (5.33)$$

$$h_{ij}(z) = \sum_{n=-\infty}^{\infty} h_{ij}[n]z^{-n}. \quad (5.34)$$

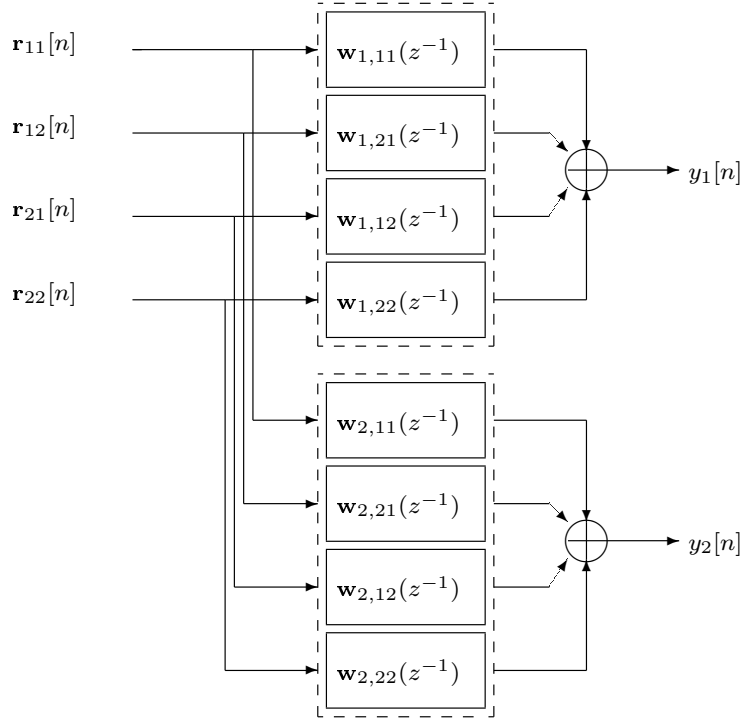


Figure 5.8: Equaliser structure for Time-Reversal STBC.

The length of the channels is assumed to be identical, denoted L_h .

Equaliser Structure

As shown in Fig. 5.8, two space-time equalisers, $\mathbf{w}_1[n]$ and $\mathbf{w}_2[n]$, are used to retrieve the transmitted data. Each space-time equaliser consists of four adaptive FIR filters of length L_w . At the n th iteration, the weight vector of the i th space-time equaliser is given by

$$\mathbf{w}_i[n] = \begin{bmatrix} \mathbf{w}_{i,11}^*[n] \\ \mathbf{w}_{i,21}^*[n] \\ \mathbf{w}_{i,12}^*[n] \\ \mathbf{w}_{i,22}^*[n] \end{bmatrix}, \quad (5.35)$$

and the corresponding output is,

$$y_i[n] = \mathbf{w}_i^H[n] \mathbf{r}_n, \quad (5.36)$$

where the regressor vector of the equaliser is given by

$$\mathbf{r}[n] = [\mathbf{r}_{11,n}^H \quad \mathbf{r}_{21,n}^H \quad \mathbf{r}_{12,n}^H \quad \mathbf{r}_{22,n}^H]^H, \quad (5.37)$$

with $\mathbf{r}_{ji,n} = [r_{ji}[n] \ r_{ji}[n-1] \ \cdots \ r_{ji}[n-L+1]]^T$.

For successful equalisation, the equaliser output should match the channel input in an appropriate sense, and also reflect the TR-STBC structure in Fig. 5.6. These properties will be used to construct a suitable cost function.

5.2.2 Cost Function

For the 2×2 TR-STBC-PDF MIMO system, the cost function was derived following the same steps as in STBC-PDF which has led to (5.17).

Choosing a stochastic gradient approach, the equaliser weights can be calculated as follows,

$$\hat{\nabla}_{w_1} \xi_{\text{PDF}} = \frac{1}{\sqrt{2\pi}} \left\{ e_1^*[n] \mathbf{r}_n e^{-\frac{(|y_1[n]|^2 - \gamma^2)^2}{2\sigma^2}} + e_2[n] \mathbf{P} \mathbf{r}_n^* e^{-\frac{(|y_2[n]|^2 - \gamma^2)^2}{2\sigma^2}} \right\}, \quad (5.38)$$

where

$$e_i[n] = (|y_i[n]|^2 - \gamma^2) y_i[n], \quad \text{for } i = 1, 2 \quad (5.39)$$

and

$$\mathbf{P} = \begin{bmatrix} 0 & 0 & -\tilde{\mathbf{I}}_{L_w} & 0 \\ 0 & 0 & 0 & -\tilde{\mathbf{I}}_{L_w} \\ \tilde{\mathbf{I}}_{L_w} & 0 & 0 & 0 \\ 0 & \tilde{\mathbf{I}}_{L_w} & 0 & 0 \end{bmatrix}, \quad (5.40)$$

with $\tilde{\mathbf{I}}_{L_w}$ being the reverse-identity matrix of size $L_w \times L_w$, e.g. $\tilde{\mathbf{I}}_2 = \begin{bmatrix} 0 & 1 \\ 1 & 0 \end{bmatrix}$.

The equaliser weights can be adjusted according to,

$$\mathbf{w}_1[n+1] = \mathbf{w}_1[n] - \mu_{\text{PDF}} \hat{\nabla}_{w_1} \xi_{\text{PDF}}, \quad (5.41)$$

where ∇_{w_1} denotes the gradient with regard to $\mathbf{w}_1[n]$, and μ_{PDF} is the step size.

The constants arising from the differentiation can be absorbed into the new step size $\tilde{\mu}_{\text{PDF}} = \frac{1}{\sqrt{2\pi}}\mu_{\text{PDF}}$ leading to,

$$\mathbf{w}_1[n+1] = \mathbf{w}_1[n] - \tilde{\mu}_{\text{PDF}} [e_1^*[n]a_1[n]\mathbf{r}_n + e_2[n]a_2[n]\mathbf{P}\mathbf{r}_n^*], \quad (5.42)$$

with

$$a_i[n] = e^{-\frac{(|y_i[n]|^2 - \gamma^2)^2}{2\sigma^2}}, \quad \text{for } i = 1, 2 \quad . \quad (5.43)$$

The relation between $w_2[n]$ and $w_1[n]$ for TR-STBC-Matched-PDF is similar to that in the Tap-Constrained-CMA for TR-STBC [96],

$$\mathbf{w}_2[n] = \mathbf{P}^T \mathbf{w}_1[n] \quad . \quad (5.44)$$

Parameters	Conjugate Gradient	FQN-CMA	TR-STBC-PDF
Remembrance factor	n/a	$\alpha_{fqn} = 0.999$	n/a
Standard deviation (Kernel Size)	n/a	n/a	$\sigma = 1$
Window of output sizes	n/a	n/a	$L = 1$
Transmit constellations	QPSK	QPSK	QPSK
Step size	$\mu_{CG} = 3 \times 10^{-4}$	$\mu_{FQN} = \frac{1}{4[\mathbf{r}^H \hat{\mathbf{R}}_{rr}^{-1} \mathbf{r} + \epsilon]}$ $\epsilon = 0.002$	$\mu_{PDF} = 2 \times 10^{-3}$
Equaliser length	$L_w = 15$	$L_w = 15$	$L_w = 15$
Correlation Matrix Estimate Initialization	n/a	$\hat{\mathbf{R}}_{rr}[0] = \mathbf{I}_{4L_w}$	n/a

Table 5.3: Simulation parameters for the different blind equalisers.

5.2.3 Algorithm Performance

This section provides details of the parameters of the algorithm, followed by simulations whose results are benchmarked against existing methods.

Implementation Details

Computer simulations have been performed in order to evaluate the performance improvement achieved by the TR-STBC-PDF equaliser. QPSK symbol mapping was used with a modulus equal to $\sqrt{2}$. An appropriate burst length was chosen to allow time for the equalisers to converge, and 1000 channel realizations were drawn from a correlated Rayleigh distribution with a normalized maximum Doppler frequency $f_d = 100\text{Hz}$, the random samples were correlated to correspond to a vehicular speed of 55km/hour. Subequalisers of order 15 were used in the simulations. The first space-time equaliser $w_1[n]$ was initialized using the central spike technique and the step sizes for the various algorithms were selected such that they provided the approximately fastest yet still stable convergence across all channel realisations. The remaining parameters were initialised according to Table 5.3.

Simulation Results

Figure 5.9 shows the MSE curves for the different TR-STBC equalisers. It can be clearly observed that the TR-STBC-PDF outperforms the standard Tap-Constrained CMA in terms of convergence speed. The FQN algorithm shows faster convergence than all other methods, followed closely by the TR-STBC-PDF.

Figure 5.10 shows the BER achieved by the different equalisers with respect to the burst length at SNR = 10dB. The channel was varied after two bursts of size 256 symbols. The channel coefficients were drawn from a 3-tap doubly dispersive Rayleigh channel with maximum Doppler frequency $f_d = 100\text{Hz}$, corresponding to a vehicular speed of 55km/hour. Comparing the performance of the simulated equalisers, a gradual decrease in the BER is observed as we move from one equaliser to the other in the same order as in the MSE performance. This translates to faster adaptation to channel variations. However, even with the FQN implementation, a burst size of at least 150 symbols is required to achieve a BER lower than 10^{-2} . This implies the channel has to be stationary over a duration longer than 300 symbols. Hence, TR-STBC with blind equalisation is generally not suitable for fast time-varying channels.

5.2.4 Complexity Study

To fairly evaluate the performance gain, the complexity of the different algorithms must be considered. Table 5.4 shows the number of complex MAC operations required by the TR-STBC-PDF and other implementations of the TR-STBC-CMA in terms of the space time (ST) equaliser of order $L_{st} = MNL_w = 4L_w$ for every iteration n . The multiplication by matrix \mathbf{P} has been ignored because it is a permutation matrix that can be implemented by indexing.

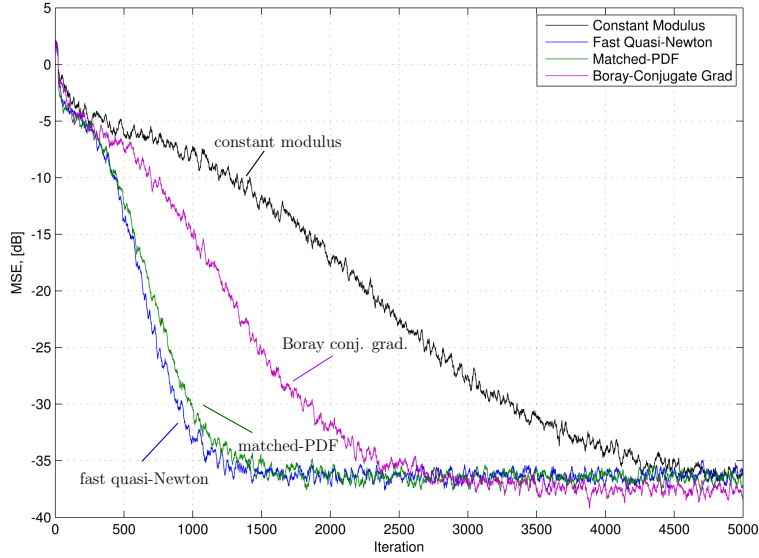


Figure 5.9: MSE curves for the different implementations of the TR-STBC-CMA

In Table 5.4, the number of recursions for the CG scheme is assumed to be $m = 5$. The division operation can be performed in a number of MACs equal to the wordlength, which is assumed 16 here. In the FQN-CMA column, the Levinson-Durbin Recursion is evaluated to invert the covariance matrix once every L_w iterations. The TR-STBC-PDF algorithm requires evaluation of the exponentials in addition to the complexity of the CMA in Table 5.4. The complexity of the exponential can be ignored assuming the use of a look-up table, where the accuracy of the result depends on the size of memory allocated to the table. Hence, the added complexity compared to the standard STBC-CMA is only one complex MAC operation for each output.

Figure 5.11 shows the complexity plot in terms of the equaliser order L_w . When weighting the gain against complexity, the TR-STBC-PDF algorithm stands out. For $L_w \gg 1$, its complexity approaches that of the TR-STBC-CMA, yet its performance approaches that of the FQN-CMA.

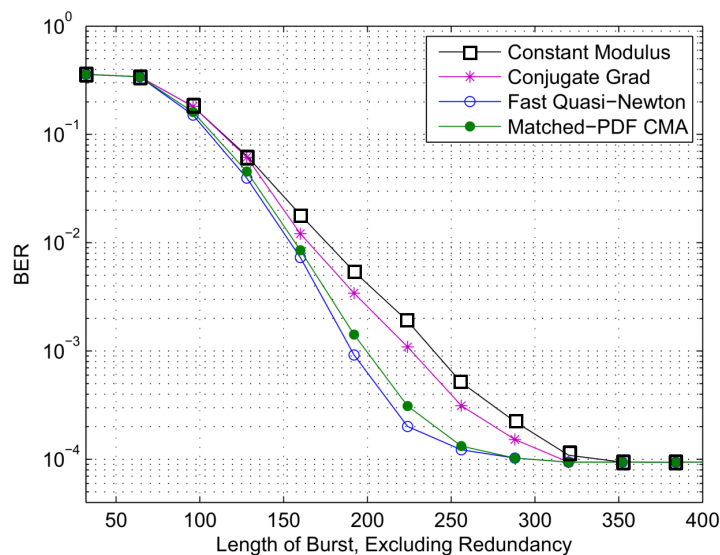


Figure 5.10: BER for the different implementations of the TR-STBC-CMA, SNR = 10dB

TR-STBC-CMA	Conjugate Gradient	FQN-CMA	TR-STBC-PDF
$4L_{st} + 6$	$47L_{st} + 116$	$4L_{st}^2 + 6L_{st} + 23$ $+C_{LDR}/L_w$	$4L_{st} + 8$

Table 5.4: Complexity of the different equalisers per iteration, in terms of complex MAC operations and the Levinson-Durbin recursion (LDR) with complexity C_{LDR} .

5.2.5 Summary

A novel algorithm (TR-STBC-PDF) has been derived for the blind adaptive equalisation of TR-STBC over doubly-dispersive channels. The proposed cost function is based on minimizing the distance between the actual PDF of the equaliser output and a desired PDF. A low-cost stochastic gradient update was derived based on this cost function. The complexity of the TR-STBC-PDF algorithm was found to be comparable to the TR-STBC-CMA, but the TR-STBC-PDF exhibited a faster convergence close to the performance of the fast but very costly recursive quasi-Newton version of the TR-STBC-CMA.

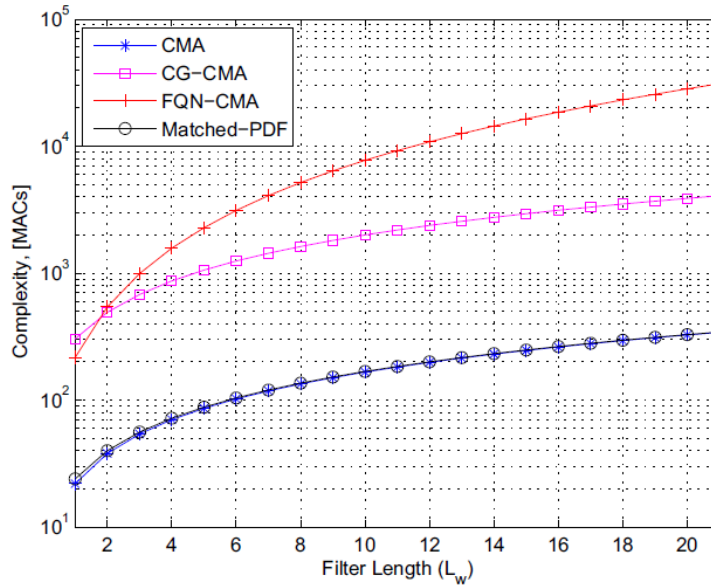


Figure 5.11: Number of MACs required per iteration for proposed algorithms.

5.3 Concluding Remarks

This chapter has looked at space-time-block-coding and time-reversal space-time-block-coding for MIMO systems under frequency selective fading channels. The tap-constrained CM receiver performs well over stationary channels but suffers from slow convergence. A different method of equalisation was investigated in this chapter, namely Matched-PDF. The proposed cost function is based on minimizing the distance between the estimated PDF of the equaliser output and a desired PDF. This equaliser has shown a fast convergence close to the performance of the Fast Quasi-Newton method, but unlike the latter its complexity was comparable to the tap-constrained CMA. However, even with this fast converging equaliser a significantly longer burst was required, for MIMO-TR-STBC as compared to MIMO-STBC, to achieve a desirable BER level. This renders the TR-STBC scheme unsuitable for use over fast time-varying channels. Furthermore, long bursts require a larger memory at the receiver, which is not always feasible.

In the next chapter, a conclusion of the work produced in this thesis will be drawn with some proposals for future work.

Chapter 6

Conclusions and Future Work

6.1 Conclusions

The main objective of this thesis was to develop blind equalisation algorithms for multiuser detection over dispersive channels. Multiuser detection has been shown to exhibit a significant improvement in capacity and spectrum efficiency over single-user detection. However, its complexity and prior knowledge requirement make it impractical for down-link (DL) transmission. Alternatively, it has been shown that blind multiuser equalisation algorithms could render multiuser detection suitable for DL applications. Motivated by the significant system capacity improvement provided by multiuser detection compared to single-user systems, the low complexity and robustness of CMA, and finally by the ability of state-of-the-art FPGA and DSP processing platforms to perform computationally complex signal processing tasks at higher sampling rates, we have investigated and proposed a robust multiuser adaptive equaliser, which has low computational complexity despite operating at the chip-level.

The general concept of adaptive filtering has been reviewed and discussed. Particular attention has been dedicated to popular algorithms such as LMS, RLS, CMA, affine projection

algorithms, and training-based and decision-directed updating schemes. We have reviewed derivations of these algorithms in a unified notational framework and highlighted some of their properties, such as their computational complexity.

A blind multiuser equalisation approach, the so-called filtered-R multiple error CM algorithm (FIRMER-CMA), has been presented. This approach has been first proposed for fully loaded systems, where it aims to enforce CM conditions on the various user signals. A stochastic gradient algorithm has been derived, which differs from previous CM algorithms by a code-prefiltering of its input. This algorithm has been extensively tested and proven itself very stable in practice. The algorithm has been modified to be implemented in different modes such as fully or partially loaded and blind and semi-blind scenarios with the latter achieved through reconfiguration for adaptation by a DD algorithm. A concurrent FIRMER-CM and DD receiver (FIRMER-CM+DD) was also developed, which takes advantage of the robustness of CMA and the fast convergence of DD in a concurrent adaptation scheme, where the slower converging CMA algorithm is complemented by a faster-converging DD step when decisions are deemed reliable. Furthermore, the FIRMER-CMA+DD algorithm can mitigate phase ambiguity found in the FIRMER-CMA case by locking the solution onto the prescribed constellation pattern through its DD mode.

By applying the APA to the concurrent filter, the so-called AP-Concurrent-CMA+DD algorithm has been formulated. This algorithm is very similar to other APA schemes, but differs in its specific application through the code filtering of the data matrix. Properties of the proposed algorithm have been investigated in simulations, and a faster convergence over the FIRMER-CMA and FIRMER-CMA+DD has been demonstrated. At the expense of a somewhat increased complexity, this blind scheme offers considerably enhanced convergence speed over previous work which makes it an attractive candidate for downlink applications.

A semi-blind equalisation approach based on the AP-Concurrent-CMA+DD algorithm

for a UMTS-TDD downlink scenario has been presented. Some unused codes in a partially loaded scenario have been exploited to load pilot signals. Supported by simulations, this pilot-assisted scheme provides continuous channel tracking and offers better convergence behaviour over the basic training equalisation even with longer training periods, whereby a gain of data rate and spectrum efficiency can be achieved. It has been shown through various simulations that the implementation of pilots enhances the system performance in terms of MSE and BER and resolves the typical CM phase ambiguity. Furthermore, a new homogeneous burst structure, which is suitable for the above pilot-assisted strategy, has been presented. The new burst structure offers a considerable gain in data rate and spectrum efficiency and ensures a continuous adaptation. Another advantage of using the proposed burst structure is that no switching is required during data transmissions, since it includes only one homogeneous field in addition to the existing guard period.

A new adaptive algorithm for blind multiuser equalisation has been developed in Chapter 4. The new cost function of this method is based on the statistical information of the transmitted sequences, by minimising the distance between the actual PDF of the equaliser output and that of the transmitted streams. This method is known as PDF-matching algorithm as it matches the PDF of the equaliser outputs to that of the transmitted sequences. The proposed method has shown faster convergence speed compared to the FIRMER-CMA using a QPSK constellation. Furthermore, the kernel size of the Parzen window estimator can be increased to accelerate the convergence speed, and once the ISI is sufficiently reduced, the kernel size can be decreased to achieve higher accuracy.

The PDF-matching algorithm has been reviewed under fast time-varying channel conditions. In simulations, the proposed method has demonstrated faster convergence speed compared to the FIRMER-CMA in constant environments. In fast time-varying systems, the proposed algorithm yields comparable performance to the FIRMER-CMA but showed a promising robustness to noise and the double dispersiveness of the channel. It can be

concluded that the proposed algorithm provides advantages over the FIRMER-CMA in constant environments while it provides a similar tracking performance when the channels are fast time-varying.

Chapter 5 has looked at space-time-block-coding (STBC) and time-reversal space-time-block-coding (TR-STBC) for MIMO systems under frequency selective channels. The tap-constrained CM receiver performs well over stationary channels but suffers from slow convergence. A different method of equalisation has been investigated in this chapter, namely PDF-matching. This equaliser has demonstrated a fast convergence and performs close to the fast quasi-Newton method, but unlike the later its complexity is comparable to tap-constrained CMA.

These developments have significantly increased the convergence speed (and tracking behaviour) compared to TR-STBC, but it has been demonstrated that further enhancements will be required to operate in fast time-varying channels; this however will be left to future endeavours.

6.2 Future Work

Based on the research outlined in this thesis, the following areas are of interest for potential further investigation:

Matched-PDF Algorithm with a Switch Between Blind and Decision-Directed

Equalisation: A switch between blind and decision directed adaptation is possible by manipulating the kernel size of the Parzen Window Estimator in the matched PDF algorithm which yields an accurate final solution [73]. Initially, a large kernel size can be employed to reinforce convergence speed. When the eye of the constellation is opened, a switch to a smaller kernel size or to decision-directed equalisation, can be performed. Therefore, adap-

tively controlling the kernel size may be a suitable approach to trade-off better between fast convergence speed and accurate steady-state performance.

Variations of the Matched PDF Algorithm: Some further combinations of the matched-PDF algorithm with other techniques are worth investigating with the aim to further improve the equaliser performance, including concurrent matched-PDF and decision directed operation. Since our proposed matched-PDF is based on the CM criterion, it is prone to achieve only moderate levels of MSE after convergence, which may not be sufficiently low for the system to attain adequate BER performance. A possible solution is to operate the DD equaliser concurrently with the matched-PDF rather than switching to a DD adaptation after the Matched-PDF has converged.

Another possibility is to operate the matched-PDF algorithm with an affine projection algorithm, since the DD part in the concurrent Matched-PDF+DD is only updated if the DD step is considered secure. Hence the adaptation is generally governed by Matched-PDF rather than DD. A possible solution to this problem is to accelerate Matched-PDF by adopting the concept of the affine projection algorithm. A concurrent matched-PDF and DD adaptation with affine projection is also worth investigating as the APA offers a flexible choice of the projection order and therefore enables different convergence speeds.

Matched-PDF algorithm for partially loaded systems: It will be interesting to see how a pilot assisted implementation of the matched-PDF algorithm affects the equalisation of a partially loaded system. In a partially loaded scenario, a number of inactive users are exploited to load pilot signals in order to enhance the system tracking performance, and we expect the pilots to enhance the system performance in terms of MSE and BER.

AP-FIRMER-CMA+DD and Matched-PDF algorithms for 5G New Radio: For 5G, most proposals are based on filter bank multi-carrier systems. In such systems, a filter bank trans-multiplexer is employed with a dispersive channel. At the receiver, equalisation

and synchronisation are required. It will be interesting to see how the schemes investigated in this thesis (AP-FIRMER-CMA+DD and Matched-PDF) can be applied to mitigate the effects of the dispersiveness of multi-carrier systems of the next generations.

Appendices

Appendix A

Wirtinger's Calculus

For a general function $f(w)$ of the complex variable $w = w_r + jw_i \in \mathbb{C}$, where w_r and w_i are the real and imaginary parts of w respectively, with $j = \sqrt{-1}$ and the assumption of statistical independence of real and imaginary parts. Using the definition of w and its complex conjugate w^* , we may express the real quantities w_r and w_i in terms of the pair of complex-conjugate coordinates w and w^* .

$$w_r = \frac{1}{2}(w + w^*), \quad (\text{A.1})$$

and

$$w_i = \frac{1}{2j}(w - w^*). \quad (\text{A.2})$$

where the asterisk denotes complex conjugation.

Using Wirtinger vector valued calculus [10, 99, 100], we may define certain complex derivatives in terms of the real derivatives $\frac{\partial}{\partial w_r}$ and $\frac{\partial}{\partial w_i}$

$$\frac{\partial}{\partial w} = \frac{1}{2} \left(\frac{\partial}{\partial w_r} - j \frac{\partial}{\partial w_i} \right) \quad (\text{A.3})$$

and

$$\frac{\partial}{\partial w^*} = \frac{1}{2} \left(\frac{\partial}{\partial w_r} + j \frac{\partial}{\partial w_i} \right) \quad (\text{A.4})$$

Hence, the function $f(w)$ can give the following derivatives

$$\frac{\partial f(w)}{\partial w} = \frac{1}{2} \left(\frac{\partial f(w)}{\partial w_r} - j \frac{\partial f(w)}{\partial w_i} \right) \quad (\text{A.5})$$

$$\frac{\partial f(w)}{\partial w^*} = \frac{1}{2} \left(\frac{\partial f(w)}{\partial w_r} + j \frac{\partial f(w)}{\partial w_i} \right) \quad (\text{A.6})$$

Applying these two equations we can find

$$\begin{aligned} \frac{\partial w}{\partial w} &= \frac{1}{2} \left(\frac{\partial w}{\partial w_r} - j \frac{\partial w}{\partial w_i} \right) \\ &= \frac{1}{2} \left(\frac{\partial(w_r + jw_i)}{\partial w_r} - j \frac{\partial(w_r + jw_i)}{\partial w_i} \right) \\ &= \frac{1}{2} (1 - j \times j) \\ &= 1 \end{aligned}$$

Hence,

$$\frac{\partial w}{\partial w} = \frac{\partial w^*}{\partial w^*} = 1 \quad , \quad (\text{A.7})$$

Following similar steps, we can deduce the following

$$\frac{\partial w^*}{\partial w} = \frac{\partial w}{\partial w^*} = 0 \quad (\text{A.8})$$

Now, we consider the differentiation with respect to a complex vector \mathbf{w} . Let \mathbf{w} be an L-by-1

vector with elements w_0, w_1, \dots, w_{L-1} . Applying equations (A.3) and (A.4) we can write

$$\frac{\partial}{\partial \mathbf{w}} = \frac{1}{2} \begin{bmatrix} \frac{\partial}{\partial w_{r_0}} - j \frac{\partial}{\partial w_{i_0}} \\ \frac{\partial}{\partial w_{r_1}} - j \frac{\partial}{\partial w_{i_1}} \\ \vdots \\ \frac{\partial}{\partial w_{r_{L-1}}} - j \frac{\partial}{\partial w_{i_{L-1}}} \end{bmatrix} \quad (\text{A.9})$$

and

$$\frac{\partial}{\partial \mathbf{w}^*} = \frac{1}{2} \begin{bmatrix} \frac{\partial}{\partial w_{r_0}} + j \frac{\partial}{\partial w_{i_0}} \\ \frac{\partial}{\partial w_{r_1}} + j \frac{\partial}{\partial w_{i_1}} \\ \vdots \\ \frac{\partial}{\partial w_{r_{L-1}}} + j \frac{\partial}{\partial w_{i_{L-1}}} \end{bmatrix} \quad (\text{A.10})$$

where $\frac{\partial}{\partial \mathbf{w}}$ is referred to as the *derivative* with respect to vector \mathbf{w} , and $\frac{\partial}{\partial \mathbf{w}^*}$ as the *conjugate derivative* with respect to vector \mathbf{w} . The asterisk $*$ represents complex conjugation as defined in (2.4). Equations (A.7) and (A.8) can be generalised using (A.9) and (A.10) to give

$$\frac{\partial \mathbf{w}^T}{\partial \mathbf{w}} = \frac{\partial \mathbf{w}^H}{\partial \mathbf{w}^*} = \mathbf{I} \quad , \quad (\text{A.11})$$

and

$$\frac{\partial \mathbf{w}^T}{\partial \mathbf{w}^*} = \frac{\partial \mathbf{w}^H}{\partial \mathbf{w}} = \mathbf{0} \quad , \quad (\text{A.12})$$

where \mathbf{I} and $\mathbf{0}$ are the L -by- L identity and null matrices, respectively.

For the convenience of this thesis we will adopt the definition of (A.10) as the *derivative* with respect to vector \mathbf{w} , as discussed in Section 2.2. Hence equation (??) has been defined

as

$$\frac{\partial}{\partial \mathbf{w}} = \begin{bmatrix} \frac{\partial}{\partial w_0} \\ \frac{\partial}{\partial w_1} \\ \vdots \\ \frac{\partial}{\partial w_{L-1}} \end{bmatrix}^* . \quad (\text{A.13})$$

Appendix B

Matched Filters

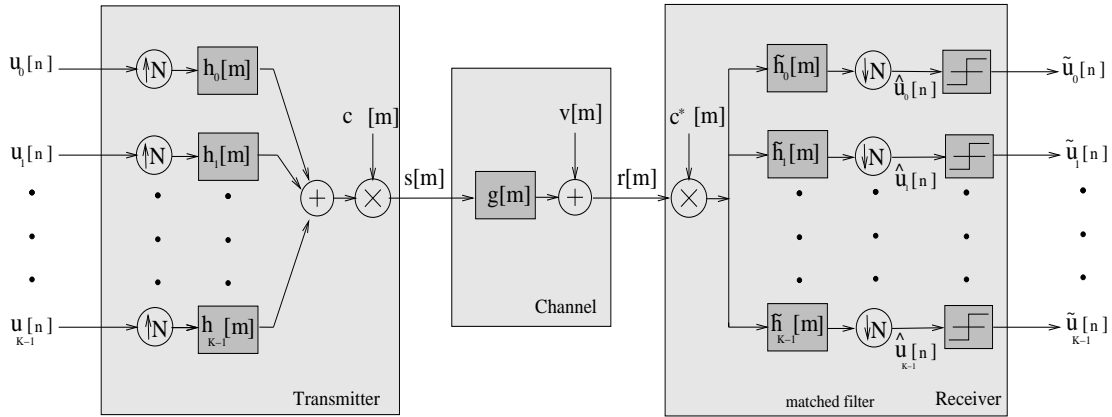


Figure B.1: Synchronous DS-CDMA system with matched filters

In DS-CDMA systems, users $u_l[n]$ ($0 \leq l < K$) transmit their signals over a common channel, and each user l is provided with a specific spreading sequence \mathbf{h}_l . During transmission, symbols will be spread by a factor called the spreading factor N [101]. After the spreading procedure is done, the resulting signals are called chips.

Let's consider the DS-CDMA system in Fig. B.1, where the spread sequences \mathbf{h}_l are synchronous and the chips can be summed up and then further scrambled by multiplying by a scrambling sequence $c[m]$ prior to transmission over a dispersive channel $g[m]$ with additive

noise $v[m]$.

In the conventional DS-CDMA receiver, the detector descrambles the received signal $r[m]$ and then correlates the resulting signal with a replica of each user's spreading code to recover the specific transmitted sequences. The output of the matched filter (MF) is sampled at the symbol rate, which yields soft estimation of transmit symbols. The final hard symbol decision is made by means of nonlinear decision devices, as shown in Fig. B.1. However this kind of detector does not take into account the effects of ISI and MAI.

Bibliography

- [1] 3rd Generation Partnership Project, “Technical Specification Group Radio Access Network, Evolved Universal Terrestrial Radio Access (E-UTRA), Physical layer procedures (Release 8)”, in 3GPP TS 36.213 V8.0.0, September 2007.
- [2] International Telecommunications Union - Radio Communications Sector, “ITU global standard for international mobile telecommunications”, in IMT-Advanced, Circular letter, March 2008.
- [3] S. Parkvall, E. Dahlman, A. Furuskär et al., “LTE-Advanced - Evolving LTE towards IMT-Advanced”, in IEEE Vehicular Technology Conference, VTC 2008-Fall, pp 1-5, Stockholm, Sweden, September 2008.
- [4] 3rd Generation Partnership Project, “Technical Specification Group Radio Access Network, Evolved Universal Terrestrial Radio Access (E-UTRA), Physical layer procedures (Release 10)”, in 3GPP TS 36.213 V10.0.0, December 2010.
- [5] L. Rugini, P. Banelli, and G. Leus, “Simple equalization of time-varying channels for OFDM”, in IEEE Communications Letters, Volume 9, pp 619-621, July 2005.
- [6] L. Rugini, P. Banelli, and G. Leus, “Low-complexity banded equalizers for OFDM systems in Doppler spread channels”, in EURASIP Journal on Applied Signal Processing, Volume 9, pp 1-13, August 2006.

-
- [7] A. A. A. Solyman, S. Weiss, and J. J. Soraghan, “Low-Complexity LSMR Equalisation of FrFT-Based Multicarrier Systems in Doubly Dispersive Channels”, in IEEE International Symposium on Signal Processing and Information Technology, pp 461-465, Bilbao, Spain, December 2011.
- [8] C. Y. Chi, C. C. Feng, C. H. Chen, and C. Y. Chen, “Blind Equalization and System Identification”, Springer, 2006.
- [9] A. Cichocki and S. Amari, “Adaptive Blind Signal and Image Processing”, John Wiley and Sons Ltd., 2002.
- [10] S. Haykin, “Adaptive Filter Theory”, Prentice Hall, Englewood Cliffs, 4th edition, 2002.
- [11] M. Hedef, A. Daas, , and S. Weiss, J. Reiss, X. Chen “A Robust Pilot-Assisted Equalizer For Partially Loaded Downlink UMTS TDD”, in Proc. European Signal Processing Conference (EUSIPCO), Poznan, Poland, September, 2007.
- [12] A. Daas, M. Hedef, and S. Weiss. “Adaptive blind multiuser equalizer based on pdf matching”, in Proc. IEEE International Conference on Telecommunications, Marrakech, Morocco, May 2009.
- [13] A. Daas, and S. Weiss. “Blind adaptive equalizer based on pdf matching for rayleigh time-varying channels”, in Proc. Asilomar Conference on Signals, Systems, and Computers, Pacific Grove, USA, November 2010.
- [14] A. Daas, S. Bendoukha, and S. Weiss. “Blind Adaptive Equaliser For Broadband MIMO STBC Based on PDF Fitting”, in proc. European Signal Processing Conference (EUSIPCO), Glasgow, Scotland, August, 2009.

-
- [15] A. Daas, S. Bendoukha, and S. Weiss. “Blind Adaptive Equaliser For Broadband MIMO Time Reversal STBC Based on PDF Fitting”, in Proc. Asilomar Conference on Signals, Systems, and Computers, Pacific Grove, USA, November 2009.
- [16] J. G. Proakis, “Digital Communications, third edition”, in McGraw-Hill Series, New York, USA, 1995.
- [17] J. G. Proakis, “Channel Equalization”, in The Mobile Communications Handbook, Jerry D. Gibson, Ed., chapter 6, pp. 56-80. CRC Press / IEEE Press, 1996.
- [18] J. R. Treichler, I. Fijalkow, and C. R. Johnson, “Fractionally Spaced Equalizers: How Long Should They Really Be?”, in IEEE Signal Processing Magazine, vol. 13, no. 3, pp. 65-81, May 1996.
- [19] T. J. Endres, “Equalizing with Fractionally-Spaced Constant Modulus and Second-Order-Statistics Blind Receivers”, Ph.D. Thesis, University of Cornell, USA, May 1997.
- [20] S. Chen, “Adaptive linear filtering design with minimum symbol error probability criterion”, in International Journal of Automation and Computing, vol. 3, no. 3, pp. 291-303, 2006.
- [21] G. H. Golub and C. F. Van Loan, “Matrix Computations, 3rd edition”, Johns Hopkins University Press, Maryland, USA, 1996.
- [22] B. Widrow and S. D. Stearns, “Adaptive Signal Processing ”, Prentice-Hall, Englewood Cliffs, New York, 1985.
- [23] B. Widrow and Hoff., “Adaptive Switching Circuits”, in IRE Western Electric Show and Convention Record, vol. 4, pp. 96-104, August 1960.
- [24] B. Widrow, J. McCool, and M. Ball, “The Complex LMS Algorithm”, in Proceedings of the IEEE, vol. 63, pp. 719-720, August 1975.

- [25] R. W. Steward, S. Weiss, and D. H. Crawford, "Convergence Behaviour of LMS-Type Algorithms for Adaptive Noise Control in Noisy Doppler Environments", in International Symposium on Methods and Models in Automation and Robotics, Volume I, pp 69-76, Miedzyzdroje, Poland, September 1996.
- [26] N. J. Bershad and O. M. Macchi, "Comparison of the RLS and LMS Algorithms for Tracking A Chirped Signal", in Proc. IEEE Conference on Acoustics, Speech, and Signal Processing, vol.2, pp. 896-899, Scotland, May 1989.
- [27] O. M. Macchi, "A General Methodology for Comparison of Adaptive Filtering Algorithms in Non-stationary Context", in Proc. European Signal Processing Conference, vol.1, pp. 189-192, Spain, September 1990.
- [28] O. M. Macchi and N. J. Bershad "Adaptive Recovery of a Chirped Sinusoid in Noise, Part 1: Performance of the RLS Algorithm", in IEEE Transactions on Signal Processing, vol.39(No.3), pp. 583-594, March 1991.
- [29] N. J. Bershad and O. M. Macchi, "Adaptive Recovery of a Chirped Sinusoid in Noise, Part 2: Performance of the LMS Algorithm", in IEEE Transactions on Signal Processing, vol.39(No.3), pp. 595-602, March 1991.
- [30] S. Makino, J. Noebauer, Y. Haneda, and A. Nakagawa "SSB Subband Echo Canceller Using Low-Order Projection Algorithm", in Proc. IEEE International Conference on Acoustics, Speech, and Signal Processing, **2**: 945-948, May 1996.
- [31] S. Weiss and R. W. Stewart, "On Adaptive Filtering in Oversampled Subbands", Shaker Verlag, Aachen, Germany, 1998.
- [32] K. Ozeki and Umeda, "An Adaptive Filtering Algorithm Using an Orthogonal Projection to an Affine Subspace and Its Properties", in Electronics and Communications in Japan, vol.67-A, no.5, pp.19-27, February 1984.

-
- [33] S. G. Sankaran and A. A. Beex, "Convergence behavior of affine projection algorithms", in *IEEE Transactions on Signal Processing*, Vol.48, No.4, pp. 1086-1096, April 2000.
- [34] N. J. Bershad, D. Linebarger, and S. McLaughlin, "A Stochastic Analysis of the Affine Projection Algorithm for Gaussian Autoregressive Inputs", in *Proc. IEEE Conference on Acoustics, Speech, Signal Processing*, vol. 6, pp. 3837-3840, May 2001.
- [35] S. J. M. De Almeida, J. C. M. Bermudez, N.J. Bershad, and M.H. Costa, "A Statistical Analysis of the Affine Projection Algorithm for Unity Step Size and Autoregressive Inputs", in *IEEE Transactions on Fundamental Theory and Applications: Circuits and Systems I*, Vol. 52, No. 7, pp. 1394-1405, July 2005.
- [36] S.L. Gay and R.J. Mammone, "Fast Converging Subband Acoustic Echo Cancellation Using Rap on WE DSP16A", in *Proc. IEEE International Conference on Acoustics, Speech, and Signal Processing*, vol.2, pp. 1141-1144, Albuquerque, NM, April 1990.
- [37] S.L. Gay and S. Tavathia, "The Fast Affine Projection Algorithm", in *Proc. IEEE International Conference on Acoustics, Speech, and Signal Processing*, vol.V, pp. 3023-3026, Detroit, Michigan, 1995.
- [38] W. A. Gardner, "A New Method of Channel Identification", in *IEEE Transactions on Communications*, vol. 39, no. 6, pp. 813-817, June 1991.
- [39] L. Tong, G. Xu, and T. Kailath, "Blind Identification and Equalization Based on Second-Order Statistics: A Time Domain Approach", in *IEEE Transactions on Information Theory*, vol.40, no.2, pp.340-349, March 1994.
- [40] M. Honig, U. Madhow, and S. Verdu, "Blind Adaptive Multiuser Detection", in *IEEE Transactions on Information Theory*, vol. 41, no. 4, pp. 944-960, July 1995.

-
- [41] R. Schober, W. H. W. H. Gerstacker, and L.H. J. Lampe, “Comparison of MOE and Blind LMS”, in *IEEE Communications Letters*, vol. 7, pp. 204-206, 2003.
- [42] R. W. Lucky, “Techniques for Adaptive Equalization of Digital Communication Systems”, in *The Bell System Technical Journal*, vol. 45, no. 2, pp.255-286, February 1966.
- [43] O. Macchi and E. Eweda, “Convergence Analysis of Self-Adaptive Equalizer”, in *IEEE Transactions on Information Theory*, vol.30, no.2, pp. 161-176, March 1984.
- [44] D. Godard, “Self-Recovering Equalization and Carrier Tracking in Two-Dimensional Data Communication Systems”, in *IEEE Transactions on Communications* [legacy, pre - 1988], vol. 28, no. 11, pp. 1867-1875, November 1980.
- [45] J. R. Treichler and B. G. Agee, “A New Approach to Multipath Correction of Constant Modulus Signals”, in *IEEE Transactions on Acoustics, Speech, and Signal Processing*, vol. 31, no. 2, pp. 459-472, February 1983.
- [46] Y. Sato, “A Method of Self-Recovering Equalization for Multilevel Amplitude-Modulation Systems”, in *IEEE Transactions on Communications*, vol. 23, no. 6, pp. 679-682, June 1975.
- [47] J. K. Byoung-Jo, “Blind Equalization for Short Burst Wireless Communications”, Ph.D. thesis, Stanford University, USA, January 1998.
- [48] S. Haykin, “Blind Deconvolution”, Prentice Hall, Englewood Cliffs, 1994.
- [49] A. Touzni, I. Fijalkow, and J.R. Treichler, “Robustness of fractionally-spaced equalization by CMA to lack of channel disparity and noise”, in *IEEE Signal Processing Workshop on Statistical Signal and Array Processing*, pp. 144-147, June 1996.

- [50] C. R. Johnson, P. Schniter, T. J. Endres, J. D. Behm, D. R. Brown, and R. A. Casas, “Blind Equalization Using the Constant Modulus Criterion: A Review”, in Proceedings of the IEEE, vol. 86, no. 10, pp. 1927-1950, October 1998.
- [51] R. Gooch, M. Ready, and J. Svoboda, “A Lattice-Based Constant Modulus adaptive filter”, in Proc. IEEE Asilomar Conference on Signals, Systems, and Computers, Pacific Grove, USA, 1987.
- [52] C. Papadias and D.T.M. Slock, “Normalized Sliding Window Constant Modulus and Decision-Directed Algorithms: a Link Between Blind Equalization and Classical Adaptive Filtering”, in IEEE Transactions on Signal Processing, vol. 45, no. 1, pp. 231-235, 1997.
- [53] E.M. Wang, and Z. Dowling, “Stochastic conjugate gradient constant modulus blind equalizer for wireless communications”, in IEEE International Conference on Communications, vol. 2, pp. 832-836, June 1996.
- [54] K. Nam Oh and Y.O. Chin, “Modified constant modulus algorithm: blind equalization and carrier phase recovery algorithm”, in IEEE International Conference on Communications, vol. 1, pp. 498-502, June 1995.
- [55] K. Nam Oh and Y.O. Chin, “New blind equalization techniques based on constant modulus algorithm”, in IEEE Global Communications Conference, vol. 2, pp. 865-869, November 1995.
- [56] K. Hilal and P. Duhamel, “A Convergence Study of the Constant Modulus Algorithm Leading to a Normalized-CMA and a Block-Normalized-CMA”, in Proc. of the European Signal Processing Conference (EUSIPCO 92), vol. 1, pp. 135-138, August 1992.
- [57] D, L, Jones, “A Normalized Constant-Modulus Algorithm”, in Proc. of Asilomar

- Conference on Signals, Systems and Computers (Asilomar 95), vol. 1, pp. 694-697, November 1995.
- [58] J. P. LeBlanc, I. Fijalkow, and C. R. Jr. Johnson, “CMA Fractionally Spaced Equalizers: Stationary Points and Stability under IID and temporally correlated sources”, in *International Journal of Adaptive Control and Signal Processing*, 1998.
- [59] I. G. Stirling, D. García-Alís, S. Weiss, G. W. Rice, and R. W. Stewart, “Adaptive Multiuser MMSE Down-Link Receiver Techniques for UTRA TDD”, in *Proc. Asilomar Conference on Signals, Systems, and Computers*, Monterey, CA, November 2000.
- [60] A.R. Margetts and P. Schniter, “Adaptive Chip-Rate Equalization of Downlink Multirate Wideband CDMA”, in *Proc. Asilomar Conference on Signals, Systems, and Computers*, pp. 1228–1232, November 2002.
- [61] S. Lambotharan, J.A. Chambers, and A.G. Constantinides, “Adaptive blind retrieval techniques for multi-user ds-cdma signals”, in *IET Electronics Letters*, vol.35, no.9, pp.693-695, 1999.
- [62] C. Papadias and A. Paulraj, “A Constant Modulus Algorithm for Multiuser Signal Separation in Presence of Delay Spread Using Antenna Arrays”, in *IEEE Signal Processing Letters*, 4(6):178–181, 1997.
- [63] 3GPP TS 25.223, “Spreading and Modulation (TDD)”, in *Third Generation Partnership Project*, Release 14, March 2017.
- [64] T. K. Moon and W. C. Stirling, “Mathematical Methods and Algorithms”, in *Prentice Hall*, Upper Saddle River, NJ, 1999.
- [65] S.J. Elliott, I.M. Stothers, and P.A. Nelson, “A Multiple Error LMS Algorithm and its

- Application to the Active Control of Sound and Vibration”, in *IEEE Transactions on Acoustics, Speech and Signal Processing*, Vol.35, No.10, pp.1423-1434, 1987.
- [66] F.C.C. De Castro, M.C.F. De Castro and D.S. Arantes, “Concurrent blind deconvolution for channel equalization”, in Proc. IEEE International Conference on Communications, vol. 2, pp. 366-371 June 2001.
- [67] M. Hedef, S. Weiss, and M. Rupp, “Adaptive Blind Multiuser DS-CDMA Downlink Equaliser”, in IET Electronics Letters, vol. 41(21), pp. 1184 - 1185, 2005.
- [68] M. Hedef, S. Weiss, “A Pilot-Assisted Equalisation Scheme for the UMTS-TDD Downlink with Partial Loading”, in IEEE 61st Semiannual Vehicular Technology Conference (VTC), Vol.1, pp.548-551, Stockholm, Sweden, June, 2005
- [69] P. Schramm, “Analysis and optimization of pilot-channel-assisted BPSK for DS-CDMA systems”, in IEEE Transactions on Communications, Vol.46, No.9, pp.1122-1124, 1998.
- [70] 3GPP TS 25.213, “Spreading and Modulation (FDD)”, in Third Generation Partnership Project, Release 15, June 2018.
- [71] I. Santamaría, C. Pantaleón, L. Vielva, and J. C. Principe “Adaptive blind equalization through quadratic pdf matching”, in Proc. European Signal Processing Conference, **2**: 289 - 292, Toulouse, France 2002.
- [72] M. Lázaro, I. Santamaría, C. Puntaleón, D. Erdogmus, and J. C. Principe “Matched-PDF Based Blind Equalization”, in Proc. IEEE International Conference on Acoustics, Speech, and Signal Processing, **4**: 297-300 , 2003.
- [73] M. Lázaro, I. Santamaría, D. Erdogmus, K. Hild, C. Puntaleón, , and J. C. Principe “Stochastic blind equalization based on PDF fitting using Parzen estimator”, in IEEE Transactions on Signal Processing, vol. 53, pp. 696-704, 2005.

- [74] C. Zhang, B. Lin, R. Liu, and B. Wang, “Low Complexity Blind Equalization Based on Parzen Window Method”, in 5th International Conference on Wireless Communications, Networking and Mobile Computing (WiCom), Beijing, China, September 2009.
- [75] M. Messai, S. Fki, T. Chonavel, and A. Aïssa-El-Bey, “An adaptive radius blind equalization algorithm based on pdf fitting”, in 21st European Signal Processing Conference, Marrakech, Morocco, September 2013.
- [76] S. Fki, M. Messai, A. Aïssa-El-Bey, and T. Chonavel, “Blind equalization based on PDF fitting and convergence analysis”, in The Signal Processing Journal, vol. 101: pp. 266-277, August 2014.
- [77] S. Fki, M. Messai, A. Aïssa-El-Bey, and T. Chonavel, “New Criteria for Blind Equalization Based on PDF Fitting”, in 15th IEEE International Workshop on Signal Processing Advances in Wireless Communications (SPAWC): pp. 489-493, Toronto, Canada, June 2014.
- [78] C. C. Calvalcante, F. R. P. Calvalcante, and J. C. M. Mota “Adaptive blind multiuser separation criterion based on log-likelihood maximisation”, in IET Electronics Letters, **38**(20): 1231 - 1233, 2002.
- [79] E. Parzen “On Estimation of Probability Density Function and Mode”, in The Annals of Mathematical Statistics Journal, **33**: pp. 1065 - 1076 , September 1962.
- [80] C. Archambeau, M. Valle, A. Assenza, and M. Verleysen, “Assessment of probability density estimation methods: Parzen window and finite Gaussian mixtures”, in Proc. IEEE International Symposium on Circuits and Systems, Kos, Greece, May 2006.
- [81] I. Santamaría, C. Pantaleón, L. Vielva, and J. C. Principe “A fast algorithm for adaptive blind equalization using order- α Renyi’s entropy”, in Proc. International Conference

- on Acoustics, Speech, Signal Processing, vol. 3, pp. 2657-2660. Orlando, Florida, USA, 2002.
- [82] E. Gokcay and J. C. Principe, “Information theoretic clustering”, in IEEE Transactions on Pattern Analysis and Machine Intelligence, vol. 24, no. 2, pp. 158-171, 2002.
- [83] J. Ossanna, “A model for mobile radio fading due to building reflections: Theoretical and experimental waveform power spectra”, in The Bell System Technical Journal, vol. 43, pp. 2935-2971, 1964.
- [84] R. H. Clarke, “Statistical theory of mobile-radio reception”, in The Bell System Technical Journal, vol. 47, pp. 957-1000, 1968.
- [85] T. S. Rappaport “Wireless Communications: Principles and Practice”, *Prentice Hall*, 1996.
- [86] R. E. Crochiere and L. R. Rabiner “Multirate Digital Signal Processing”, *Prentice Hall*, 1983.
- [87] G. J. Foschini and M. J. Gans. “On limits of wireless communication in a fading environment when using multiple antennas”, in Wireless Personal Communications Journal, **6**(3): 311–335, March 1998.
- [88] S.M Alamouti, “A simple transmit diversity technique for wireless communication”, in IEEE Journal on Selected Areas in Communications, **16**(8): 1451 – 1458, 1998.
- [89] S. N. Diggavi, N. Al-Dhahir, A. Stamoulis, and A. R. Calderbank, “Differential space-time coding for frequency-selective channels”, in IEEE Communications Letters, **6**(6): 253 - 255, June 2002.
- [90] N. Al-Dhahir, “Overview and comparison of equalization schemes for space-time-coded

- signals with application to EDGE”, *IEEE Transactions on Signal Processing*, **50**(10): 2477–2488, Oct. 2002.
- [91] T. Jiang and Y. W. Wu, “An overview: Peak to average power ratio reduction techniques for OFDM signals”, in *IEEE Transactions on Broadcasting*, vol. 54, no. 2, pp. 257-268, June 2008.
- [92] R. Schober, H. Z. B. Chen, and W. H. Gerstacker. “Decision-feedback sequence estimation for timereversal space-time block-coded transmission”, in *IEEE Transactions on Vehicular Technology*, **53**(4): 12732–1278, July 2004.
- [93] S. Bendoukha and S. Weiss, “Blind CM equalisation for STBC over multipath fading”, in *IET Electronics Letters*, **44**(15): 922-923, July 2008.
- [94] S. Bendoukha and S. Weiss, “A Fast Converging Blind Receiver for Space-Time Block Codes over Frequency Selective Channels”, in *Proc. IEEE International Conference on Signal Processing and Communications*, 169-172 , Nov. 2007.
- [95] E. Lindskog and A. Paulraj, “A transmit diversity scheme for channels with intersymbol interference”, in *Proc. IEEE International Conference on Communications*, **vol. 1**: 307-311, June 2000.
- [96] Y. Luo and S. Lambbotharan, “A new tap constrained constant modulus algorithm for blind equalization of time reversal space time block codes”, in *Proc. IEEE 5th Workshop on Signal Processing Advances in Wireless Communications*, **vol(1)**: 273-277, 2004.
- [97] G. Boray and M. Srinath, “Conjugate gradient techniques for adaptive filtering”, in *IEEE Transactions on Circuits and Systems I: Regular Papers*, **39**: 1-10, 1992.
- [98] S. Barbarossa and A. Scaglione, “Blind equalization using cost function matched to the

- signal constellation”, in Proc. Asilomar Conference on Signals, Systems & Computers, **1**: 550-554, 1997.
- [99] R. F. H. Fischer, “Precoding and Signal Shaping for Digital Transmission”, John Wiley & Sons Inc., New York, 2005.
- [100] A. Hjørungnes and D. Gesbert, “Complex-Valued Matrix Differentiation: Techniques and Key Results”, in IEEE Transactions on Signal Processing, 2006.
- [101] S. Verdu, “Multiuser Detection”, Cambridge University Press, Cambridge, UK, 1998